Midterm Report

Multi-Disciplinary Design and Optimisation of a Long-Range eVTOL Aircraft

Group 06

Student Name	Student Number
Alba Maestre, Javier	4844009
Beyne, Egon	4797957
Buszek, Michael	4773934
Cuadrat-Grzybowski, Miguel	4838726
Montoya Santamaría, Alejandro	4789946
Poliakov, Nikita	4804236
Prud'homme van Reine, Koen	4878965
Salvador López, Noah	4882512
Schoser, Jakob	4843754
Wadia, Kaizad	4789849

Tutor: Saullo Giovani Pereira Castro
Coaches: Davide Biagini and Ali Nokhbatolfoghahai
Teaching Assistant: Paula Meseguer Berroy

Institution: Delft University of Technology
Place: Faculty of Aerospace Engineering, Delft

Submission Date: Tuesday 19th October, 2021

TU Delft Delft University of Technology

Summary

The issue of adequate transportation is widespread. Not only are many modes of transportation expensive, but they often require dedicated infrastructure and are prone to traffic and congestion. In an attempt to attenuate this costly problem an electrical Vertical Takeoff and Landing (eVTOL) aircraft concept is proposed. To be precise, three such concepts are proposed. One with a tandem wing configuration, another with a box wing and a third with a single wing. While there can be three such solutions, the objective remains the same, which is to provide sustainable, personal aerial transportation for inter-city travel that is competitive with the current transportation methods while requiring minimal infrastructure. In order to accomplish this goal, several steps are taken, which are hereby explained.

In Chapter 2 the organisational structure of the group is explained, which allows for the project plan to be explicated in Chapter 3. After the planning is complete the trade-off criteria is listed in Chapter 4 and possible solutions can be graphed by means of a design option tree in Chapter 5.

However, out of the realm of possibility, one is likely to be the most suitable for the problem at hand. The purpose of this report is to select the concept which performs the best under the requirements previously formulated, that state what the solution shall do and how it shall do it. Through these requirements, it is possible to establish the relevant trade-off criteria and thereby create a trade-off matrix. That being said the criteria of the trade-off matrix have yet to be defined, for which preliminary values are necessary. For these, Chapter 6 outlines the method used to size the vehicle, using a set of statistical models after the concepts are illustrated. In this, the stall speed, climb rate, turning load factor, and other parameters pertaining to the aircraft is estimated, including the mass.

Then the flight performance is discussed in Chapter 7. Therein the aircraft is analysed during the different phases of flight. This leads to its energy consumption being considered during different phases. Thereafter its climb performance is evaluated as well as aspects of the passengers. After that the aerodynamics of the aircraft is explicated in Chapter 8. This includes estimations of the lift and drag coefficients, the design of the wing (if applicable) and the selection of airfoils for the concepts. Once that is complete the drag estimation can be concretised and a more accurate version of the drag polar can be made.

The discussion of the design continues with the Propulsion & Power subsystem in Chapter 9, the crux of which lies in selecting a proper and adequate source of power. Several options were considered, including a variety of hydrogen fuel cells and batteries. The design of the propulsion subsystem of the vehicle also presented itself as a challenge, but it could be overcome with Actuator Disk Theory, which exploits the relationship between the area of a propeller and the weight of the aircraft.

The stability and control of any aircraft not only constitutes passenger comfort, but also governs their safety during flight, an essential discipline that is presented in Chapter 10. In this chapter, the controllability is explained in hover, through a set of state space models that govern the output of a system, given the inputs. An aircraft is only as good as the loads it is capable to withstand, which implicates another crucial aspect of the design of an aircraft, namely the structure thereof. Chapter 11 presents the structural design envelope. These are done with the critical failure modes: fatigue and yield. This is coupled with the estimation of the aircraft weight and centre of gravity, as well as its crash-worthiness.

After the technical aspects of the design are discussed, the finances can then be planned, as in Chapter 13. In this, the unit cost analysis is performed as well as the direct operational cost. Upon completion of this analysis the project development and design is also discussed, as well as the plan for sustainability in Chapter 14. The Reliability, Availability, Maintainability and Safety characteristics are then elucidated in Chapter 15. The Technical Risk Analysis is also performed in Chapter 16 in order to determine any foreseeable malignant circumstances and plan for all contingencies.

With all of the above in mind, the trade-off can then be conducted in Chapter 17. Wherein the selection criteria and weights are defined, as well as how well it complies to its constraints. Thereafter the Trade-Off matrix is generated. With all of this done, the purpose of this is thereby fulfilled and the final design is presented in Chapter 18, wherein the Tandem configuration is selected.

Contents

1 Introduction

When confronted with a number of different conceptual design options for the design of an eVTOL aircraft, constructing a thorough and extensive technical and logistic analysis of all the available concepts is key. By doing this, a detailed and integral trade-off can be performed allowing the selection of the most optimal choice. Once a concept is chosen, it is possible to continue the design process in a more detailed level for each discipline, followed by an optimisation process to refine the final design.

Thus, the aim of this report is to present and justify the selection of a final design concept for the eVTOL aircraft project, out of 3 concepts which are chosen for further analysis. In order to achieve this, it is necessary to plan all the design activities in a detailed manner in order to ensure that the assignments are completed when required. The first step of the preliminary sizing for each concept is to analyse existing eVTOL aircraft of similar characteristics, in order to obtain initial estimates of important parameters, such as weight, to initiate the design and analysis of each concept. Once this is achieved, each discipline is able to perform a preliminary design and sizing of the relevant subsystems, with the focus of the analysis being the main differences between the concepts, and by extension being related to the trade-off. In order to complete an accurate and coherent analysis, an iterative process is necessary to ensure continuity between the interfaces of the different disciplines.

The outline of the report is as follows. Chapters 2 and 3 present the organisation of the project, while Chapters 4 and 5 discuss the selection criteria (to be used in the trade-off) and the design options respectively. After that, Chapters 6 to 11 focus on the technical design and analysis of the concepts per discipline, followed by Chapters 12 to 14 presenting the non-technical aspects of the aircraft concepts. Chapter 15 provides a RAMS analysis of the concepts, and Chapter 16 presents an analysis of the risks. Finally, the results from all the different processes comes together in the trade-off in Chapter 17 with concluding remarks to be found in Chapter 18.

2 Human Resources

In this chapter the task division of both the technical and non-technical roles can be found. The team structure and the relations between members will also be seen. More details about both the technical an non-technical roles can be found in the project plan [2, Chapter 5].

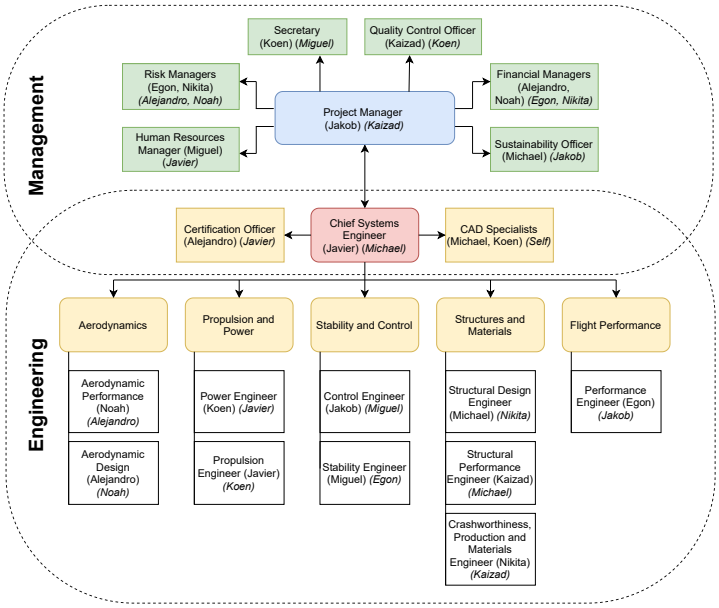

Figure 2.1: Organogram

The different roles can be seen in the organogram in Figure 2.1. This figure includes the relations between the roles, and the task and role allocation. Every function also needs a backup, to make sure the team can still function when a group member is absent. The backup roles for each team member is shown in italic in the organogram.

There have not been any changes in the task division since the project plan. After working with the structure shown above for the past weeks, no need was found to change the allocation. Each team member has adjusted to their roles, knows what to expect from other members, and who to approach when a question arises.

3 Project Plan

This chapter includes the diagrams used for project planning.

The first one is the Work Breakdown Structure (WBS), which includes the list of tasks to be performed throughout the project. These tasks are listed in no particular order and classified in different trees by discipline or category. The tasks are classified in four different levels, corresponding to their level of detail and length. The lowest level corresponds to tasks that could be completed within half a working day. Two WBS are presented in this chapter (divided only for the sake of representation in this report): the first one (Diagram 1) contains the non-technical tasks, the second one contains the technical tasks (Diagram 2).

Diagram 3 is the Work Flow Diagram (WFD), which contains the 3 levels of tasks of the WBS. These tasks are mostly estimated to have a throughput time up to 2 days (16 hours). In this diagram the tasks are ordered chronologically, and contain their throughput time (in hours) and the people allocated to each task. In order to improve readability, the tasks have been colour-coded into the following categories: Stability and Control, Structures, Aerodynamics, Propulsion and Power, Flight Performance, Sustainability, Finances, PMSE, and Report, Document and Present. The reason that these categories are not the same as in the WBS is that there were too many categories to reasonably colour code.

The chronological order of the WFD is combined with the level of detail of the WBS in the Gantt chart. It contains resources, start and end dates, duration, as well as the relations between the tasks (predecessors).

The last diagram is the N^2 chart, which contains the technical disciplines and the relations between them, i.e. the outputs and inputs that the disciplines share. The subsystems and disciplines are located on the diagonal (marked in yellow). The outputs of a subsystem are arranged in the same row, whereas its inputs can be found in the same column as the yellow box. The N^2 chart was essential to planning the technical analysis of the different subsystems during the midterm phase, and helped organised the code architecture for the repository.

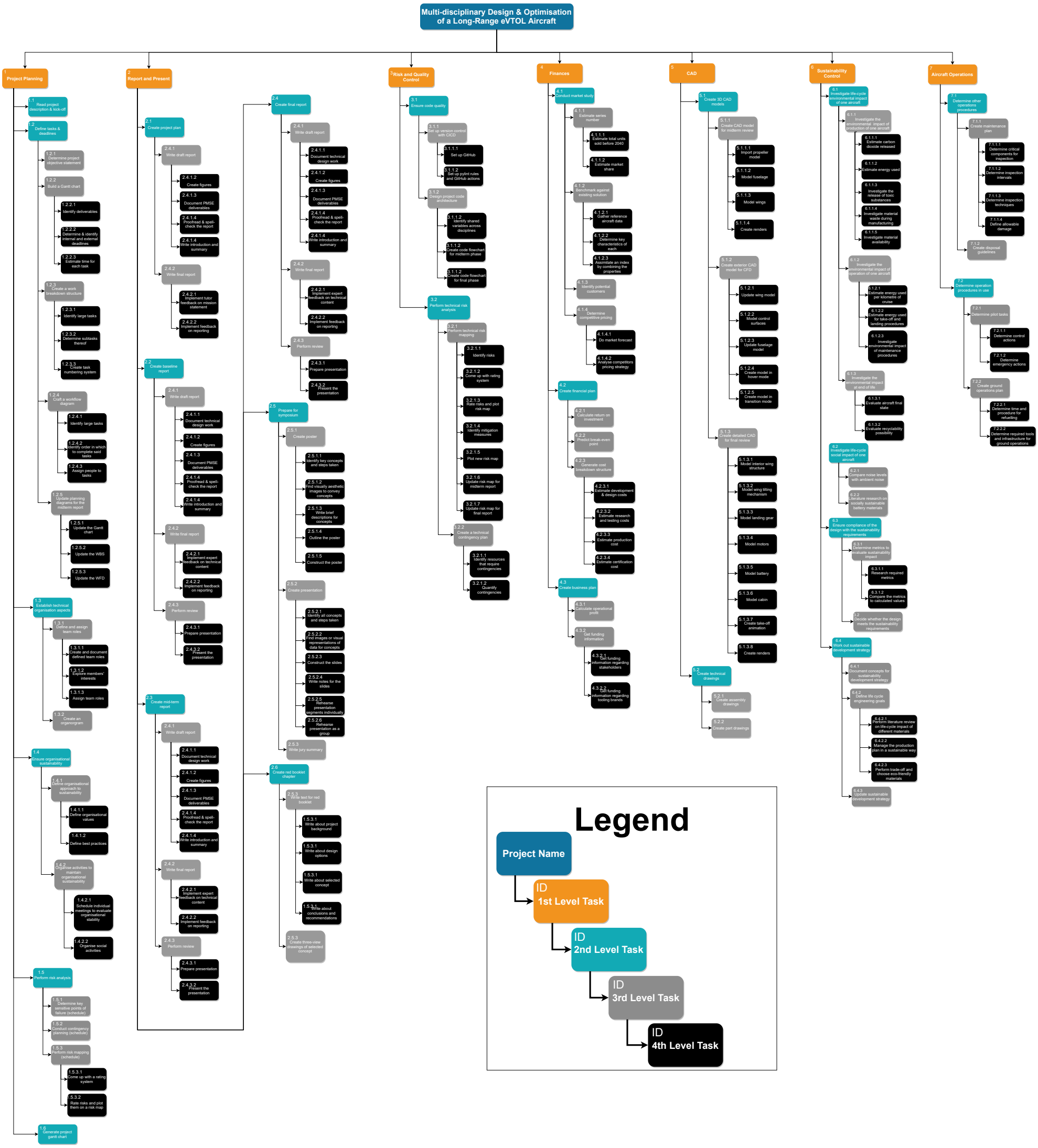

Diagram 1: Non-technical Work Breakdown Structure.

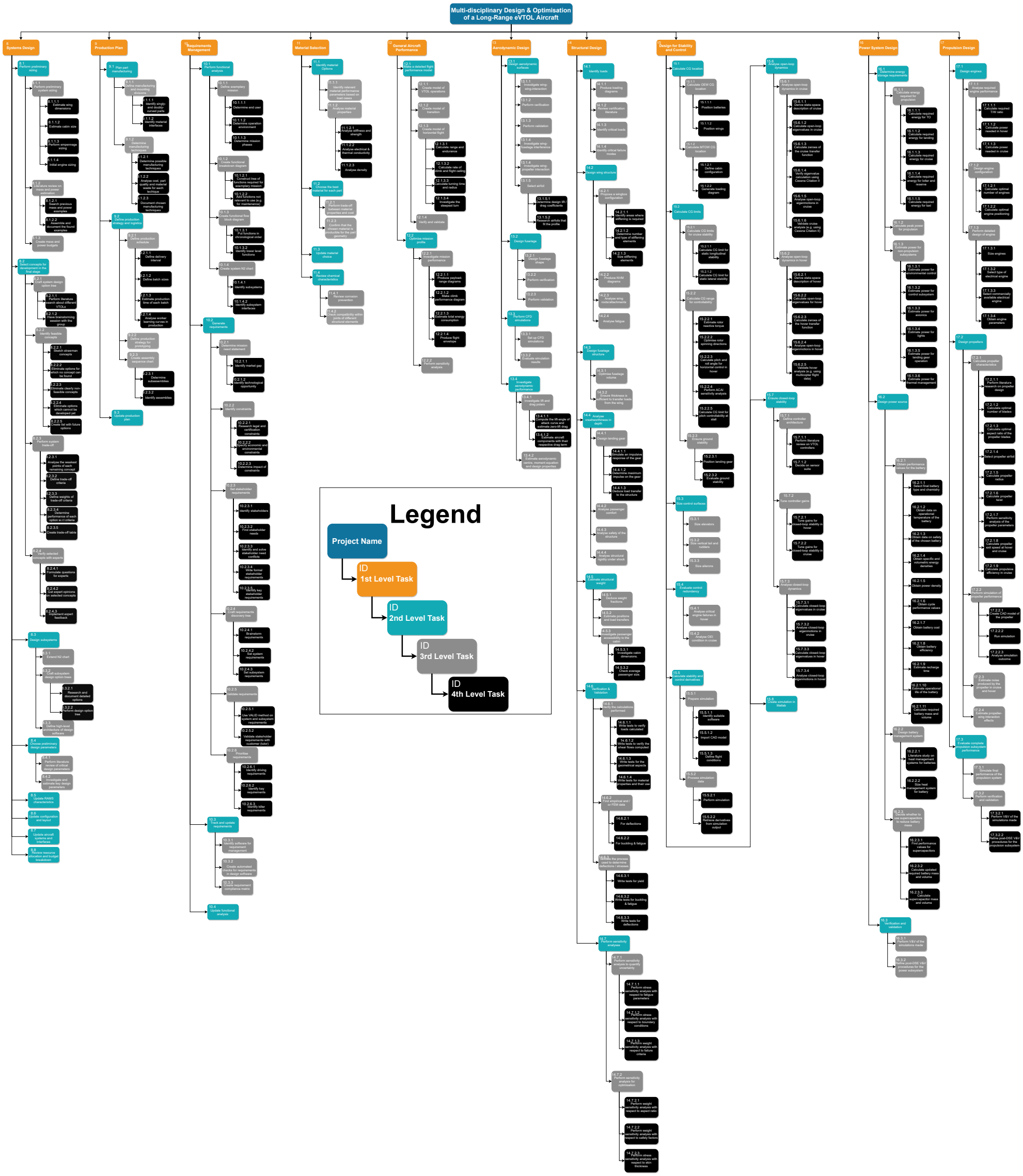

Diagram 2: Technical Work Breakdown Structure.

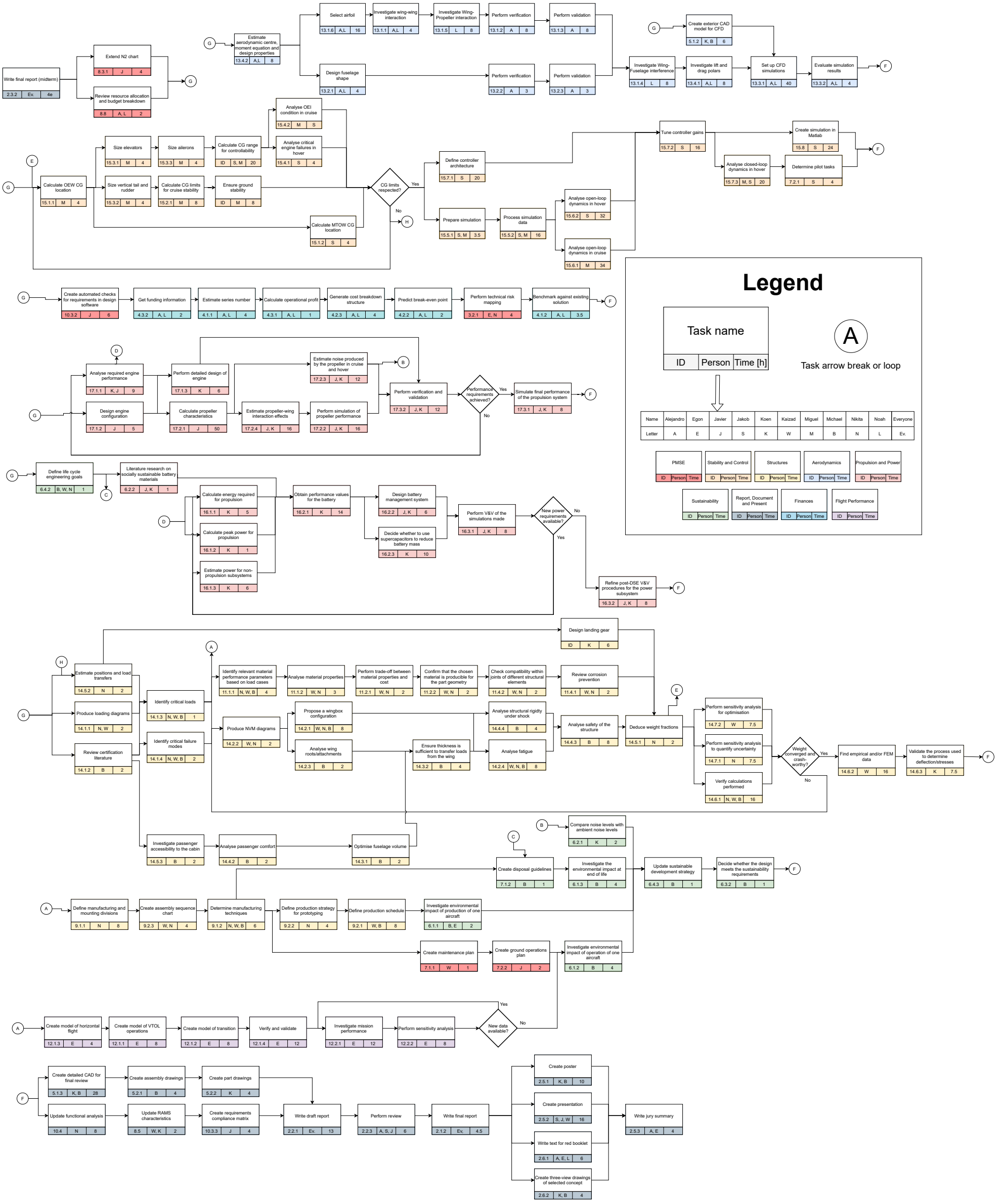

Diagram 3: Work Flow Diagram for the final project phase.

Table 3.1: N^2 chart with subsystem interfaces.

Wing	Induced drag coefficient, Aerodynamic wing-propeller interactions	Vertical take-off loads, Geometrical wing parameters, Lift distribution			CG location	Maximum lift during take-off, Induced drag coefficient
Propeller geometry, Propeller placement	**Propulsion subsystem**	Thrust loads, Propeller placement	Take-off power required, Cruise power required		CG location, Propeller placement	
Geometrical wing parameters	Structures operational empty weight	**Structures**			CG location, Maximum allowable load factor	Maximum allowable load factor, Parasite drag coefficient
	Battery weight, Electrical power	Compliant fuel storage, Wing loads (if applicable)	**Power subsystem**	Electrical power available	CG location, Electrical power	Power consumption
Cabin geometry	Cabin operational empty weight, Payload weight, Parasite drag coefficient	Cabin operational empty weight, Payload weight, Cabin geometry	Power required	**Cabin**	CG location, Maximum allowable acceleration	
Longitudinal wing position	Throttle, Propeller direction		Power required	Longitudinal cabin position	**Control subsystem**	
Optimal cruise speed, Altitude, Wing loading	Optimal cruise speed, Altitude		Total energy required		Optimal cruise speed, Optimal take-off and landing trajectory	**Flight performance**

In Table 3.1 the N^2 chart shows the interfaces and inputs and outputs of each subsystem. Above that the work breakdown structure can be observed and below the Gantt Chart for the design process from this point on.

ID	WBS	Task Name	Duration	Start
1	**1**	**Project Planning**	**159 hrs**	**Mon 19-4-21**
2	1.1	Read project description & kick-off	2 hrs	Mon 19-4-21
3	**1.2**	**Define tasks & deadlines**	**151 hrs**	**Mon 19-4-21**
5	**1.2.2**	**Build a Gantt chart**	**12,5 hrs**	**Mon 19-4-21**
6	1.2.2.1	Identify deliverables	1 hr	Mon 19-4-21
7	1.2.2.2	Determine & identify internal and external deadlines	1 hr	Mon 19-4-21
8	1.2.2.3	Estimate time for each task	6 hrs	Tue 20-4-21
9	**1.2.3**	**Create a work breakdown structure**	**10 hrs**	**Thu 22-4-21**
10	1.2.3.1	Identify large tasks	2 hrs	Thu 22-4-21
11	1.2.3.2	Determine subtasks thereof	4 hrs	Thu 22-4-21
12	1.2.3.3	Create task numbering system	4 hrs	Thu 22-4-21
13	**1.2.4**	**Craft a workflow diagram**	**18,5 hrs**	**Mon 19-4-21**
14	1.2.4.1	Identify large tasks	4 hrs	Mon 19-4-21
15	1.2.4.2	Identify order in which to complete said tasks	8 hrs	Tue 20-4-21
16	1.2.4.3	Assign people to tasks	7,5 hrs	Mon 19-4-21
17	**1.2.5**	**Update planning diagrams for the midterm report**	**15 hrs**	**Tue 18-5-21**
18	1.2.5.1	Update the Gantt chart	7,5 hrs	Wed 19-5-21
20	1.2.5.3	Update the WFD	7,5 hrs	Wed 19-5-21
19	1.2.5.2	Update the WBS	7,5 hrs	Tue 18-5-21
4	1.2.1	Determine project objective statement	2 hrs	Mon 19-4-21
21	**1.3**	**Establish technical organisation aspects**	**11,5 hrs**	**Mon 19-4-21**
22	**1.3.1**	**Define and assign team roles**	**10 hrs**	**Mon 19-4-21**
24	1.3.1.2	Explore members' interests	0,5 hrs	Mon 19-4-21
23	1.3.1.1	Create and document defined team roles	1 hr	Tue 20-4-21
25	1.3.1.3	Assign team roles	0,5 hrs	Tue 20-4-21
26	1.3.2	Create an organogram	2 hrs	Tue 20-4-21
27	**1.4**	**Ensure organisational sustainability**	**7,5 hrs**	**Tue 20-4-21**
28	**1.4.1**	**Define organisational approach to sustainability**	**7,5 hrs**	**Tue 20-4-21**
29	1.4.1.1	Define organisational values	4 hrs	Tue 20-4-21
30	1.4.1.2	Define best practices	4 hrs	Wed 21-4-21
31	**1.4.2**	**Organise activities to maintain organisational sustainability**	**2 hrs**	**Wed 21-4-21**
33	1.4.2.2	Organise social activities	1 hr	Wed 21-4-21
32	1.4.2.1	Schedule individual meetings to evaluate organisational stability	1 hr	Wed 21-4-21
34	**1.5**	**Perform risk analysis**	**6 hrs**	**Mon 19-4-21**
37	**1.5.3**	**Perform risk mapping (schedule)**	**2 hrs**	**Tue 20-4-21**
38	1.5.3.1	Come up with a rating system	1 hr	Tue 20-4-21
39	1.5.3.2	Rate risks and plot them on a risk map	1 hr	Tue 20-4-21
35	1.5.1	Determine key sensitive points of failure (schedule)	2 hrs	Mon 19-4-21
36	1.5.2	Conduct contingency planning (schedule)	2 hrs	Tue 20-4-21
40	1.6	Generate project Gantt chart	2 hrs	Thu 20-5-21
41	**2**	**Report and Present**	**368 hrs**	**Wed 21-4-21**
42	**2.1**	**Create project plan**	**60,5 hrs**	**Wed 21-4-21**
43	**2.1.1**	**Write draft report**	**16 hrs**	**Wed 21-4-21**
44	2.1.1.1	Create figures	2 hrs	Wed 21-4-21
45	2.1.1.2	Document PMSE deliverables	4 hrs	Wed 21-4-21
46	2.1.1.3	Proofread & spell-check the report	2 hrs	Wed 21-4-21
47	2.1.1.4	Write introduction and summary	1 hr	Thu 22-4-21
48	2.1.1.5	Deliver project plan draft	0 hrs	Fri 23-4-21
49	**2.1.2**	**Write final report**	**4,5 hrs**	**Mon 3-5-21**
51	2.1.2.2	Implement feedback on reporting	4 hrs	Mon 3-5-21
52	2.1.2.3	Deliver final project plan	0 hrs	Mon 3-5-21
50	2.1.2.1	Implement tutor feedback on mission statement	0,5 hrs	Mon 3-5-21
53	**2.2**	**Create baseline report**	**40 hrs**	**Thu 29-4-21**
54	**2.2.1**	**Write draft report**	**13 hrs**	**Thu 29-4-21**
55	2.2.1.1	Document technical design work	4 hrs	Thu 29-4-21
56	2.2.1.2	Create figures	2 hrs	Thu 29-4-21
57	2.2.1.3	Document PMSE deliverables	4 hrs	Thu 29-4-21
58	2.2.1.4	Proofread& spell-check the report	2 hrs	Fri 30-4-21
59	2.2.1.5	Write introduction and summary	1 hr	Fri 30-4-21
60	2.2.1.6	Deliver baseline report draft	0 hrs	Fri 30-4-21
61	**2.2.2**	**Write final report**	**16 hrs**	**Tue 4-5-21**
62	2.2.2.1	Implement expert feedback on technical content	4 hrs	Tue 4-5-21
63	2.2.2.2	Implement feedback on reporting	4 hrs	Tue 4-5-21
64	2.2.2.3	Deliver final baseline report	0 hrs	Thu 6-5-21
65	**2.2.3**	**Perform review**	**11 hrs**	**Fri 30-4-21**
66	2.2.3.1	Prepare presentation	8 hrs	Fri 30-4-21
67	2.2.3.2	Present the presentation	2 hrs	Mon 3-5-21
68	**2.3**	**Create mid-term report**	**55,5 hrs**	**Mon 17-5-21**
83	**2.4**	**Create final report**	**56,5 hrs**	**Thu 17-6-21**
84	**2.4.1**	**Write draft report**	**31 hrs**	**Thu 17-6-21**
85	2.4.1.1	Document technical design work	8 hrs	Thu 17-6-21
86	2.4.1.2	Create figures	8 hrs	Fri 18-6-21
87	2.4.1.3	Document PMSE deliverables	8 hrs	Mon 21-6-21
88	2.4.1.4	Proofread & spell-check the report	4 hrs	Tue 22-6-21
89	2.4.1.5	Write introduction and summary	2 hrs	Tue 22-6-21
90	2.4.1.6	Deliver final report draft	0 hrs	Tue 22-6-21
91	**2.4.2**	**Write final report**	**16 hrs**	**Thu 24-6-21**
93	2.4.2.2	Implement feedback on reporting	8 hrs	Fri 25-6-21
94	2.4.2.3	Deliver final report	0 hrs	Mon 28-6-21
92	2.4.2.1	Implement expert feedback on technical content	8 hrs	Thu 24-6-21
95	**2.4.3**	**Perform review**	**9,5 hrs**	**Tue 22-6-21**
96	2.4.3.1	Prepare presentation	7,5 hrs	Tue 22-6-21
97	2.4.3.2	Present the presentation	2 hrs	Wed 23-6-21
98	**2.5**	**Prepare for symposium**	**77 hrs**	**Thu 17-6-21**
99	**2.5.1**	**Create poster**	**11 hrs**	**Thu 24-6-21**
100	2.5.1.1	Identify key concepts and steps taken	2 hrs	Thu 24-6-21
101	2.5.1.2	Find visually aesthetic images to convey concepts	2 hrs	Thu 24-6-21
102	2.5.1.3	Write brief descriptions for concepts	2 hrs	Thu 24-6-21
103	2.5.1.4	Outline the poster	2 hrs	Thu 24-6-21
104	2.5.1.5	Construct the poster	2 hrs	Fri 25-6-21
105	2.5.1.6	Deliver poster	0 hrs	Fri 25-6-21
106	**2.5.2**	**Create presentation**	**16 hrs**	**Tue 29-6-21**
107	2.5.2.1	Identify all concepts and steps taken	4 hrs	Tue 29-6-21
108	2.5.2.2	Find images or visual representations of data for concepts	2 hrs	Tue 29-6-21
109	2.5.2.3	Construct the slides	4 hrs	Tue 29-6-21
110	2.5.2.4	Write notes for the slides	2 hrs	Wed 30-6-21
111	2.5.2.5	Rehearse presentation segments individually	2 hrs	Wed 30-6-21
112	2.5.2.6	Rehearse presentation as a group	2 hrs	Wed 30-6-21
113	2.5.3	Write jury summary	4 hrs	Thu 17-6-21
114	2.5.4	Deliver jury summary	0 hrs	Fri 18-6-21
115	**2.6**	**Create red booklet chapter**	**14 hrs**	**Tue 29-6-21**
116	**2.6.1**	**Write text for red booklet**	**12 hrs**	**Tue 29-6-21**
117	2.6.1.1	Write about project background	3 hrs	Tue 29-6-21
118	2.6.1.2	Write about design options	3 hrs	Tue 29-6-21
119	2.6.1.3	Write about selected concept	3 hrs	Tue 29-6-21
120	2.6.1.4	Write about conclusions and recommendations	3 hrs	Wed 30-6-21
121	2.6.2	Create three-view drawings of selected concept	4 hrs	Tue 29-6-21
122	2.6.3	Deliver red booklet chapter	0 hrs	Wed 30-6-21
123	**3**	**Risk and Quality Control**	**157 hrs**	**Mon 26-4-21**
124	**3.1**	**Ensure code quality**	**101 hrs**	**Fri 7-5-21**
125	**3.1.1**	**Set up version control with CICD**	**3 hrs**	**Fri 7-5-21**
126	3.1.1.1	Set up GitHub	1 hr	Fri 7-5-21
127	3.1.1.2	Set up pylint rules and GitHub actions	2 hrs	Fri 7-5-21
128	**3.1.2**	**Design project code architecture**	**77 hrs**	**Wed 12-5-21**
130	3.1.2.2	Create code flowchart for midterm phase	2 hrs	Mon 17-5-21
131	3.1.2.3	Create code flowchart for final phase	4 hrs	Fri 28-5-21
129	3.1.2.1	Identify shared variables across disciplines	2 hrs	Wed 12-5-21
132	**3.2**	**Perform technical risk analysis**	**33 hrs**	**Mon 26-4-21**
133	**3.2.1**	**Perform technical risk mapping**	**29 hrs**	**Mon 26-4-21**
134	3.2.1.1	Identify risks	2 hrs	Mon 26-4-21
135	3.2.1.2	Come up with rating system	4 hrs	Mon 26-4-21
136	3.2.1.3	Rate risks and plot risk map	2 hrs	Mon 26-4-21
137	3.2.1.4	Identify mitigation measures	4 hrs	Mon 26-4-21
138	3.2.1.5	Plot new risk map	0,5 hrs	Wed 28-4-21
139	3.2.1.6	Update risk map for midterm report	8 hrs	Wed 28-4-21
140	3.2.1.7	Update risk map for final report	8 hrs	Wed 28-4-21
141	**3.2.2**	**Create a technical contingency plan**	**16,5 hrs**	**Thu 29-4-21**
142	3.2.2.1	Identify resources that require contingencies	4 hrs	Thu 29-4-21
143	3.2.2.2	Quantify contingencies	4 hrs	Thu 29-4-21
144	**4**	**Finances**	**183 hrs**	**Wed 12-5-21**
145	**4.1**	**Conduct market study**	**42 hrs**	**Wed 12-5-21**
146	**4.1.1**	**Estimate series number**	**10 hrs**	**Thu 20-5-21**
148	4.1.1.2	Estimate market share	2 hrs	Fri 21-5-21
147	4.1.1.1	Estimate total units sold before 2040	2 hrs	Thu 20-5-21
149	**4.1.2**	**Benchmark against existing solution**	**21,5 hrs**	**Wed 12-5-21**
150	4.1.2.1	Gather reference aircraft data	2 hrs	Wed 12-5-21
151	4.1.2.2	Determine key characteristics of each	1 hr	Wed 19-5-21
152	4.1.2.3	Assimilate an index by combining the properties	0,5 hrs	Wed 19-5-21
154	**4.1.4**	**Determine competitive pricing**	**4 hrs**	**Thu 20-5-21**
155	4.1.4.1	Do market forecast	2 hrs	Thu 20-5-21
156	4.1.4.2	Analyse competitors pricing strategy	2 hrs	Thu 20-5-21
153	4.1.3	Identify potential customers	2 hrs	Wed 19-5-21
157	**4.2**	**Create financial plan**	**8 hrs**	**Wed 16-6-21**
160	**4.2.3**	**Generate cost breakdown structure**	**4 hrs**	**Wed 16-6-21**
162	4.2.3.2	Estimate research and testing costs	1 hr	Wed 16-6-21
163	4.2.3.3	Estimate production cost	1 hr	Wed 16-6-21
164	4.2.3.4	Estimate certification cost	1 hr	Wed 16-6-21
161	4.2.3.1	Estimate development & design costs	1 hr	Wed 16-6-21
159	4.2.2	Predict break-even point	2 hrs	Wed 16-6-21
158	4.2.1	Calculate return on investment	2 hrs	Wed 16-6-21
165	**4.3**	**Create business plan**	**3 hrs**	**Thu 17-6-21**
167	**4.3.2**	**Get funding information**	**2 hrs**	**Thu 17-6-21**
168	4.3.2.1	Get funding information regarding stakeholders	1 hr	Thu 17-6-21
169	4.3.2.2	Get funding information regarding tooling brands	1 hr	Thu 17-6-21
166	4.3.1	Calculate operational profit	1 hr	Thu 17-6-21
170	**5**	**CAD**	**246 hrs**	**Tue 18-5-21**
171	**5.1**	**Create 3D CAD models**	**246 hrs**	**Tue 18-5-21**
172	**5.1.1**	**Create CAD model for midterm review**	**12 hrs**	**Thu 20-5-21**
173	5.1.1.1	Import propeller model	2 hrs	Thu 20-5-21
174	5.1.1.2	Model fuselage	4 hrs	Thu 20-5-21
175	5.1.1.3	Model wings	4 hrs	Thu 20-5-21
176	5.1.1.4	Create renders	2 hrs	Fri 21-5-21
177	**5.1.2**	**Create exterior CAD model for CFD**	**6 hrs**	**Tue 18-5-21**
179	5.1.2.2	Model control surfaces	4 hrs	Tue 18-5-21
181	5.1.2.4	Create model in hover mode	2 hrs	Tue 18-5-21
182	5.1.2.5	Create model in transition mode	2 hrs	Tue 18-5-21
178	5.1.2.1	Update wing model	2 hrs	Tue 18-5-21
180	5.1.2.3	Update fuselage model	2 hrs	Tue 18-5-21
183	**5.1.3**	**Create detailed CAD for final review**	**164 hrs**	**Wed 2-6-21**
185	5.1.3.2	Model wing tilting mechanism	4 hrs	Mon 7-6-21
186	5.1.3.3	Model landing gear	4 hrs	Wed 9-6-21
187	5.1.3.4	Model motors	2 hrs	Thu 3-6-21
188	5.1.3.5	Model battery	2 hrs	Thu 3-6-21
189	5.1.3.6	Model cabin	4 hrs	Fri 4-6-21
190	5.1.3.7	Create take-off animation	8 hrs	Tue 29-6-21
191	5.1.3.8	Create renders	8 hrs	Tue 22-6-21
184	5.1.3.1	Model interior wing structure	4 hrs	Wed 2-6-21
192	**5.2**	**Create technical drawings**	**44 hrs**	**Fri 4-6-21**
194	5.2.2	Create part drawings	4 hrs	Fri 4-6-21
193	5.2.1	Create assembly drawings	4 hrs	Fri 11-6-21
195	**6**	**Sustainability Control**	**140 hrs**	**Thu 27-5-21**
196	**6.1**	**Investigate life-cycle environmental impact of one aircraft**	**41,5 hrs**	**Wed 9-6-21**
197	**6.1.1**	**Investigate the environmental impact of production of one aircraft**	**33,5 hrs**	**Wed 9-6-21**
199	6.1.1.2	Estimate energy used	2 hrs	Wed 9-6-21
200	6.1.1.3	Investigate the release of toxic substances	0,5 hrs	Wed 9-6-21
201	6.1.1.4	Investigate material waste during manufacturing	2 hrs	Wed 9-6-21
202	6.1.1.5	Investigate material availability	2 hrs	Tue 15-6-21
198	6.1.1.1	Estimate carbon dioxide released	2 hrs	Wed 9-6-21
203	**6.1.2**	**Investigate the environmental impact of operation of one aircraft**	**4 hrs**	**Tue 15-6-21**
204	6.1.2.1	Estimate reference grid carbon intensity	2 hrs	Tue 15-6-21
205	6.1.2.2	Investigate environmental impact of maintenance procedures	2 hrs	Tue 15-6-21
206	**6.1.3**	**Investigate the environmental impact at end of life**	**4 hrs**	**Tue 15-6-21**
207	6.1.3.1	Evaluate aircraft final state	2 hrs	Tue 15-6-21
208	6.1.3.2	Evaluate recyclability possibility	2 hrs	Wed 16-6-21
209	**6.2**	**Investigate life-cycle social impact of one aircraft**	**130 hrs**	**Thu 27-5-21**
210	6.2.1	Compare noise levels with ambient noise	2 hrs	Fri 18-6-21
211	6.2.2	Literature research on socially sustainable battery materials	1 hr	Thu 27-5-21
212	**6.3**	**Ensure compliance of the design with the sustainability requirements**	**3 hrs**	**Wed 16-6-21**
213	**6.3.1**	**Determine metrics to evaluate sustainability impact**	**2 hrs**	**Wed 16-6-21**
214	6.3.1.1	Research required metrics	1 hr	Wed 16-6-21
215	6.3.1.2	Compare the metrics to calculated values	1 hr	Wed 16-6-21
216	6.3.2	Decide whether the design meets the sustainability requirements	1 hr	Wed 16-6-21
217	**6.4**	**Work out sustainable development strategy**	**23,5 hrs**	**Wed 16-6-21**
219	**6.4.2**	**Define life cycle engineering goals**	**20,5 hrs**	**Wed 16-6-21**
220	6.4.2.1	Perform literature review on life-cycle impact of different materials	2 hrs	Wed 16-6-21
221	6.4.2.2	Manage the production plan in a sustainable way	1 hr	Mon 21-6-21
222	6.4.2.3	Perform trade-off and choose eco-friendly materials	1 hr	Mon 21-6-21
218	6.4.1	Document concepts for sustainability development strategy	2 hrs	Wed 16-6-21
223	6.4.3	Update sustainable development strategy	1 hr	Mon 21-6-21
224	**7**	**Aircraft Operations**	**113 hrs**	**Tue 1-6-21**
225	**7.1**	**Determine other operations procedures**	**5 hrs**	**Mon 21-6-21**
226	**7.1.1**	**Create maintenance plan**	**4 hrs**	**Mon 21-6-21**
227	7.1.1.1	Determine critical components for inspection	1 hr	Mon 21-6-21
228	7.1.1.2	Determine inspection intervals	1 hr	Mon 21-6-21
229	7.1.1.3	Determine inspection techniques	1 hr	Mon 21-6-21
230	7.1.1.4	Define allowable damage	1 hr	Mon 21-6-21
231	7.1.2	Create disposal guidelines	1 hr	Mon 21-6-21
232	**7.2**	**Determine operation procedures in use**	**107 hrs**	**Tue 1-6-21**
233	**7.2.1**	**Determine pilot tasks**	**41,5 hrs**	**Fri 11-6-21**
235	7.2.1.2	Determine emergency actions	2 hrs	Fri 18-6-21
234	7.2.1.1	Determine control actions	2 hrs	Fri 11-6-21
236	**7.2.2**	**Create ground operations plan**	**107 hrs**	**Tue 1-6-21**
238	7.2.2.2	Determine required tools and infrastructure for ground operations	1 hr	Mon 21-6-21
237	7.2.2.1	Determine time and procedure for refuelling	1 hr	Tue 1-6-21
239	**8**	**Systems Design**	**111 hrs**	**Thu 29-4-21**
240	**8.1**	**Perform preliminary sizing**	**31 hrs**	**Fri 7-5-21**
241	**8.1.1**	**Perform preliminary system sizing**	**31 hrs**	**Fri 7-5-21**
243	8.1.1.2	Estimate cabin size	4 hrs	Wed 12-5-21
244	8.1.1.3	Perform empennage sizing	7 hrs	Mon 10-5-21
242	8.1.1.1	Estimate wing dimensions	4 hrs	Fri 7-5-21
245	8.1.1.4	Initial engine sizing	5 hrs	Wed 12-5-21
246	**8.1.2**	**Literature review on mass and power estimation**	**11 hrs**	**Tue 11-5-21**
247	8.1.2.1	Search previous mass and power examples	6 hrs	Tue 11-5-21
248	8.1.2.2	Assemble and document the found examples	2 hrs	Tue 11-5-21
249	8.1.3	Create mass and power budgets	2 hrs	Wed 12-5-21
250	**8.2**	**Select concepts for development in the final stage**	**86 hrs**	**Thu 29-4-21**
251	**8.2.1**	**Craft system design option tree**	**4 hrs**	**Thu 6-5-21**
252	8.2.1.1	Perform literature search about different VTOLs	2 hrs	Thu 6-5-21
253	8.2.1.2	Have a brainstorming session with the group	2 hrs	Thu 6-5-21
254	**8.2.2**	**Identify feasible concepts**	**28 hrs**	**Thu 6-5-21**
255	8.2.2.1	Sketch strawman concepts	4 hrs	Thu 6-5-21
256	8.2.2.2	Eliminate options for which no concept can be found	1 hr	Tue 11-5-21
257	8.2.2.3	Eliminate clearly non-feasible concepts	1 hr	Tue 11-5-21
258	8.2.2.4	Eliminate options which cannot be developed yet	1 hr	Tue 11-5-21
259	8.2.2.5	Create list with future options	1 hr	Wed 12-5-21
260	**8.2.3**	**Perform system trade-off**	**27 hrs**	**Tue 11-5-21**
261	8.2.3.1	Analyse the weakest points of each remaining concept	3 hrs	Tue 11-5-21
262	8.2.3.2	Define trade-off criteria	3 hrs	Wed 12-5-21
263	8.2.3.3	Define weights of the trade-off criteria	3 hrs	Mon 17-5-21
264	8.2.3.4	Determine performance of each option wrt criteria	3 hrs	Mon 17-5-21
265	8.2.3.5	Create trade-off table	3 hrs	Tue 18-5-21
266	**8.2.4**	**Verify selected concepts with experts**	**4 hrs**	**Thu 29-4-21**
267	8.2.4.1	Formulate questions for experts	1 hr	Thu 29-4-21
268	8.2.4.2	Get expert opinions on selected concepts	1 hr	Thu 29-4-21
269	8.2.4.3	Implement expert feedback	2 hrs	Thu 29-4-21
270	**8.3**	**Design subsystems**	**52 hrs**	**Mon 10-5-21**
272	**8.3.2**	**Craft subsystem design option tree**	**18 hrs**	**Mon 10-5-21**
273	8.3.2.1	Research and document detailed options	2 hrs	Mon 10-5-21
274	8.3.2.2	Perform design option tree	2 hrs	Wed 12-5-21
271	8.3.1	Extend N2 chart	4 hrs	Thu 20-5-21
275	8.3.3	Define high level architecture of design software	7 hrs	Wed 12-5-21
276	**8.4**	**Choose preliminary design parameters**	**8 hrs**	**Fri 7-5-21**
277	8.4.1	Perform literature review of critical design paramaters	4 hrs	Fri 7-5-21
278	8.4.2	Investigate and estimate key design parameters	4 hrs	Fri 7-5-21
282	8.8	Review resource allowcation and budget breakdown	2 hrs	Fri 21-5-21
280	8.6	Update configuration and layout	2 hrs	Fri 21-5-21
281	8.7	Update aircraft systems and interfaces	2 hrs	Fri 21-5-21
279	8.5	Update RAMS characteristics	2 hrs	Mon 17-5-21
283	**9**	**Production Plan**	**39 hrs**	**Mon 14-6-21**
284	**9.1**	**Plan part manufacturing**	**25 hrs**	**Mon 14-6-21**
285	**9.1.1**	**Define manufacturing and mounting divisions**	**19 hrs**	**Mon 14-6-21**
287	9.1.1.2	Identify material interfaces	4 hrs	Mon 14-6-21
286	9.1.1.1	Identify singly- and doubly- curved parts	4 hrs	Wed 16-6-21
288	**9.1.2**	**Determine manufacturing techniques**	**6 hrs**	**Wed 16-6-21**
289	9.1.2.1	Determine possible manufacturing techniques	2 hrs	Wed 16-6-21
290	9.1.2.2	Analyse cost, part quality and material waste for each technique	2 hrs	Thu 17-6-21
291	9.1.2.3	Document chosen manufacturing techniques	2 hrs	Thu 17-6-21
292	**9.2**	**Define production strategy and logistics**	**12 hrs**	**Thu 17-6-21**
293	**9.2.1**	**Define production schedule**	**10,5 hrs**	**Thu 17-6-21**
294	9.2.1.1	Define delivery interval	2 hrs	Thu 17-6-21
295	9.2.1.2	Define batch sizes	2 hrs	Thu 17-6-21
296	9.2.1.3	Estimate production time of each batch	4 hrs	Fri 18-6-21
297	9.2.1.4	Analyse worker learning curves in production	4 hrs	Fri 18-6-21
299	**9.2.3**	**Create assembly sequence chart**	**4 hrs**	**Fri 18-6-21**

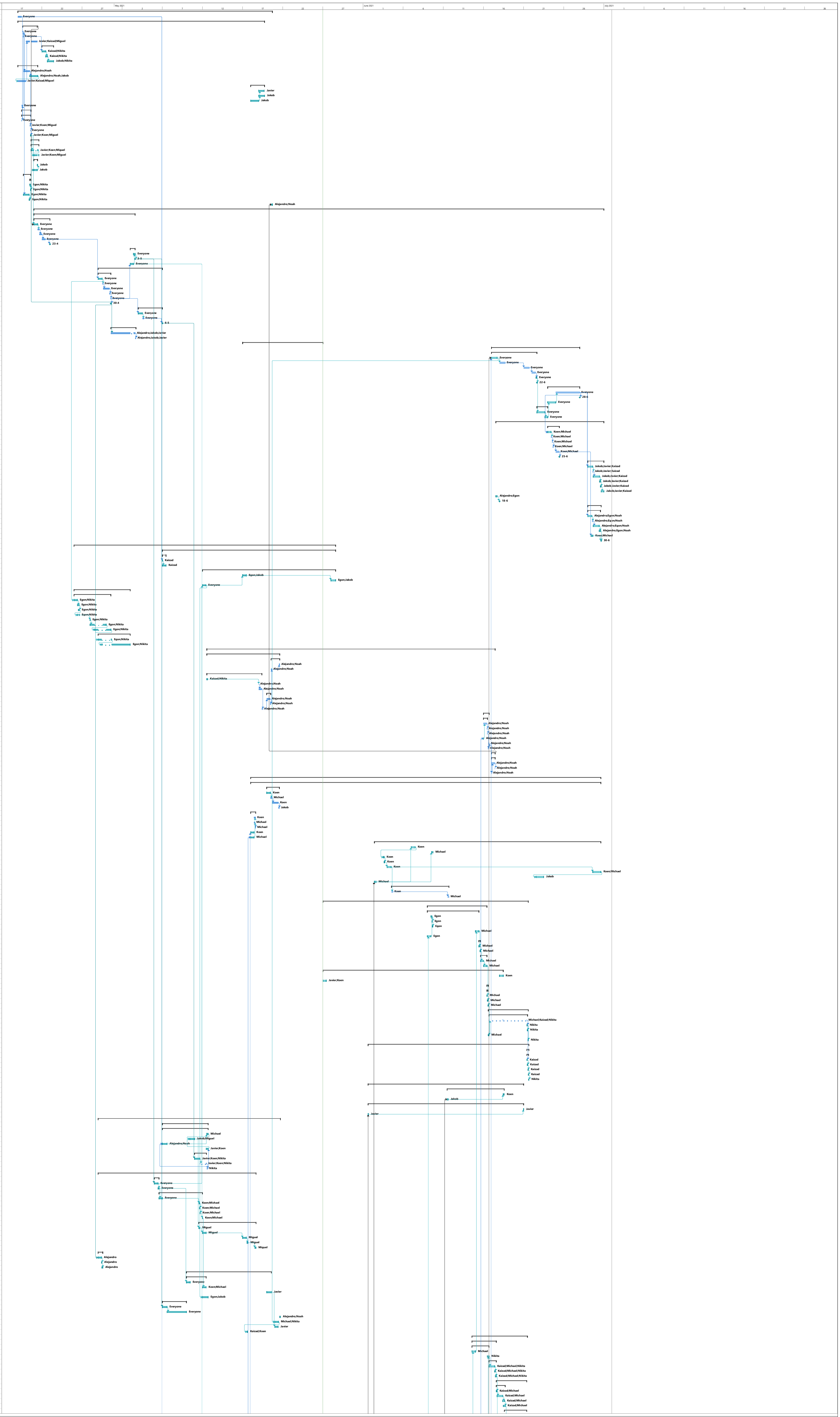

Project: GanttMidterm
Date: Thu 27-5-21

Task | Split | Milestone | Summary | Project Summary | Inactive Task | Inactive Milestone | Inactive Summary | Manual Task | Duration-only | Manual Summary Rollup | Manual Summary | Start-only | Finish-only | External Tasks | External Milestone | Deadline | Progress | Manual Progress

ID	WBS	Task Name	Duration	Start
300	9.2.3.1	Determine subassemblies	2 hrs	Fri 18-6-21
301	9.2.3.2	Identify assemblies	2 hrs	Fri 18-6-21
298	9.2.2	Define production strategy for prototyping	4 hrs	Thu 17-6-21
302	9.3	Update production plan	2 hrs	Mon 21-6-21
303	**10**	**Requirements Management**	**239,5 hrs**	**Tue 6-4-21**
304	**10.1**	**Perform functional analysis**	**64 hrs**	**Mon 3-5-21**
305	**10.1.1**	**Define exemplary mission**	**17 hrs**	**Fri 7-5-21**
306	10.1.1.1	Determine end user	2 hrs	Fri 7-5-21
307	10.1.1.2	Determine operation environment	2 hrs	Mon 10-5-21
308	10.1.1.3	Determine mission phases	2 hrs	Fri 7-5-21
309	**10.1.2**	**Create functional breakdown diagram**	**16 hrs**	**Wed 12-5-21**
310	10.1.2.1	Construct tree of functions required for exemplary mission	8 hrs	Wed 12-5-21
311	10.1.2.2	Add functions not relevant to use (e.g. for maintenance)	8 hrs	Mon 17-5-21
312	**10.1.3**	**Create functional flow block diagram**	**12 hrs**	**Thu 6-5-21**
313	10.1.3.1	Put functions in chronological order	4 hrs	Thu 6-5-21
314	10.1.3.2	Identify lower level functions	8 hrs	Thu 6-5-21
315	**10.1.4**	**Create system N2 chart**	**24 hrs**	**Mon 3-5-21**
316	10.1.4.1	Identify subsystems	8 hrs	Mon 3-5-21
317	10.1.4.2	Identify subsystem interfaces	8 hrs	Tue 4-5-21
318	**10.2**	**Generate requirements**	**182 hrs**	**Tue 6-4-21**
319	**10.2.1**	**Determine mission need statement**	**3 hrs**	**Tue 6-4-21**
320	10.2.1.1	Identify market gap	1 hr	Tue 6-4-21
321	10.2.1.2	Identify technological opportunity	2 hrs	Tue 6-4-21
322	**10.2.2**	**Identify constraints**	**9 hrs**	**Tue 6-4-21**
323	10.2.2.1	Research legal and certification constraints	3 hrs	Tue 6-4-21
324	10.2.2.2	Specify economic and environmental constraints	3 hrs	Tue 6-4-21
325	10.2.2.3	Determine impact of constraints	3 hrs	Wed 7-4-21
326	**10.2.3**	**Set stakeholder requirements**	**6,5 hrs**	**Mon 26-4-21**
327	10.2.3.1	Identify stakeholders	1 hr	Mon 26-4-21
328	10.2.3.2	Find stakeholder needs	2 hrs	Mon 26-4-21
329	10.2.3.3	Identify and solve stakeholder need conflicts	0,5 hrs	Mon 26-4-21
330	10.2.3.4	Write formal stakeholder requirements	3 hrs	Mon 26-4-21
331	10.2.3.5	Identify key stakeholder requirements	2 hrs	Mon 26-4-21
332	**10.2.4**	**Craft requirements discovery tree**	**18 hrs**	**Wed 28-4-21**
333	10.2.4.1	Brainstorm requirements	6 hrs	Wed 28-4-21
334	10.2.4.2	Set system requirements	6 hrs	Wed 28-4-21
335	10.2.4.3	Set subsystem requirements	6 hrs	Thu 29-4-21
336	**10.2.5**	**Validate requirements**	**21 hrs**	**Fri 30-4-21**
337	10.2.5.1	Use VALID method on system and subsystem requirements	8 hrs	Fri 30-4-21
338	10.2.5.2	Validate stakeholder requirements with customer (tutor)	13 hrs	Mon 3-5-21
339	**10.2.6**	**Prioritise requirements**	**29 hrs**	**Tue 4-5-21**
340	10.2.6.1	Identify driving requirements	13 hrs	Tue 4-5-21
341	10.2.6.2	Identify key requirements	13 hrs	Thu 6-5-21
342	10.2.6.3	Identify killer requirements	13 hrs	Fri 7-5-21
343	**10.3**	**Track and update requirements**	**4,5 hrs**	**Fri 21-5-21**
344	10.3.1	Identify software for requirement management	0,5 hrs	Fri 21-5-21
345	10.3.2	Create automated checks for requirements in design software	2 hrs	Fri 21-5-21
346	10.3.3	Create requirement compliance matrix	2 hrs	Fri 21-5-21
347	10.4	Update functional analysis	2 hrs	Fri 21-5-21
348	**11**	**Material Selection**	**19 hrs**	**Mon 14-6-21**
349	**11.1**	**Identify material Options**	**7 hrs**	**Mon 14-6-21**
351	**11.1.2**	**Analyse material properties**	**3 hrs**	**Mon 14-6-21**
352	11.1.2.1	Analyse stiffness and strength	1 hr	Mon 14-6-21
353	11.1.2.2	Analyse electrical & thermal conductivity	1 hr	Mon 14-6-21
354	11.1.2.3	Analyse density	1 hr	Mon 14-6-21
350	11.1.1	Identify relevant material performance parameters based on load cases	4 hrs	Mon 14-6-21
355	**11.2**	**Choose the best material for each part**	**6 hrs**	**Mon 14-6-21**
356	11.2.1	Perform trade-off between material properties and cost	2 hrs	Mon 14-6-21
357	11.2.2	Confirm that the chosen material is producible for the part geometry	2 hrs	Tue 15-6-21
358	11.2.3	Check material interactions between adjacent parts	2 hrs	Tue 15-6-21
360	**11.4**	**Review chemical characteristics**	**4 hrs**	**Tue 15-6-21**
361	11.4.1	Review corrosion prevention	2 hrs	Tue 15-6-21
362	11.4.2	Check compatibility within joints of different structural elements	2 hrs	Wed 16-6-21
359	11.3	Update material choice	2 hrs	Tue 15-6-21
363	**12**	**General Aircraft Performance**	**72,5 hrs**	**Thu 27-5-21**
364	**12.1**	**Make a detailed flight performance model**	**52,5 hrs**	**Thu 27-5-21**
367	**12.1.3**	**Create model of horizontal flight**	**16 hrs**	**Tue 1-6-21**
368	12.1.3.1	Calculate range and endurance	4 hrs	Tue 1-6-21
369	12.1.3.2	Calculate rate of climb and flight ceiling	4 hrs	Tue 1-6-21
370	12.1.3.3	Calculate turning time and radius	4 hrs	Wed 2-6-21
371	12.1.3.4	Investigate the steepest turn	4 hrs	Wed 2-6-21
365	12.1.1	Create model of VTOL operations	8 hrs	Thu 27-5-21
366	12.1.2	Create model of transition	8 hrs	Mon 31-5-21
372	12.1.4	Verify and validate	12 hrs	Thu 3-6-21
373	**12.2**	**Optimise mission profile**	**20 hrs**	**Fri 4-6-21**
374	**12.2.1**	**Investigate mission performance**	**12 hrs**	**Fri 4-6-21**
375	12.2.1.1	Produce payload-range diagrams	2 hrs	Fri 4-6-21
376	12.2.1.2	Make climb performance diagram	2 hrs	Fri 4-6-21
377	12.2.1.3	Estimate total energy consumption	4 hrs	Mon 7-6-21
378	12.2.1.4	Produce flight envelope	4 hrs	Mon 7-6-21
379	12.2.2	Perform sensitivity analysis	8 hrs	Tue 8-6-21
380	**13**	**Aerodynamic Design**	**253,5 hrs**	**Mon 19-4-21**
381	**13.1**	**Design aerodynamic surfaces**	**100,5 hrs**	**Mon 10-5-21**
387	**13.1.6**	**Select Airfoil**	**16 hrs**	**Mon 10-5-21**
388	13.1.6.1	Determine design lift / drag coefficients	8 hrs	Mon 10-5-21
389	13.1.6.2	Research airfoils that fit the profile	8 hrs	Tue 11-5-21
382	13.1.1	Investigate wing-wing-interaction	4 hrs	Thu 27-5-21
383	13.1.2	Perform verification	8 hrs	Thu 27-5-21
385	13.1.4	Investigate wing-fuselage interference	8 hrs	Thu 27-5-21
384	13.1.3	Perform validation	8 hrs	Fri 28-5-21
386	13.1.5	Investigate wing-propeller interaction	8 hrs	Fri 28-5-21
390	**13.2**	**Design fuselage**	**10 hrs**	**Mon 31-5-21**
391	13.2.1	Design fuselage shape	4 hrs	Mon 31-5-21
392	13.2.2	Perform verification	3 hrs	Tue 1-6-21
393	13.2.3	Perform validation	3 hrs	Tue 1-6-21
394	**13.3**	**Perform CFD simulations**	**253,5 hrs**	**Mon 19-4-21**
395	13.3.1	Set up CFD simulations	40 hrs	Tue 1-6-21
396	13.3.2	Evaluate simulation results	4 hrs	Mon 19-4-21
397	**13.4**	**Investigate aerodynamic performance**	**25 hrs**	**Wed 12-5-21**
398	**13.4.1**	**Investigate lift and drag polars**	**17 hrs**	**Wed 12-5-21**
399	13.4.1.1	Compute the lift-angle of attack curve and estimate zero-lift drag	8 hrs	Wed 12-5-21
400	13.4.1.2	Estimate aircraft components with their respective drag term	8 hrs	Mon 17-5-21
401	13.4.2	Estimate aerodynamic center, moment equation and design properties	8 hrs	Tue 18-5-21
402	**14**	**Structural Design**	**96,5 hrs**	**Thu 27-5-21**
403	**14.1**	**Identify loads**	**6 hrs**	**Thu 27-5-21**
404	14.1.1	Produce loading diagrams	2 hrs	Thu 27-5-21
405	14.1.2	Review certification literature	2 hrs	Thu 27-5-21
406	14.1.3	Identify critical loads	1,5 hrs	Thu 27-5-21
407	14.1.4	Identify critical failure modes	2,5 hrs	Thu 27-5-21
408	**14.2**	**Design wing structure**	**26,5 hrs**	**Thu 27-5-21**
409	**14.2.1**	**Propose a wingbox configuration**	**8,5 hrs**	**Thu 27-5-21**
410	14.2.1.1	Identify areas where stiffening is required	2,5 hrs	Thu 27-5-21
411	14.2.1.2	Determine number and type of stiffening elements	4 hrs	Fri 28-5-21
412	14.2.1.3	Size stiffening elements	2 hrs	Fri 28-5-21
413	14.2.2	Produce NVM diagrams	2 hrs	Fri 28-5-21
414	14.2.3	Analyse wing roots/attachments	2 hrs	Fri 28-5-21
415	14.2.4	Analyse fatigue	16 hrs	Mon 31-5-21
416	**14.3**	**Design fuselage structure**	**10 hrs**	**Tue 1-6-21**
417	14.3.1	Optimise fuselage volume	2 hrs	Wed 2-6-21
418	14.3.2	Ensure thickness is sufficient to transfer loads from the wing	4 hrs	Tue 1-6-21
419	**14.4**	**Analyse crashworthiness in depth**	**20 hrs**	**Wed 2-6-21**
420	**14.4.1**	**Design landing gear**	**12 hrs**	**Wed 2-6-21**
421	14.4.1.1	Simulate an impulsive response of the gear	4 hrs	Wed 2-6-21
422	14.4.1.2	Determine maximum impulse on the gear	4 hrs	Wed 2-6-21
423	14.4.1.3	Deduce load transfer to the structure	4 hrs	Thu 3-6-21
424	14.4.2	Analyse Passenger comfort	2 hrs	Thu 3-6-21
425	14.4.3	Analyse safety of the structure	8 hrs	Thu 3-6-21
426	14.4.4	Analyse structural rigidity under shock	4 hrs	Fri 4-6-21
427	**14.5**	**Estimate structural weight**	**10 hrs**	**Thu 3-6-21**
430	**14.5.3**	**Investigate passenger accessibility to the cabin**	**2 hrs**	**Fri 4-6-21**
431	14.5.3.1	Investigate cabin dimensions	1 hr	Fri 4-6-21
432	14.5.3.2	Check average passenger size	1 hr	Fri 4-6-21
428	14.5.1	Deduce weight fractions	2 hrs	Thu 3-6-21
429	14.5.2	Estimate positions and load transfers	2 hrs	Fri 4-6-21
433	**14.6**	**Verification & Validation**	**73 hrs**	**Mon 31-5-21**
434	**14.6.1**	**Verify the calculations performed**	**57 hrs**	**Mon 31-5-21**
435	14.6.1.1	Write tests to verify loads calculated	8 hrs	Mon 31-5-21
436	14.6.1.2	Write tests to verify the shear flows computed	4 hrs	Mon 7-6-21
437	14.6.1.3	Write tests for the geometrical aspects	4 hrs	Tue 8-6-21
438	14.6.1.4	Write tests for the geometrical aspects	4 hrs	Tue 8-6-21
439	**14.6.2**	**Find empirical and / or FEM data**	**16 hrs**	**Wed 9-6-21**
440	14.6.2.1	For deflections	8 hrs	Wed 9-6-21
441	14.6.2.2	For buckling & fatigue	8 hrs	Thu 10-6-21
442	**14.6.3**	**Validate the process used to determine deflections / stresses**	**7,5 hrs**	**Wed 9-6-21**
443	14.6.3.1	Write tests for yield	2,5 hrs	Wed 9-6-21
444	14.6.3.2	Write tests for buckling & fatigue	2,5 hrs	Wed 9-6-21
445	14.6.3.3	Write tests for deflections	2,5 hrs	Wed 9-6-21
446	**14.7**	**Perform sensitivity analyses**	**16 hrs**	**Thu 10-6-21**
447	**14.7.1**	**Perform sensitivity analysis to quantify uncertainty**	**7,5 hrs**	**Thu 10-6-21**
448	14.7.1.1	Perform stress sensitivity analysis with respect to fatigue parameters	2,5 hrs	Thu 10-6-21
449	14.7.1.2	Perform stress sensitivity analysis with respect to boundary conditions	2,5 hrs	Thu 10-6-21
450	14.7.1.3	Perform weight sensitivity analysis with respect to failure criteria	2,5 hrs	Thu 10-6-21
451	**14.7.2**	**Perform sensitivity analysis for optimisation**	**7,5 hrs**	**Fri 11-6-21**
452	14.7.2.1	Perform weight sensitivity analysis with respect to aspect ratio	2,5 hrs	Fri 11-6-21
453	14.7.2.2	Perform weight sensitivity analysis with respect to safety factors	2,5 hrs	Fri 11-6-21
454	14.7.2.3	Perform stress sensitivity analysis with respect to skin thickness	2,5 hrs	Fri 11-6-21
455	**15**	**Design for Stability and Control**	**147 hrs**	**Thu 27-5-21**
456	**15.1**	**Calculate CG location**	**12,5 hrs**	**Thu 27-5-21**
457	**15.1.1**	**Calculate OEW CG location**	**12,5 hrs**	**Thu 27-5-21**
458	15.1.1.1	Position batteries	2 hrs	Thu 27-5-21
459	15.1.1.2	Position wings	2 hrs	Fri 28-5-21
460	**15.1.2**	**Calculate MTOW CG location**	**4 hrs**	**Thu 27-5-21**
461	15.1.2.1	Define cabin configuration	2 hrs	Thu 27-5-21
462	15.1.2.2	Generate loading diagram	2 hrs	Thu 27-5-21
463	**15.2**	**Calculate CG limits**	**21 hrs**	**Fri 28-5-21**
464	**15.2.1**	**Calculate CG limits for cruise stability**	**8 hrs**	**Fri 28-5-21**
465	15.2.1.1	Calculate CG limit for static longitudinal stability	4 hrs	Fri 28-5-21
466	15.2.1.2	Calculate CG limit for static lateral stability	4 hrs	Mon 31-5-21
467	**15.2.2**	**Calculate CG range for controllability**	**16 hrs**	**Fri 28-5-21**
468	15.2.2.1	Estimate rotor reactive torque	4 hrs	Fri 28-5-21
472	15.2.2.5	Calculate CG limit for pitch controllability at stall	4 hrs	Mon 31-5-21
469	15.2.2.2	Optimise rotor spinning directions	4 hrs	Fri 28-5-21
470	15.2.2.3	Calculate pitch and roll angle for horizontal control in hover	4 hrs	Mon 31-5-21
471	15.2.2.4	Perform ACAI sensitivity analysis	4 hrs	Mon 31-5-21
473	**15.2.3**	**Ensure ground stability**	**6 hrs**	**Tue 1-6-21**
474	15.2.3.1	Position landing gear	4 hrs	Tue 1-6-21
475	15.2.3.2	Evaluate ground stability	2 hrs	Tue 1-6-21
476	**15.3**	**Size control surfaces**	**12 hrs**	**Tue 1-6-21**
477	15.3.1	Size elevators	4 hrs	Tue 1-6-21
478	15.3.2	Size vertical tail and rudders	4 hrs	Wed 2-6-21
479	15.3.3	Size ailerons	4 hrs	Wed 2-6-21
480	**15.4**	**Evaluate control redundancy**	**8 hrs**	**Tue 1-6-21**
481	15.4.1	Determine critical engine failures in hover	4 hrs	Tue 1-6-21
482	15.4.2	Analyse OEI condition in cruise	4 hrs	Tue 1-6-21
483	**15.5**	**Calculate stability and control derivatives**	**44,5 hrs**	**Wed 2-6-21**
484	**15.5.1**	**Prepare simulation**	**11 hrs**	**Wed 2-6-21**
487	15.5.1.3	Define flight conditions	2 hrs	Thu 3-6-21
485	15.5.1.1	Identify suitable software	1 hr	Wed 2-6-21
486	15.5.1.2	Import CAD model	0,5 hrs	Wed 2-6-21
488	**15.5.2**	**Process simulation data**	**43 hrs**	**Wed 2-6-21**
489	15.5.2.1	Perform simulation	29,5 hrs	Wed 2-6-21
490	15.5.2.2	Retrieve derivatives from simulation output	8 hrs	Mon 7-6-21
491	**15.6**	**Analyse open-loop dynamics**	**47,5 hrs**	**Fri 4-6-21**
492	**15.6.1**	**Analyse open-loop dynamics in cruise**	**38 hrs**	**Tue 8-6-21**
493	15.6.1.1	Derive state-space description of cruise	4 hrs	Tue 8-6-21
494	15.6.1.2	Calculate open-loop eigenvalues in cruise	2 hrs	Tue 8-6-21
495	15.6.1.3	Calculate zeroes of the cruise transfer function	2 hrs	Tue 8-6-21
496	15.6.1.4	Verify eigenvalue calculation using Cessna Citation II	2 hrs	Wed 9-6-21
497	15.6.1.5	Analyse open-loop eigenmotions in cruise	8 hrs	Wed 9-6-21
498	15.6.1.6	Validate cruise analysis (e.g. using Cessna Citation II)	16 hrs	Thu 10-6-21
499	**15.6.2**	**Analyse open-loop dynamics in hover**	**36 hrs**	**Fri 4-6-21**
500	15.6.2.1	Derive state-space description of hover	4 hrs	Fri 4-6-21
501	15.6.2.2	Calculate open-loop eigenvalues for hover	2 hrs	Mon 7-6-21
502	15.6.2.3	Calculate zeroes of the hover transfer function	2 hrs	Tue 8-6-21
503	15.6.2.4	Analyse open-loop eigenmotions in hover	8 hrs	Tue 8-6-21
504	15.6.2.5	Validate hover analysis (e.g. using multicopter flight data)	16 hrs	Wed 9-6-21
505	**15.7**	**Ensure closed-loop stability**	**41,5 hrs**	**Fri 11-6-21**
506	**15.7.1**	**Define controller architecture**	**18 hrs**	**Fri 11-6-21**
507	15.7.1.1	Perform literature review on VTOL controllers	14 hrs	Fri 11-6-21
508	15.7.1.2	Decide on sensor suite	4 hrs	Tue 15-6-21
509	**15.7.2**	**Tune controller gains**	**28,5 hrs**	**Mon 14-6-21**
511	15.7.2.2	Tune gains for closed-loop stability in cruise	16 hrs	Mon 14-6-21
510	15.7.2.1	Tune gains for closed-loop stability in hover	16 hrs	Wed 16-6-21
512	**15.7.3**	**Analyse closed-loop dynamics**	**23,5 hrs**	**Tue 15-6-21**
513	15.7.3.1	Calculate closed-loop eigenvalues in cruise	2 hrs	Tue 15-6-21
514	15.7.3.2	Analyse closed-loop eigenmotions in cruise	8 hrs	Wed 16-6-21
515	15.7.3.3	Calculate closed-loop eigenvalues in hover	2 hrs	Wed 16-6-21
516	15.7.3.4	Analyse closed-loop eigenmotions in hover	8 hrs	Thu 17-6-21
517	15.8	Create simulation in Matlab	16 hrs	Fri 18-6-21
518	**16**	**Power System Design**	**147 hrs**	**Thu 27-5-21**
519	**16.1**	**Determine energy storage requirements**	**13 hrs**	**Thu 27-5-21**
534	**16.2**	**Design power source**	**32 hrs**	**Thu 27-5-21**
535	**16.2.1**	**Obtain performance values for the battery**	**15 hrs**	**Fri 28-5-21**
536	16.2.1.1	Select final battery type and chemistry	1 hr	Fri 28-5-21
537	16.2.1.2	Obtain data on operational temperature of the battery	2 hrs	Fri 28-5-21
538	16.2.1.3	Obtain data on safety of the chosen battery	2 hrs	Mon 31-5-21
539	16.2.1.4	Obtain specific and volumetric energy densities	1 hr	Mon 31-5-21
540	16.2.1.5	Obtain power density	1 hr	Mon 31-5-21
541	16.2.1.6	Obtain cycle performance values	1 hr	Mon 31-5-21
542	16.2.1.7	Obtain battery cost	1 hr	Mon 31-5-21
543	16.2.1.8	Obtain battery efficiency	1 hr	Mon 31-5-21
544	16.2.1.9	Estimate recharge time	2 hrs	Tue 1-6-21
545	16.2.1.1	Estimate operational life of the battery	1 hr	Tue 1-6-21
546	16.2.1.1	Calculate required battery mass and volume	1 hr	Tue 1-6-21
547	**16.2.2**	**Design battery management system**	**6 hrs**	**Tue 1-6-21**
548	16.2.2.1	Literature study on heat management systems for batteries	2 hrs	Tue 1-6-21
549	16.2.2.2	Size heat management system for battery	4 hrs	Tue 1-6-21
550	**16.2.3**	**Decide on the use of supercapacitors to reduce battery mass**	**10 hrs**	**Thu 27-5-21**
551	16.2.3.1	Find performance values for supercapacitors	4 hrs	Thu 27-5-21
552	16.2.3.2	Calculate updated required battery mass and volume	3 hrs	Thu 27-5-21
553	16.2.3.3	Calculate supercapacitor mass and volume	3 hrs	Fri 28-5-21
554	**16.3**	**Verification and validation**	**14 hrs**	**Fri 18-6-21**
556	16.3.2	Refine post-DSE V&V procedures for the power subsystem	4 hrs	Mon 21-6-21
555	16.3.1	Perform V&V of the simulations made	8 hrs	Fri 18-6-21
557	**17**	**Propulsion Design**	**135 hrs**	**Fri 28-5-21**
558	**17.1**	**Design engines**	**28 hrs**	**Fri 28-5-21**
559	**17.1.1**	**Analyse required engine performance**	**9 hrs**	**Fri 28-5-21**
560	17.1.1.1	Calculate required T/W ratio	1 hr	Fri 28-5-21
561	17.1.1.2	Calculate power needed in hover	4 hrs	Fri 28-5-21
562	17.1.1.3	Calculate power needed in cruise	4 hrs	Mon 31-5-21
563	**17.1.2**	**Design engine configuration**	**5 hrs**	**Mon 31-5-21**
564	17.1.2.1	Calculate optimal number of engines	3 hrs	Mon 31-5-21
565	17.1.2.2	Calculate optimal engine positioning	2 hrs	Tue 1-6-21
566	**17.1.3**	**Perform detailed design on engine**	**7 hrs**	**Wed 2-6-21**
567	17.1.3.1	Size engines	1 hr	Wed 2-6-21
568	17.1.3.2	Select type of electrical engine	1 hr	Wed 2-6-21
569	17.1.3.3	Select commercially available electrical engine	2 hrs	Wed 2-6-21
570	17.1.3.4	Obtain engine parameters	2 hrs	Wed 2-6-21
571	**17.2**	**Design propellers**	**93 hrs**	**Tue 1-6-21**
572	**17.2.1**	**Calculate propeller characteristics**	**51 hrs**	**Tue 1-6-21**
573	17.2.1.1	Perform literature research on propeller design	4 hrs	Tue 1-6-21
574	17.2.1.2	Calculate optimal number of blades	8 hrs	Tue 1-6-21
575	17.2.1.3	Calculate optimal aspect ratio of the propeller blades	8 hrs	Wed 2-6-21
576	17.2.1.4	Select propeller airfoil	8 hrs	Thu 3-6-21
577	17.2.1.5	Calculate propeller radius	4 hrs	Fri 4-6-21
578	17.2.1.6	Calculate propeller twist	8 hrs	Mon 7-6-21
579	17.2.1.7	Perform sensitivity analysis of the propeller parameters	4 hrs	Tue 8-6-21
580	17.2.1.8	Calculate propeller exit speed at hover and cruise	4 hrs	Tue 8-6-21
581	17.2.1.9	Calculate propulsive efficiency in cruise	2 hrs	Wed 9-6-21
582	**17.2.2**	**Perform simulation of propeller performance**	**49 hrs**	**Thu 3-6-21**
583	17.2.2.1	Create CAD model of the propeller	4 hrs	Thu 3-6-21
584	17.2.2.2	Run simulation	6 hrs	Wed 9-6-21
585	17.2.2.3	Analyse simulation outcome	6 hrs	Thu 10-6-21
586	17.2.3	Estimate noise produced by the propeller in cruise and hover	12 hrs	Fri 11-6-21
587	17.2.4	Estimate propeller-wing interaction effects	18 hrs	Mon 14-6-21
588	**17.3**	**Evaluate complete propulsion subsystem performance**	**28 hrs**	**Wed 16-6-21**
590	**17.3.2**	**Perform verification and validation**	**14 hrs**	**Fri 18-6-21**
591	17.3.2.1	Perform V&V of the simulations made	8 hrs	Fri 18-6-21
592	17.3.2.2	Refine post-DSE V&V procedures for the propulsion subsystem	4 hrs	Mon 21-6-21
589	17.3.1	Simulate final performance of the propulsion system	10 hrs	Wed 16-6-21

Project: GanttMidterm
Date: Thu 27-5-21

Task | Split | Milestone

4 Trade-Off Selection Criteria

In this chapter the selection criteria will be presented in Section 4.1, which will be followed by the importance of the technical analysis described in Section 4.2.

4.1. Selection Criteria and Weights

In order to perform a trade-off which will be used to select the best configuration, a various range of tools will be needed. First, the selection criteria from which the configurations will be graded on must be defined. Secondly, the weights of each selection criterion must be given. Depending on their importance and relevance, the weights of each selection criterion can be derived. The selection criteria are derived from previously defined requirements (please see [1]). These selection criteria for the design trade-off are the following:

- **Control and Stability**: This criterion relates to the stability and controllability properties of the system, especially related to quantitative measures of the allowable cg range and number of redundancies during hover flight. There is an additional qualitative aspect related to how damped and stable the aircraft's motion is for longitudinal and lateral open-loop stability. This selection criterion relates to requirements VTOL-STK-01, VTOL-STK-13, and VTOL-STK-22. These requirements are very important to the pilot so that the aircraft can be manned and stable during all flight conditions. The failing engines relate to VTOL-SAF-4 and VTOL-SAF-6 which are essential to guarantee the safety of passengers. Due to the previously explained importance of this selection criterion it is given a weight of **4/20**.
- **Energy Consumption**: This relates to how much energy the aircraft consumes for a trip of 300 km. This selection criterion derives itself from VTOL-STK-02 and VTOL-STK-03 which relate to the 300 km range and 1 to 3 hours endurance limits. Indeed the aircraft must be able to consume a limited amount of energy per kilometre in order to improve its capability to achieve the previously mentioned requirements but also respect the of set environmental requirements such as VTOL-STK-12. As it is related to not only technical aspects associated to the performance of the aircraft but also to other environmental aspects, this selection criterion is very important and as a consequence receives a weight of **5/20**.
- **Power**: This relates to the maximum required power provided by the battery and needed for various phases of the mission. This criterion relates to numerous system and subsystem requirements which define the minimum and maximum required power that the battery needs to provide. If this power is not achieved, it can lead to the failure of the mission, which shows its high importance, giving it a weight of **5/20**.
- **Noise**: The noise criterion relates specifically to how much noise each configuration would create during its mission, specifically during hover which is the critical case when the aircraft is in an urban environment. This selection criterion is derived from VTOL-STK-11 and is also critical for urban mobility where as little noise as possible must be emitted. Due to the fact that it is a regulation requirement, this selection criterion is of high importance to not only the governmental agencies but also to the customer. This high importance in terms of certification relates to a weight of **3/20**.
- **Cost**: The cost criterion is an essential criterion as it will allow the aircraft to be competitive in the market. The unitary cost per aircraft will be taken as a quantitative measure of compliance. First, it will be verified if all configuration meet the cost requirement VTOL-STK-09 of $6 million. Secondly, all configurations will be compared in terms of cost and graded accordingly. Due to its importance as previously explained it receives a weight of **2/20**.
- **Passenger Comfort**: It can be mainly associated to how easily passengers can board into the plane and their associated comfort. This criterion is the least critical, however still relates to specific stakeholders such as passengers or customers who wish to buy the aircraft. This results in it having the lowest weight of **1/20**.

4.2. Technical Analysis

Due to the importance of the selection criteria for the trade-off process, it is essential to provide a good technical analysis from which the results will be used in order to grade the different selected configurations. This technical analysis will provide the necessary results from all disciplines.

In fact, a preliminary sizing will first be performed in order to initialise the analysis for all disciplines. From there, the flight performance of all configurations will be estimated (in Chapter 7) which will result in an energy estimate used for the **Energy Consumption** criterion. Furthermore, an aerodynamic sizing and analysis will be required in order to obtain the necessary aerodynamic variables for both the $Propulsion$ & $Power$ and $Control$ & $Stability$ departments. From Propulsion and Power (see Chapter 9) both peak power and noise estimates will be obtained, which will be directly used to assess the **Power** and **Noise** selection criteria respectively. The required results for the **Control and Stability** criterion will be obtained and analysed in Chapter 10. These will include the allowable CG range wished to be as large and aft as possible, the number of allowable engines to fail and the overall open-loop stability characteristics of the configuration. The combination of all three aspects will result in a particular performance for **Control and Stability**. Finally, the **Cost** and **Passenger Comfort** criteria will be assessed using the results obtained in Chapter 13 with the association of Chapter 11 and Chapter 12 respectively.

Before the technical analysis can be presented, the team must select its three configurations, which will be the topic of the next chapter.

5 Design Option Tree and Selected Configurations

The chapter presents the Design Option Tree (DOT) and gives a short description of all the three design considered for the trade-off, pointing out some of the possible benefits and differences between the designs.

The DOT can be found below. It can be seen that it includes the initial elimination process, represented by the black and purple crosses, for non feasible concepts, and concepts which are not worth pursuing further respectively. Thus, the last type of elimination happens during the trade off between the 3 options presented in Chapter 17, which uses the results of the multidisciplinary analysis of the aircraft concepts to grade the three concepts, based on a number of selection criteria are presented in Chapter 4. Other concepts however were eliminated before the trade because they were not directly related to one of the aircraft concepts, but could be included in any of them, such as the energy source, as discussed in Chapter 9.

Figure 5.1a shows the Tandem wing concept. It features distributed propulsion, spread out over both wings. The aircraft has two wings, one on the front and one on the rear. To achieve vertical take-off and landing, the entire wing rotates.

The next concept is illustrated in Figure 5.1b, named the Box wing. This design, much like the previous one, features two wings.The sketch shows multiple differences, one being the wings connected at their tips and therefore featuring a box wing. The engines are ducted and mounted on the trailing edge,as opposed to the Tandem wing concept. Only the flaps rotate, instead of the entire wing.

The remaining design, which is presented in Figure 5.1c, features dedicated engines for take-off inside the wing. These engines get covered during cruise. The four other engines tilt, and are used both during cruise and take-off and landing. It consists of only one wing, which makes it significantly different from the other two designs.

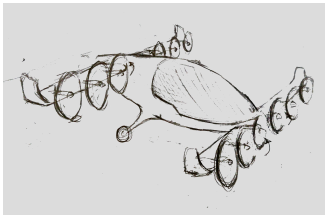

(a) Tandem wing concept

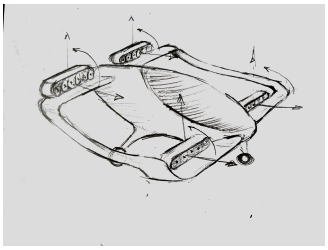

(b) Box wing concept

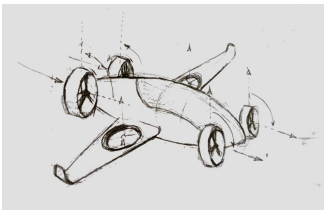

(c) Single wing concept

Figure 5.1: Drawings of all three proposed concepts

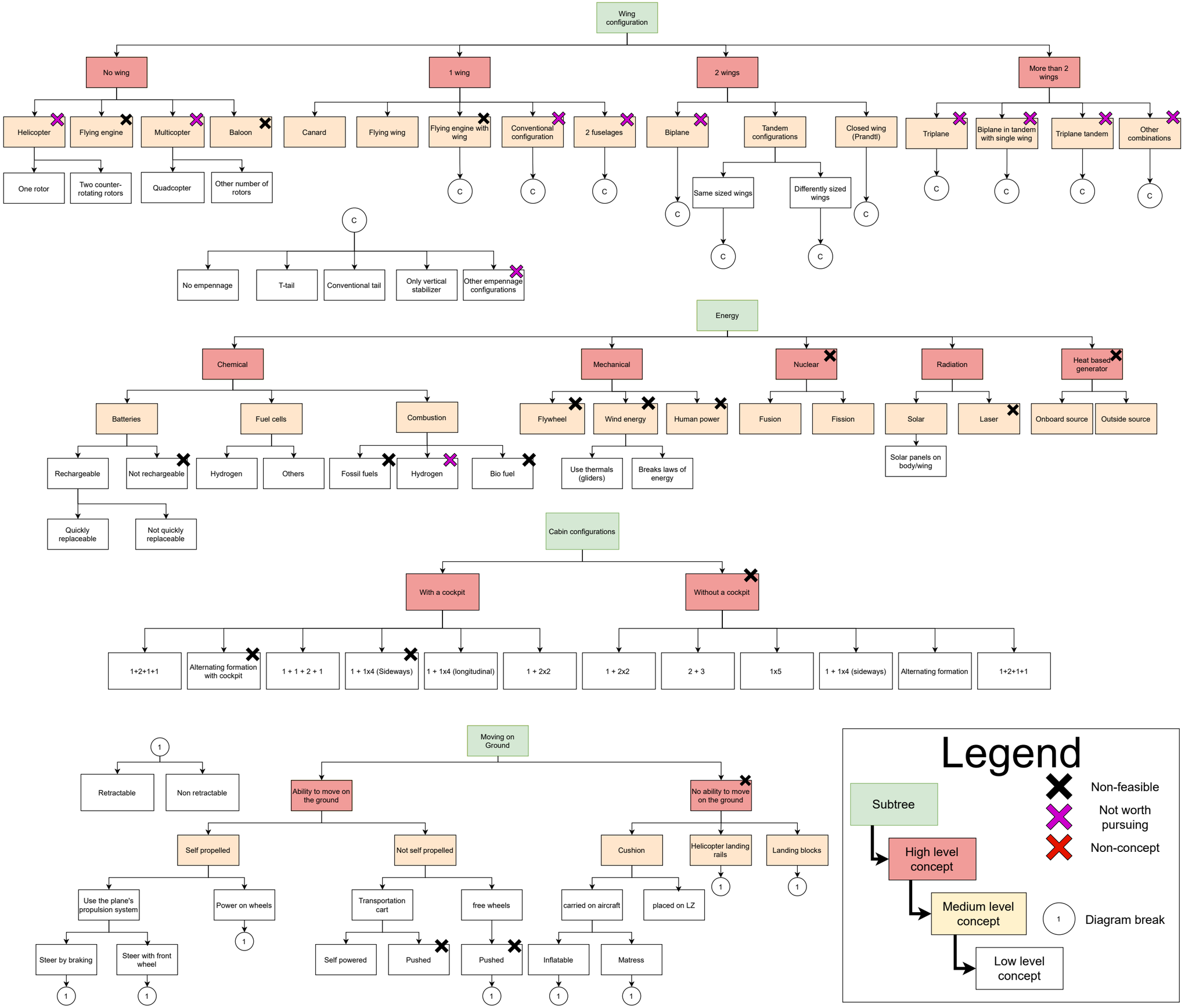

Diagram 5: Design Option Tree part 1

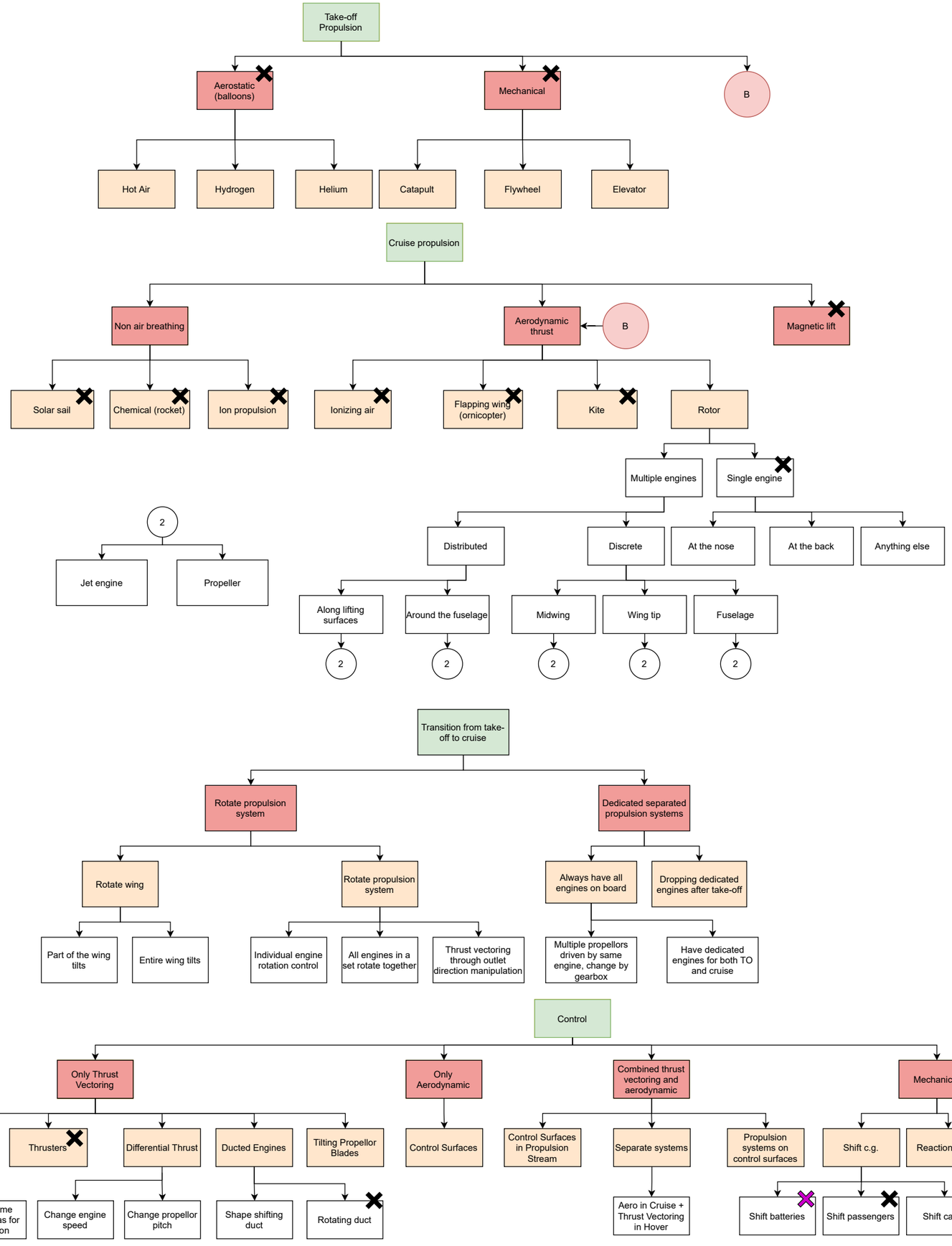

Diagram 6: Design Option Tree part 2

6 Preliminary Sizing

This chapter will cover the process followed to perform the preliminary sizing of the aircraft. In Section 6.1, the wing and power loading diagrams are constructed for each concept. Then, an estimate of the maximum take-off weight and empty operative weight is made in Section 6.2

6.1. Wing and Power Loading

One of the first steps in the design of an aircraft is the sizing of the wing and propulsion system. These are sensitive to the weight of the aircraft, which is not yet known accurately at this design stage. Therefore, the wing size and shaft power are estimated per unit weight of the aircraft. The parameters to be estimated are then the wing loading W/S and power loading W/P.

6.1.1. Relevant equations and requirements

To estimate the wing and power loading, some equations to analyse flight performance are rewritten, such that they represent the power loading in function of the wing loading or vice versa. This was done for the turning and climbing performance, stall speed, hover power and maximum speed of the aircraft. Apart from a requirement with respect to these performance parameters, some other aircraft parameters need to be estimated first. These include the propulsive efficiency of the propeller at different speeds, the drag polar of the aircraft and the maximum lift coefficient. These estimations stem from different departments, such as structures, aerodynamics and power and propulsion. For more information on the estimations, please refer to their respective chapters.

Stall speed

Equation 6.1 shows the wing loading based on the stall speed requirement of the aircraft. Note that this represents an upper bound on the wing loading, and is not dependent on the power loading. As stall is mainly relevant during transition, which takes place right after take-off, the density here is that of the take-off altitude. More on the selection of a relevant stall speed can be found in Section 7.2.1.

$$\left(\frac{W}{S}\right)_{stall} = 0.5\rho V_{stall}^2 C_{L_{max}} \tag{6.1}$$

Climb rate

The equation used for the power and wing loading related to climb can be found in Equation 6.2. The $\frac{C_D}{C_L^{3/2}}$ term should be the optimal and thus minimal value, such that minimal power is required for a certain rate of climb. The density here is that of the cruise altitude, because the climb rate requirement should be satisfied until cruise is reached. The required climb rate (ROC) was set to 10 [m/s]. Although this value is somewhat high, it is chosen such that the aircraft can reach cruise as fast as possible. This is beneficial for passenger comfort (more time in cruise) and travel times. In a later design stage, a more optimal value will be selected.

$$\frac{W}{P_{br}} = \left(ROC + \left(\frac{2W/S}{\rho}\right)^{1/3} \left(\frac{C_D}{C_L^{3/2}}\right)_{opt}\right)^{-1} \eta_{prop,climb} \tag{6.2}$$

Turning load factor

Equation 6.3 is used to asses the ability of the aircraft to sustain speed in a turn with a certain load factor. The effect of the turn is present in the drag coefficient, shown in Equation 6.4. In this equation the lift coefficient for steady, symmetric, horizontal flight is multiplied by the load factor of the turn. The drag polar model is further discussed in Chapter 8. Because it is not yet known at this point at which speed the turning requirement will be most critical, it will be considered at cruise speed and at maximum speed.

$$\frac{W}{P_{br}} = \frac{C_D \rho V^3}{2W/S} \eta_{prop,cruise} \tag{6.3}$$

$$C_D = C_{D_{min}} + k(nC_L - C_{L_{min}})^2 \tag{6.4}$$

Maximum speed
If a constraint on maximum speed would be chosen, Equation 6.3 and Equation 6.4 can be used as well, setting the load factor equal to 1. The value for a maximum speed was based on the maximum speed obtained from structural considerations, as explained later in Chapter 11. There a maximum speed is selected of 1.25 times the cruise speed [15]. Since the cruise speed cannot be estimated accurately at this stage, after a number of iterations, a maximum speed of 65 m/s was selected.

Vertical flight
Because the aircraft needs to be able to take off and land vertically, also a constraint on the power and wing loading for hover was added. First the required thrust-to-weight ratio was determined. This was done using Equation 6.5, obtained from [61]. Here the parameter $\frac{S_{TOT}}{S}$ represents the ratio between the total projected area and the wing surface area, as seen from the top. A factor of 1.2 was applied to allow for accelerations. The rate of climb (ROC) used here is the required rate of climb during hover.

Since the requirement for hover has to be expressed in terms of W/P instead of T/W, the thrust has to be converted to power. This was done using Equation 6.6 [38]. In this equation, T/A represents the disk loading of the aircraft, which is estimated in Section 9.2.3.

$$\frac{T}{W} = 1.2\left(1 + \frac{1}{W/S}\rho ROC^2 \frac{S_{TOT}}{S}\right) \tag{6.5}$$

$$\frac{W}{P_{br}} = \left(\frac{T}{W}\sqrt{\frac{T/A}{2\rho}}\right)^{-1} \eta_{prop,hover} \tag{6.6}$$

6.1.2. Plotting and design point selection

The requirements set on stall speed, climb rate, turning load factor, maximum speed and hover are all listed in Table 6.1.

Table 6.1: List of additional requirements on aircraft performance

Requirement	Value	Unit	Requirement	Value	Unit
Stall speed	40	[m/s]	**Maximum speed**	65	[m/s]
Climb rate	10	[m/s]	**Take-off climb rate**	2	[m/s]
Turn load factor	2	[-]	**Landing descend rate**	-1	[m/s]

The wing and power loading diagrams for all three eVTOL concept can be found in Figure 6.1. Since the wing surface and shaft power should be as low as possible, the design point should be as closer to the top right as possible. The design region has been indicated in green. Note that two regions are present. The dark green area represents the design space including the vertical flight requirements, while the lighter area does not consider these. The reason for this is that some concepts can have dedicated engines for vertical flight, which can ease the power requirement on the cruise engines.

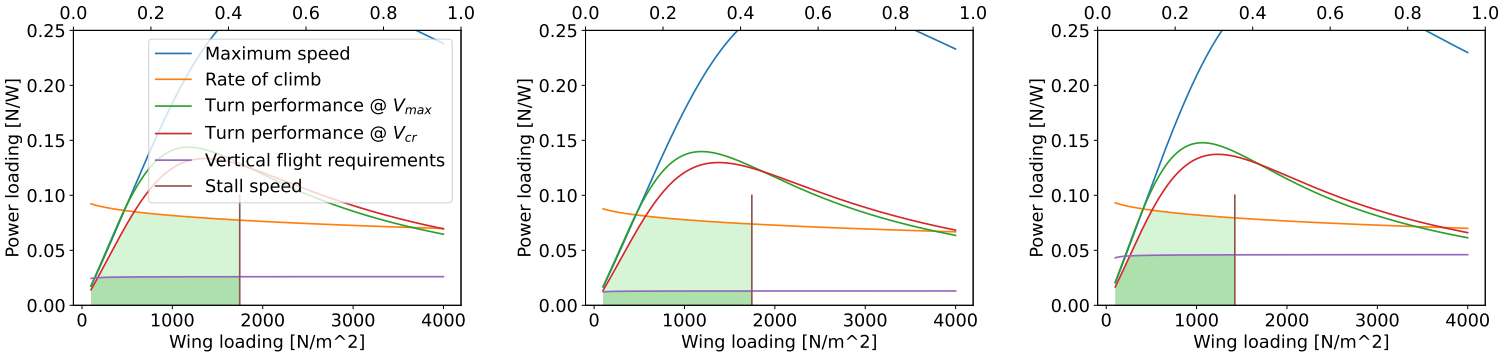

(a) Tandem wing **(b)** Box wing **(c)** Single wing

Figure 6.1: Wing and power loading diagrams for all three eVTOL concepts

In Table 6.2 the design points for each concept are listed. Note that the two double wing concepts have no dedicated hover engines, therefore their power loading requirement in hover is the same as that in cruise. In terms of required brake power, the single wing concept needs the least power, followed by the tandem

wing concept. The box wing concept is the most power-intensive in flight. For the sizing of the wing, the first and second concepts need the smallest wing.

Table 6.2: Design points for each concept

Concept	W/S [N/m^2]	$(W/P)_{hover}$ [N/W]	$(W/P)_{cruise}$ [N/W]
Tandem wing	1745	0.026	0.026
Box wing	1745	0.013	0.013
Single wing	1422	0.046	0.0795

6.2. Mass Estimation

Using data from several sources, such as "A review of current technology and research in urban on-demand air mobility applications"[36] and database of an eVTOL directory [54], it was possible to plot a regression line of Operational Empty Mass versus Maximum Take-off Mass and Maximum Take-off Mass versus Payload. The resulted plots are depicted in Figure 6.2. The data retrieved includes short, medium and long range eVTOLs, which is not ideal for the estimation of the long-range eVTOL, but due to the scarcity of the available data, this method was used. It is obvious that Figure 6.2a provides a much better fit, with RMSE of 166. Figure 6.2b has an RMSE of 814. It was decided not to remove the outliers as most of these are high range eVTOLs, hence relate most to the mission of the project. Including only high-range eVTOLs provided an even worse fit due to having only 5 data points.

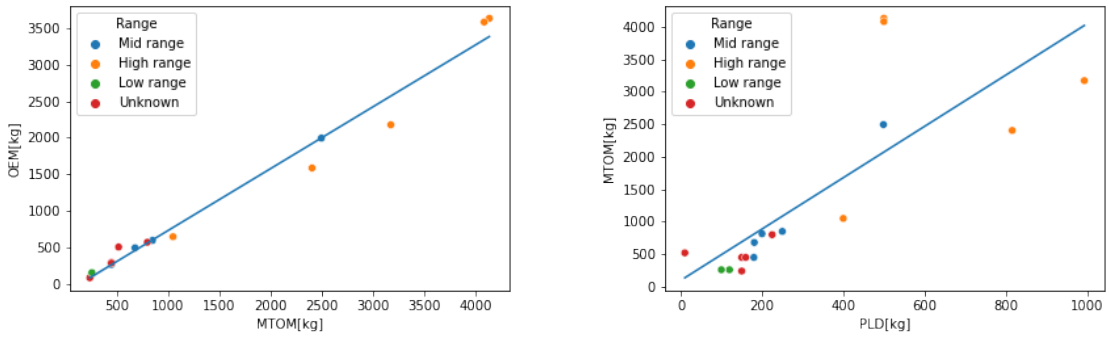

(a) Take off Mass versus Operational Empty Mass

(b) Payload versus Take off Mass

Figure 6.2: Mass Estimation Relationships

Using the lines plotted in Figure 6.2, firstly it is possible to find the required Maximum Take-off Mass based on the payload requirement. The payload requirement is 475 kg, 95 kg per each passenger and the pilot. From this, $MTOM = 1930.62\ kg$ and $OEM = 1565.15\ kg$ was retrieved, which is used as preliminary weight estimation.

7 Flight Performance

In this chapter, the performance of the different concepts will be evaluated. First, in Figure 7.1, a typical mission is presented. In Section 7.2, the energy needed to fulfil such a typical mission is calculated for each concept. The influence of the payload on the range of the aircraft is evaluated in Section 7.3. In Section 7.5, the climb performance of each concept is presented, in the form of climb performance charts. Finally, Section 7.6, some elaboration on verification and validation is given.

7.1. Mission profile

To consider the performance of the aircraft in different phases of the flight, it can be useful to define a typical mission profile. The mission profile for an eVTOL aircraft is shown in Figure 7.1. This mission profile is used to estimate the energy needed for a typical mission. In the next design stage, optimisations will be made to the profile, and individual flight phases to minimise the required energy.

In the list below, all flight phases from Figure 7.1 are listed.

1. Take-off
2. Transition from hover to climb
3. Climb to cruising altitude
4. Cruise
5. Loiter in case of an unavailable landing zone
6. Descent
7. Transition to hover
8. Loiter near landing zone while hovering
9. Landing

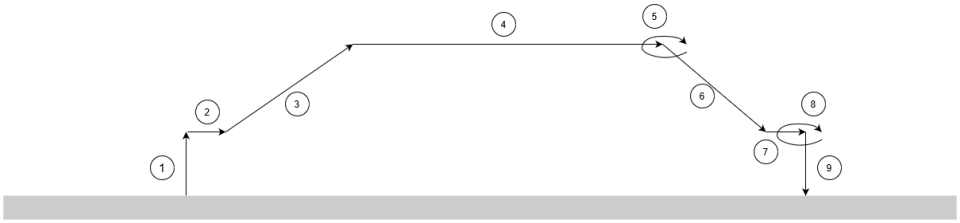

Figure 7.1: Profile of a typical eVTOL mission, including some loiter time if the landing zone is unavailable.

7.2. Energy Consumption

Because the range requirement of 300 km is only just possible with current or near future technologies, the energy consumption can be considered an important trade-off criterion. The energy consumption of a concept is evaluated by considering the power and duration of each flight phase.

7.2.1. Energy per phase

In this subsection, the calculation of the energy consumption per flight phase for each configuration is explained.

Take-off

The energy during take-off was found by calculating the thrust required for a constant rate of climb of 2 [m/s], using Equation 6.5. This was converted to power using Equation 7.1 [8]. Since the only component of the velocity is the rate of climb, V can be replaced by the ROC during vertical flight. The factor k corrects for simplifications made when deriving the equation, and is assumed to be 1.2 [8].

$$P = T + kT\left(-V_{\perp}/2 + \sqrt{\frac{V_{\perp}^2}{4} + \frac{T}{2\rho A_{prop}}}\right) \tag{7.1}$$

Assuming a time spent in vertical flight for take-off of 20 [s], the energy used during vertical flight can be estimated by multiplying the power use by the time spent in vertical flight.

Transition to climb

To estimate the energy used during transition from take-off to climb, a simplified model was made. This model assumed a constant altitude during the initial phase of transition, to simplify the analysis. This is likely not the optimal trajectory, but since the scope of this report is to compare different configurations, optimization is not performed. From this assumption it follows that the acceleration in y-direction (altitude) can be assumed to be zero, allowing the equilibrium equation in y (Equation 7.2) to be rewritten such that the required thrust can be obtained.

$$ma_y = L + \sin\alpha_T T - W \tag{7.2}$$

$$T = (W - L)/\sin\alpha_T \tag{7.3}$$

Another assumption was that the angle of attack is kept constant, such that C_L can also be considered constant. This means lift is only dependent on speed. In order to find the required thrust, also the engine angle has to be found. This was done by assuming a constant rotational speed of the engine angle of attack. Since this can lead to insufficient thrust when the engine is rotated too much, the engine stops rotating when this is the case, and waits for the speed and thus lift to increase before continuing to rotate.

The acceleration in x-direction was evaluated using Equation 7.4. The drag was evaluated using the drag model explained in Chapter 8. Also this equation can be rewritten to obtain a minimum thrust required to maintain speed, see Equation 7.5. This thrust is used as a lower bound to the thrust found in Equation 7.3. Note that if the thrust needed to maintain altitude is lower than that for speed, the aircraft will start climbing.

As an upper bound, the maximum thrust at a certain speed can be found by finding the thrust associated with the maximum power, by numerically finding the roots of Equation 7.1. Also using Equation 7.1, the power associated with a certain thrust can be found.

$$a_x = (-D + \cos\alpha_T T)/m \qquad (7.4) \qquad\qquad T = \frac{D}{\cos\alpha_T} \qquad (7.5)$$

The simulation itself is performed by calculating the acceleration, engine angle and required thrust at a certain point in time, and performing a discrete time stepping numerical integration. The simulation is stopped once the engines are completely rotated to the cruise configuration. The total energy is found by multiplying the power at a certain time with the time step, and summing it for the entire simulation.

Apart from estimating the required energy for transition, the simulation was also used to select a stall speed for the aircraft. As soon as the aircraft reaches the stall speed during transition, it can in principle completely transition to cruise configuration, as no additional thrust is needed to lift the aircraft. Based on the simulation of the transition to climb of the first configuration, which ended at a speed of 47 m/s, a stall speed of 40 m/s was selected.

Climb

For the climb to cruise it was assumed that the aircraft flies at the optimal climb speed. The power can then be evaluated using Equation 7.6. Both the V_{climb} and $(C_D/C_L)_{climb}$ were those at the optimal point for climb, namely were C_L^3/C_D^2 is the highest.

The time it takes to climb to cruise altitude is found using Equation 7.7. The rate-of-climb during take-off in vertical flight was assumed to be 2 m/s, with a take-off duration of 20 s. This gives a transition altitude of 40 m. The cruise altitude was set to be 400 m, since the cruising altitudes encountered during operation are likely in this range. It is slightly above the 305 m recommended by Uber [22] for additional safety. Since the scope of this report is to compare configurations, no further optimisations were performed.

$$P = W\frac{V_{climb}(C_D/C_L)_{climb} + ROC}{\eta_{prop,climb}} \qquad (7.6) \qquad t_{climb} = \frac{h_{cruise} - h_{trans}}{ROC} \qquad (7.7)$$

A rate of climb of 10 m/s was assumed, although this is likely not the most optimum rate of climb, it serves to compare the performance of different configurations. The energy needed for climb is then found by multiplying the power with t_{climb}.

Cruise

For cruise, a similar procedure as for climb was used. The power required for cruise can be found in Equation 7.8. Here the V_{cruise} and $(C_D/C_L)_{cruise}$ are the value at maximum C_L/C_D, which gives the maximum range.

The time spent in cruise was done by first calculating the distance needed for climb and descent, and subtracting these from the total mission distance. This gave the distance spent cruising, from which the time spent in cruise can be obtained using the cruise speed. Multiplying this with the cruise power gave the energy required for cruise.

Descent

To simplify calculations, the descent was performed at an angle that required zero power. This angle is found by Equation 7.9.

$$P = \frac{WV_{cruise}(C_D/C_L)_{cruise}}{\eta_{prop,cruise}} \qquad (7.8) \qquad \gamma = \arctan\left(C_D/C_L\right)_{cruise} \qquad (7.9)$$

Transition to landing configuration

After descending to the transition altitude, the aircraft transitions to vertical flight. To simplify the analysis, the energy required to do this was assumed to be equal to that needed to transition to cruising altitude. In reality, less energy will likely be needed, since the aircraft the aircraft needs to decelerate instead of accelerate.

Loiter

The power used during loiter in cruise configuration can be found in the same way as the power during climb, but setting the climb rate equal to zero. This can be done since both maximum endurance and maximum climb rate require minimum power. 30 min. of loiter time was reserved for loiter in cruise configuration.

Some loiter time while hovering was added in the mission profile, if the landing pad would be occupied unexpectedly by people. Since most of these occurrences should not take long, only 30 seconds of hover time was allocated to this. The energy needed was calculated in a similar fashion as take-off, but with a rate of climb equal to zero.

Landing
Also the landing energy was done in the same way as the take-off energy. Here the rate of climb was replaced with a rate of descent of -1 m/s. The time needed to descent was estimated to be 40 seconds.

7.2.2. Energy balance

Summing all the energies from Section 7.2.1 gave an estimate for the total energy consumption during flight. The results for each aircraft concept can be found in Table 7.1. It can be concluded that the energy requirement for the different aircraft varies significantly. Unsurprisingly, the ranking of aircraft based on energy requirement follows the same order as that based on the estimated weights (Section 11.3), highlighting the importance of a lightweight structure.

Additionally, to visualise which flight phases contribute the most to the total energy, a pie chart was made, see Figure 7.2. Cruise is the most energy-intensive phase for all concepts. For the second concept, vertical flight contributes more than for the other concepts, due to the low hover efficiency of its ducted fans.

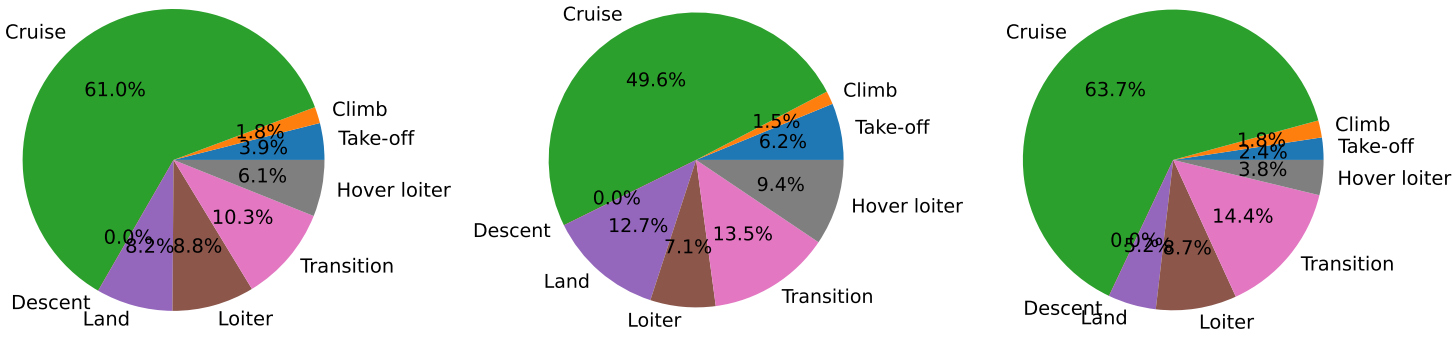

(a) Tandem wing **(b)** Box wing **(c)** Single wing

Figure 7.2: Fractions of the total energy used for each flight phase

Table 7.1: Total energy needed for a typical mission

	Tandem wing	**Box wing**	**Single wing**
Total Energy (MJ)	422	557	389

7.3. Influence of Payload Mass

For a transport aircraft, the weight can vary between different flights. To assess the effect of a different payload mass on the range of an aircraft, payload range diagrams were constructed. To make these, the energy capacity of the aircraft was set equal to the estimated required energy for a typical mission, as given in Table 7.1. Based on this, the range was calculated for a range of payload masses. The maximum payload was set equal to the difference between the maximum take-off mass and the empty operative mass.

The resulting payload range diagrams can be found in Figure 7.3. These are useful when considering the operations of an aircraft. In this design stage however, they are mainly there as a sensitivity analysis with respect to the aircraft weight. From the diagrams, it can be concluded that the range depends strongly on the payload mass for all aircraft concepts.

7.4. Influence of Cruising Altitude

Figure 7.4 shows the relationship between the required energy to complete a 300 km mission and the cruising altitude, including a linear function plotted to the data points. As can be expected, the required energy increases with altitude, since extra energy is required to climb. The relationship is not very strong

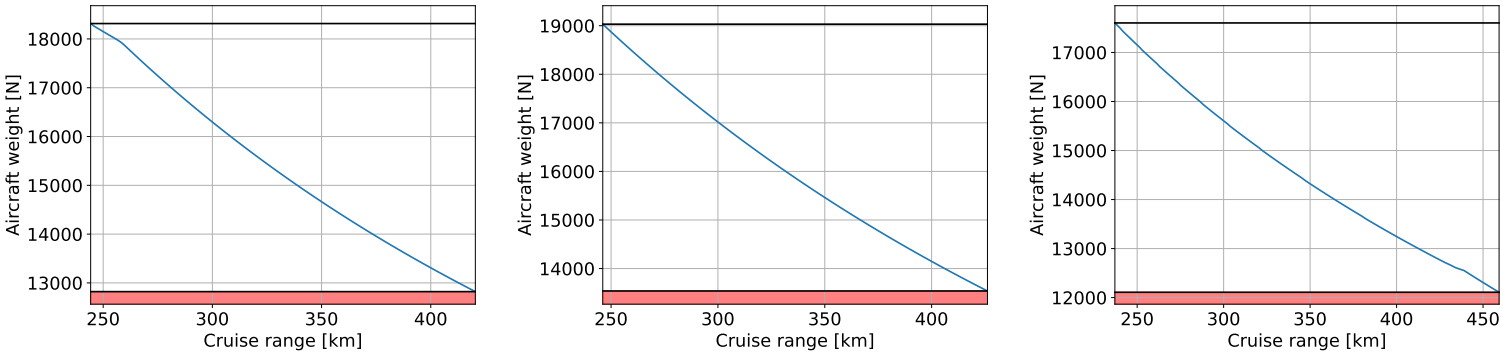

(a) Tandem wing **(b)** Box wing **(c)** Single wing

Figure 7.3: Payload-range diagrams for each eVTOL concept

however, varying around 10% for the 3 concepts in the operating altitude range (Assuming the cabin will be unpressurized). The influence of altitude is different for each concept. It can be noted that the dependency varies in a similar manner as the total energy required, with the most energy intensive concept also exhibiting the largest variation in energy with cruising altitude. This can likely be explained by the weight distribution found in Section 11.3. A heavier aircraft not only needs more energy for a certain mission, but also needs more power to climb to a certain altitude, explaining the higher dependency on cruising altitude for the heavier concepts.

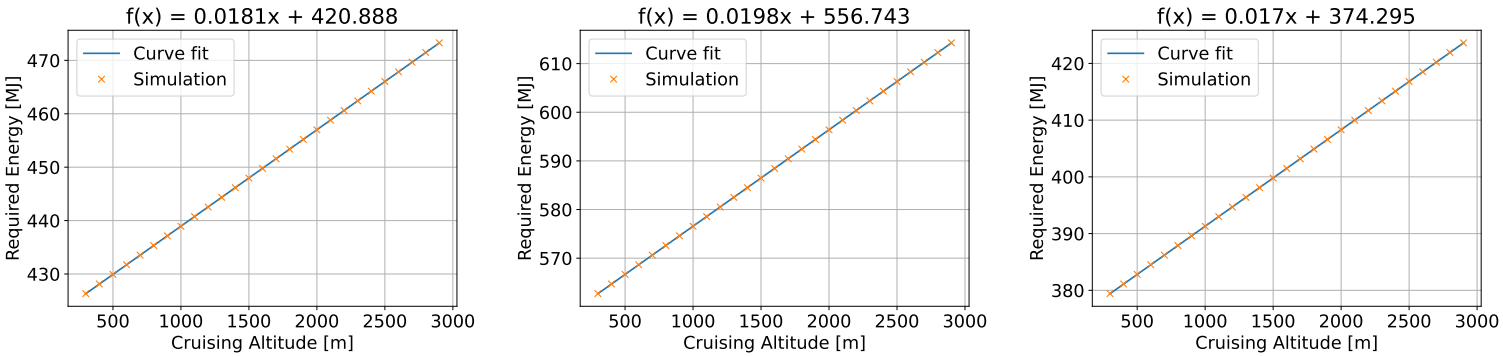

(a) Tandem Wing **(b)** Box wing **(c)** Single wing

Figure 7.4: Effect of cruising altitude on total energy consumption

7.5. Climb Performance

The climb performance of each aircraft was also considered. The rate of climb of each concept was calculated using Equation 7.10 at different speeds. Even though the propulsive efficiency will vary with airspeed, it is assumed constant for now. Since the brake power is also assumed constant for a propeller aircraft, only the second term varies with speed. The required power $P_{req.}$ for steady, symmetric, horizontal flight was obtained using Equation 7.11, where the drag coefficient was found based on the C_L needed for level flight.

$$ROC = \eta_{prop,climb}\left(\frac{W}{P_{br}}\right)^{-1} - \frac{P_{req.}}{W} \qquad (7.10)$$

$$P_{req.} = 0.5\rho V^3 S C_D \qquad (7.11)$$

The climb rates were also calculated for different altitudes, to assess the effect of different air densities on climb rate. The resulting climb performance charts are shown in Figure 7.5. As can be seen, the dependency of altitude on climb rate is minor. Another important consideration is the big difference in climb rate and maximum speed for each concept. The maximum speed is the speed at which the maximum climb rate equals zero, so no excess power is available. In the climb performance charts it can also be observed that some of the climb rates are extremely high. This is because the tandem and box wing do not have dedicated hover engines, so all the engines are sized based on the vertical flight requirements. This leads to a lot of

reserve power during horizontal flight. This is most pronounced for the box wing concept, where the high disk loading of the ducted fans is very inefficient for vertical flight. This leads to a high power requirement. In horizontal flight, where the speeds are higher, the ducted fans are more efficient, and can provide high climb rates. Note the discontinuous slope in Figure 7.5b, there the aircraft is climbing at an angle of 90 degrees, meaning that the climb rate is limited only by the speed of the aircraft.

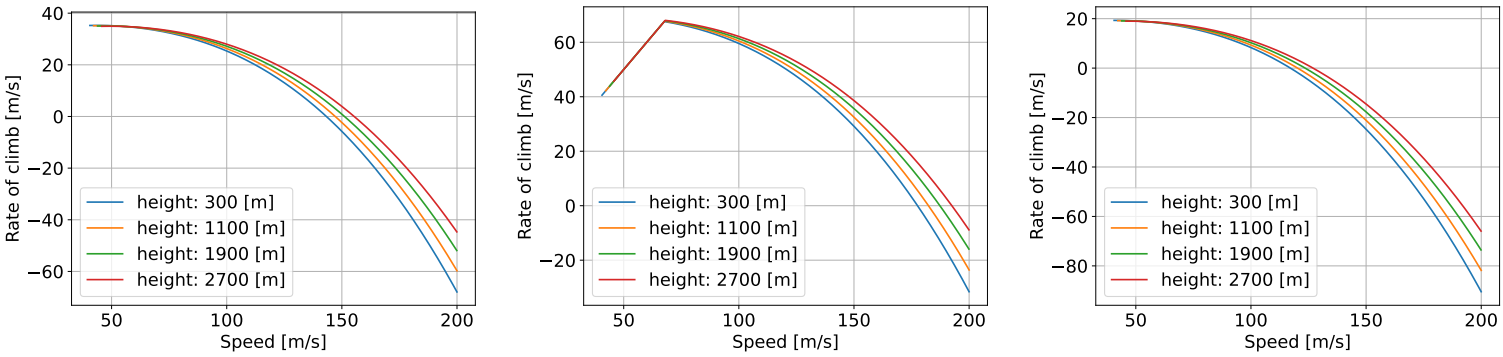

(a) Tandem wing **(b)** Box wing **(c)** Single wing

Figure 7.5: Climb performance charts for each eVTOL concept

7.6. Verification and Validation

This section will address the verification and validation procedure for the flight performance calculations.

7.6.1. Verification and validation for preliminary design tools.

In order to verify the implementation of the different models, simple unit tests were used, including verifying that no negative power, thrust or energy resulted from any of the calculations. Furthermore, the pie charts in Figure 7.2 served as a tool to check if the energy fractions do not take on unrealistic values.

Due to the lack of resources, the models used to assess the flight performance of each concept where not validated extensively. The main method used was to check whether results made physical sense or comparing them to similar aircraft. For example, the 7-seat Lilium jet with a 200 km range needs about 1100 MJ of energy [38]. Comparing this with the energy capacity of the three concepts considered here, which were around 450 MJ, leads to the conclusion that the energy needed is not unrealistic, more so since the Lilium almost weighs twice as much (3175 kg [38] vs an average of 1870 [kg] for the concepts considered here).

The main reason for not performing a detailed validation on the models is that they are mainly used to compare concepts, the difference between concepts is considered more important than the actual values. However, it is still required that the models represent reality accurately enough to enable a reliable comparison.

7.6.2. Verification plan

To verify the models that will be used in the next design phase, units tests will be used. It will be tested whether each model behaves as expected when changing the inputs. Furthermore, the outputs of the model will be compared to simplified analytical results where possible.

7.6.3. Validation plan

Where possible, to save resources, validated models developed by previous research will be used. If new models have to be made, or if existing models need to be modified, validation will be performed. This will be done by comparing the final outputs to aircraft with similar characteristics. These are not limited to eVTOLs, but can also include propeller aircraft with similar power and wing loading as one of the concepts. This allows validation of performance parameters such as climb rate, maximum speed and power consumption. For the vertical flight phases, data from multicopters may be used. In a late stage, also flight testing can be performed, with power measurements at each flight phase. These can be compared to the prediction made

by the models.

8 Aerodynamic Sizing

This chapter will focus on the preliminary design of lifting surfaces for each of the three concepts and the estimation of their aerodynamic characteristics. Section 8.1 performs the initial lift and drag estimations which are then used in Section 8.2 to conduct the wing design. A more thorough drag estimation is then detailed in Section 8.3. The chapter concludes with a sensitivity analysis in Section 8.4 and a verification and validation plan in Section 8.5.

8.1. Initial Lift and Drag Estimations

In order to get an initial estimation of the area of the lifting surfaces, and initial weight estimations, a first estimate of the drag polar is needed in order to obtain the L/D ratio of the aircraft for cruise and loiter. For the zero lift drag estimation, a simple method was used based on the ratio of wet area to reference area and the skin friction coefficient, shown in equation 8.1 [56].

$$C_{D_0} = C_{f_e} \frac{S_{wet}}{S_{ref}} \tag{8.1}$$

$$C_{D_i} = \frac{{C_L}^2}{\pi ARe} \tag{8.2}$$

Assuming a skin friction coefficient of 0.0045, an estimate for twin engine light aircraft, and a $S_{wet}/S_{ref} = 4.5$ for all three concepts based on similar aircraft [41], this results in an initial estimate of 0.02025 for all concepts.

Regarding induced drag, described by formula 8.2, the estimates for the drag polar do differ between the different concepts. Aspect ratio, AR is a design decision, and e is dependent on the lift distribution along the span of the aircraft. For the single wing aircraft an estimate of 0.85 is made [56]. For the two double wing concepts, a different method has to be used and a number of aspects have to be clarified. For the initial estimate, wings of equal span are assumed, as studies show that this results in the lowest induced drag [49]. In this case the following formulas are true. For equal spanned wings, Schiktanz et al. propose Equations 8.3, 8.4, 8.5 and 8.6, which are based on wing area fractions [48]. Henceforth, the subscript 1 refers to the frontal wing, while the subscript 2 does that for the rear wing in the case of the dual wing concepts.

$$s_i = \frac{S_i}{S_{ref}} \tag{8.3}$$

$$AR_i = \frac{b_i^2}{S_i} \tag{8.4}$$

$$AR = \frac{b^2}{S_1 + S_2} \tag{8.5}$$

$$S_{ref} = S_1 + S_2 \tag{8.6}$$

Regarding the Oswald efficiency factor the following formulas based partly in the work of Prandtl and Rizzo are presented [48].

$$e_{\text{box}} = e_{\text{ref}} \cdot \frac{0,44 + 2,219h/b}{0,44 + 0,9594h/b} \tag{8.7}$$

$$\frac{e_{\text{bi}}}{e_{\text{ref}}} = 0,5 + \frac{1 - 0,66 \cdot h/b}{2,1 + 7,4 \cdot h/b} \tag{8.8}$$

Equations 8.7 and 8.8 refer to a box wing and tandem respectively, where h refers to the vertical distance between the wings. e_{ref} is the Oswald efficiency factor of a single wing aircraft with the same AR. Assuming that the reference single wing aircraft for the double wing concepts also has $e = 0.85$ results in Oswald efficiency factors of 1.145 and 1.189 for the tandem and box wing respectively. Furthermore, for the initial estimations, aspect ratios of 8 and 10 are chosen as initial estimates for the double and single wing concepts respectively.

8.2. Wing Design and Planform

Based on the design point, the wing loading of the aircraft is found as presented in Chapter 6. Using this and the first class weight estimation, an initial value for the surface area can be calculated. A factor to take into account when selecting the aspect ratio of the aircraft is that the span is limited to 14m to satisfy the requirement that the plane must fit into a standard heliport [1].

In order to simplify the initial sizing process, trapezoidal wing planforms without twist are assumed. Since the aircraft will fly at Mach numbers significantly below transonic speeds, the sweep at quarter chord is chosen to be 0 for all lifting surfaces. Furthermore, the taper ratio is chosen to be 0.4 in order to obtain

a lift distribution as close to elliptical as possible with a trapezoidal wing without sweep [56]. For now, the wing will be assumed to be planar, meaning the dihedral angle is 0, although this will change in further iterations in order to improve lateral stability.

Using the surface area, taper ratio and aspect ratio, a number of relevant wing parameters can be computed. The wingspan can be found using equation 8.4, and the root and tip chords are calculated with formulae 8.9 and 8.11 respectively. The MGC and MAC are assumed to be equal, and thus the c_{MAC} can be computed using equation 8.12, and its location along the span is calculated with equation 8.10. The X_{LEMAC} is found with formula 8.13 and the sweep at any position along the chord is found with 8.14 [56].

$$c_r = \frac{2S}{(1+\lambda)b} \tag{8.9}$$

$$c_{MAC} = \frac{2}{3} \cdot c_r \cdot \frac{1+\lambda+\lambda^2}{1+\lambda} \tag{8.12}$$

$$Y_{MAC} = \frac{b}{6} \cdot \frac{1+2\lambda}{1+\lambda} \tag{8.10}$$

$$X_{LEMAC} = Y_{MAC} \cdot tan(\Lambda_{LE} \cdot \frac{\pi}{180}) \tag{8.13}$$

$$c_t = \lambda c_r \tag{8.11}$$

$$tan(\Lambda_{x/c}) = tan(\Lambda_{LE}) - \frac{x}{c}\frac{2C_r}{b}(1-\lambda) \tag{8.14}$$

In the table below, the values of these parameters for both the single wing and the two double wing configurations are presented. The aspect ratio for the double wing configurations was reduced from 8 to 7 in order to reduce the structural weight of the wings. The reason why the same aspect ratio was chosen for both configurations is that it makes it easier to analyse the strengths and weaknesses of each option in terms of weight, and induced drag if this important control parameter is equal for both options.

Table 8.1: Wing planform parameters for the three concepts. For the double wing configurations, the values for one of the two wings are given.

Parameter	Tandem wing	Box wing	Single wing
S [m^2]	5.25	5.45	13.32
b [m]	8.57	8.73	11.5412
A [-]	14	14	10
C_r [m]	0.875	0.892	1.59
C_t [m]	0.350	0.357	0.636
c_{MAC} [m]	0.650	0.662	1.18
$\Lambda_{c/4}$ [rad]	0	0	0
λ [-]	0.4	0.4	0.4

8.2.1. Airfoil selection

For the airfoil selection, the value for the design lift coefficient must be found. The design lift coefficient can be found by rearranging the lift equation to yield C_L:

$$C_{L_{des}} = \frac{W}{0.5\rho V^2 S} \tag{8.15}$$

$$C_{l_{des}} = \frac{C_{L_{des}}}{\cos^2 \Lambda_{LE}} \tag{8.16}$$

In order to obtain the design lift coefficient for the airfoil, the leading edge sweep of the wing must be taken into account, which can be done using Equation 8.16.

The selection criteria that are used to select the airfoil are listed below:

- Lift slope:A higher lift slope for the airfoil is considered to be better, as it should improve stability.
- $C_{d_{min}}$: The lower the minimum drag of the airfoil, the more efficient cruise will be.
- C_L at $C_{d_{min}}$: The closer this value is to the design lift coefficient, the better.
- Drag bucket range: The larger the drag bucket is the better, as the airfoil can be used for a different design lift coefficient in case it changes.
- C_m at $C_{L_{des}}$: The higher the C_m the better for the controllability of the aircraft, as trimming should be easier during cruise.
- $\frac{C_l}{C_d}$ at $C_{L_{des}}$: The higher the lift drag ratio the more efficient cruise will be.
- $C_{L_{max}}$: The higher the maximum lift coefficient the better. A higher lift coefficient will increase the wing loading, which will therefore reduce the surface area of the wing.
- Stall characteristics: An airfoil which has an smoother stall curve and does not experience a extremely sudden loss of lift is consider safer and thus better in this criteria.

- Thickness over chord ratio:A higher thickness over chord is considered better as it reduces the structural weight of the wing.

All the criteria had equal weight except for $C_{L_{max}}$ which has twice the weight of the others. The reasoning behind this choice is that having higher $C_{L_{max}}$ allows for an increased wing loading, as the limiting requirement for selecting the design point was the stall speed. Two separate selection procedures are carried out, one for the double wing aircraft and another for the single wing. The reasoning for this is that for the single wing it is important that the $C_{m_{ac}}$ is higher than 0 in order to make it possible to trim the aircraft without needing to use the thrust, thus reflex airfoils will be used. The airfoils are evaluated using XFOIL software. 6 airfoils were considered for the double wing concepts and 7 different ones for the single wing concepts.

The characteristics of the chosen airfoils are summarised in the table below. The EPPLER 335 is for the single wing concept, and the NASA LANGLEY LS1 0417 for the double wing concepts:

Table 8.2: Summary of characteristics of the chosen airfoils Simulation settings: M = 0, Ncrit = 9, Re= 12100000 for EPPLER 335 and Re = 6194000 for NASALANGLEY.

Criteria	EPPLER 335	NASA LANGLEY
C_{L_α} [1/deg]	0.109	0.108
$C_{d_{min}}$	0.00347	0.00445
C_l for $C_{d_{min}}$	0.241	0.293
Drag bucket	Big	Average
Minimum C_m at $C_{l_{des}}$	0.0489	-0.0648
C_l/C_d at $C_{l_{des}}$	52.1	35.6
$C_{L_{max}}$ [2]	1.61	1.98
Stall characteristics	Average	Safe
t/c	0.126	0.170

It must be noted that the Reynolds number and the $C_{l_{des}}$ changed significantly after the airfoil selection due to changes in wing loading and cruising speed, thus the process will be repeated at a later stage to optimise the airfoil for the new cruising conditions.

8.2.2. Wing performance

The performance of airfoil has to be transformed to that of a finite wing with the characteristics of the wing planform. To achieve this the DATCOM method is used. Below, equation 8.17 illustrates how to compute the lift slope [41] [42].

$$\frac{dC_L}{d\alpha} = C_{L_\alpha} = \frac{C_{l_\alpha}\ AR}{2 + \sqrt{4 + \left(\frac{AR\ \beta}{\eta}\right)\left(1 + \frac{\tan(\Lambda_{0.5C})^2}{\beta^2}\right)}} \tag{8.17}$$

Where β is the Prandtl-Glauert correction for compressibility and η is the airfoil efficiency factor which can be assumed to be 0.95. For the double wing concepts the downwash on the second wing has to be taken into account. As a first estimate, a 10% reduction in lift slope due to downwash can be expected [10]. The formula used is shown below:

$$C_L = s_1 \cdot \frac{dC_{L1}}{d\alpha}\alpha + s_2 \cdot \frac{dC_{L2}}{d\alpha}\alpha\left(1 - \frac{d\epsilon}{d\alpha}\right) \tag{8.18}$$

Having a finite wing also changes the $C_{L_{max}}$. From DATCOM formula 8.19 can be found [41] [42]. Also, the stall angle can be estimated using formula 8.20:

$$C_{L\ max} = \left[\frac{C_{L\ max}}{C_{l\ max}}\right] C_{l\ max} + \Delta C_{Lmax} \tag{8.19}$$

$$\alpha_s = \frac{C_{L\ max}}{C_{L_\alpha}} + \alpha_{0L} \tag{8.20}$$

For the eVTOL concepts, since they all have a very low leading edge sweep, the $\left[\frac{C_{L\ max}}{C_{l\ max}}\right]$ ratio can be estimated to be 0.9[41]. ΔC_{Lmax} is a constant to account for compressibility effects, however, due to the low speed of the aircraft which is below 0.2 M during both cruise and landing, this term can be ignored. For the double wing concepts this formula had to be modified to account for the effect of the down wash. This

is shown in equation 8.21.

$$C_{L\ max} = s_1 \left[\frac{C_{L\ max}}{C_{l\ max}}\right] C_{l\ max} + s_2 \left[\frac{C_{L\ max}}{C_{l\ max}}\right] C_l \left(\alpha_s - \frac{d\epsilon}{d\alpha}\alpha_s\right) \tag{8.21}$$

The lift curve characteristics for the table can be observed in the table below:

Table 8.3: Lift curve characteristics for the double and single wing.

	Single wing	**Double wing**
α_{0L}	0.008	-2.622
C_{L_α}	4.908	4.910
C_L for $C_{d_{min}}$	0.2401	0.2927
α_s	16.96	17.90
$C_{L_{max}}$	1.452	1.759

8.3. Class II Drag Estimations

For the class II drag estimation the component drag method is used. This method divides the drag into its different sources and allows for a more accurate estimation of the drag polar of the aircraft. The first component is the skin friction drag, which can be calculated separately for the fuselage and the wing and then summed [41]. This is shown in equation 8.22.

$$C_{D_0} = \frac{1}{S_{ref}} \sum_c C_{f_c} \cdot FF_c \cdot IF_c \cdot S_{wet_c} + C_{D_{misc}} \tag{8.22}$$

Here, FF is the form factor for estimating the pressure drag due to viscosity, the interference factor , IF is the interference factor to take into account the drag resulting from the interactions of different components and S_{wet} which is the wet surface area of the component. C_f, the skin friction coefficient is computed based on the Reynolds number and the type of flow. For the fuselage it was assumed that 10% of the flow is laminar, while for the wing 35% of the flow was assumed to be laminar [41]. Then the skin friction coefficient can be computed using equation 8.23.

$$C_f = \begin{cases} \frac{1.328}{\sqrt{Re}} & \text{Laminar} \\ \frac{0.455}{(\log Re)^{2.58}(1+0.144M^2)^{0.65}} & \text{Turbulent} \end{cases} \tag{8.23}$$

For the wet area of the fuselage a preliminary sizing of the fuselage was used. A width of 1.3 m and a height of 1.6 m were used, as well as a length of 4 meters. By assuming a parabolic shape for the first 2 meters and a conical shape for the last 2 meters the wet area was obtained using the following formula [41]:

$$S_{w,f} = \frac{\pi D}{4}\left(\frac{1}{3L_1^2}\left[\left(4L_1^2 + \frac{D^2}{4}\right)^{1.5} - \frac{D^3}{8}\right] - D + 4L_2 + 2\sqrt{L_3^2 + \frac{D^2}{4}}\right) \tag{8.24}$$

Where L1 is the length of the parabolic section, L2 is the length of the cylindrical section and L3 is the length of the conical section. Another drag component that will be used is the base drag of the fuselage, which can be estimated using the formula presented below. Where, A_{base} is the base area of the fuselage, for which a value of 0.04 m^2 is estimated based on the preliminary fuselage design, as presented in Section 11.4, and M is the Mach number during cruise.

$$C_{D_b} = \frac{\left[0.139 + 0.419(M - 0.161)^2\right] A_{\text{base}}}{S_{ref}} \tag{8.25}$$

Another component for the drag is the upsweep drag, which from empirical data can be estimated according to Equation 8.26 [41]. For the upsweep, a few assumptions were made from the drawings. Assuming a cone length of 3 meters and a vertical distance of 0.7 meters between the centre of the fuselage cross-section and the most aft point of the fuselage, a value for u of 0.229 radians is obtained [41]. Finally, the last drag component is the induced drag due to lift. Since the airfoil chosen is cambered, Equation 8.2 has to be slightly modified to better simulate the behaviour of the cambered wing:

$$C_{D_u} = \frac{3.83u^{2.5}A_{\max}}{S_{ref}} \tag{8.26}$$

$$C_{D_i} = \frac{(C_L - C_{L\ C_{D\ min}})^2}{\pi ARe} \tag{8.27}$$

Where e, the Oswald efficiency factor is calculated using the same method as discussed in section 8.1. However, the reference Oswald efficiency factor was recalculated using the formula below [41]:

$$e = 1.78\left(1 - 0.045AR^{0.68}\right) - 0.64 \tag{8.28}$$

This yields the following results for the drag components for the different configurations:

Table 8.4: The components of minimum drag, the constant of the drag polar and the maximum lift over drag ratio for all three configurations.

	Tandem wing	**Box wing**	**Single wing**
C_{D_0} [-]	0.0168	0.0170	0.0150
C_{D_u} [-]	0.0150	0.00144	0.00127
C_{D_b} [-]	0.000530	0.000510	0.000449
$C_{D_{min}}$ [-]	0.0324	0.0320	0.0283
$C_{D_{min}}S_{ref}$ $[m^2]$	0.343	0.351	0.352
K [-]	0.0402	0.0387	0.0421
$\frac{C_L}{C_{D\ max}}$ [-]	19.1	19.5	19.3

The drag polar can then be plotted for the three different configurations as shown in figure 8.1. This results are then used to calculate the energy needed from the battery during the mission as presented in Chapter 7, which is one of the criteria considered in Chapter 17.

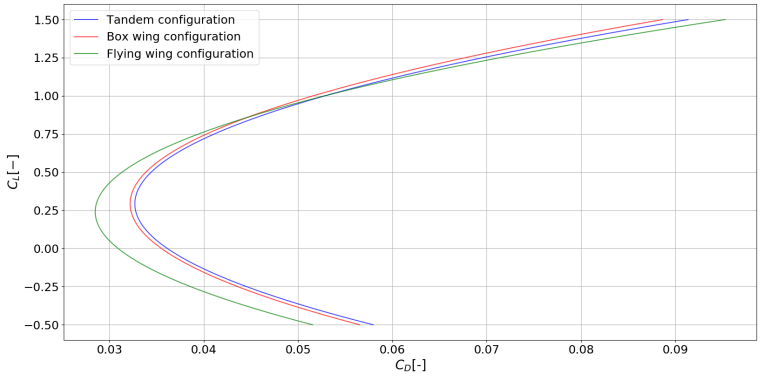

Figure 8.1: The drag polars for the 3 different concepts based on their current geometry.

8.4. Sensitivity Analysis

An important wing parameter which was chosen, and therefore, for which a sensitivity analysis can be insightful, is the aspect ratio. The change in the maximum aerodynamic efficiency of the aircraft configurations based on the aspect ratio of the wing planform can be observed in Figure 8.2:

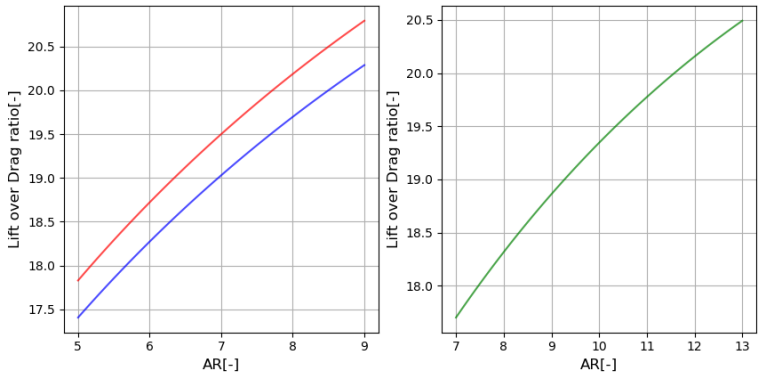

Figure 8.2: Aspect ratio against maximum lift over drag for the three configurations. The tandem and box wing are placed on the left graph, where as the single wing is on the right graph. The colour code is the same as for the previous figure.

As can be discerned, higher aspect ratio results in a greater aerodynamic efficiency; however, this improvement can be observed to decline the greater the aspect ratio, as a higher aspect ratio also causes the Oswald efficiency factor to become lower. Another aspect of the wing affected by the aspect ratio is the lift slope. By increasing the aspect ratio, the lift slope of the aircraft is increased, however, the effect is not too significant. For the double wing concepts an increase of AR from 7 to 7.5 causes a 0.87% increase in C_{L_α} for the single wing, a 0.9% increase.

Another significant parameter, which is not related to the wing is the fuselage upsweep. It is clear from testing different upsweep numbers that excessive upsweep can result in large amounts of drag. Also, the sensitivity of this number has been tested to be high according to semi empirical methods . Using the preliminary calculation method provided by Equation 8.26, an increase of 1 degree in the upsweep from the currently assumed value can lead to an increase of approximately 9 % in the parasitic drag of the aircraft. Thus, reducing this parameter as much as possible during the next design phase will be important.

8.5. Verification and Validation

This section will focus on describing the procedures planned for verification and validation of the aerodynamic behaviour of the eVTOL design.

8.5.1. Verification and validation for preliminary design tools.

Currently, a number of procedures have been created for the current code of the design tools. Firstly, for code verification, the compiler checks that no syntax errors exist in the code. Apart from this, a number of unit tests are coded to test different calculations that are made during aerodynamic design some of this calculations are for instance: zero lift drag, the drag polar, the lift slope, and the wing planform characteristics. These tests work by using test values as inputs for functions, or by checking that the functions respond as expected to changes in value, for instance, a higher aspect ratio should result in a higher lift slope.

8.5.2. Verification plan

For code verification, the current tests will be refined if needed due to changes in the functions, furthermore new tests will have to be made for new units of code, such as the effect of the propellers on the lift curve, the fuselage wing interaction and the wing wing interaction. For calculation verification the quality of the models used, and therefore its results will be assessed. In order to do this, the plan is to use CFD simulation of the model to obtain the lift and drag characteristics of the design using a CAD model. At the same time, the results from the CFD simulation will be used to iterate on the model and generate a new design, which will then again be verified using a CFD simulation.

8.5.3. Validation plan

For the validation of the aerodynamics there are three main steps planned. Firstly, after the DSE, it is planned to carry out a qualitative wind tunnel experiment using a 3D printed model of the aircraft based on the CAD model of the final design. This test will not provide quantitative validation, but it will prove whether the behaviour of the airflow around the aircraft occurs as expected from the CFD simulations. The next step would be to create a bigger model of the aircraft that can be tested in a bigger wind tunnel with

higher speeds, this will give a more accurate depiction of the aerodynamic forces and moments acting on the vehicle. The final step is to do a test flight once the first prototype has been manufactured to provide flight test data which can validate whether the aerodynamic characteristics of the final aircraft are accurately predicted by the models and simulations.

9 Propulsion and Power

This chapter will cover the preliminary design and trade-off of the power and propulsion subsystems. In Section 9.1, the power subsystem will be discussed. The second section is about the propulsion system. Finally, Section 9.3 will discuss the verification and validation methods for both subsystems.

9.1. Power Subsystem

The first subsystem is the power subsystem, which provides power and energy to the aircraft. This section will discuss the different options for the power subsystem of the aircraft, and how the trade-off was made.

9.1.1. Options

For energy storage, several different options were considered. The two main options that were considered were batteries and hydrogen fuel-cells. Besides these two options, a third option to be consider are supercapacitors. However, supercapacitors are primarily suitable for bursts of power during short periods, and not for the long periods of relatively low power required for most of the mission. Therefore, they will be considered as a source of peak power during the final design but not as the primary energy storage system, so they are excluded from this trade-off.

9.1.2. Hydrogen fuel-cells versus batteries

This subsection will qualitatively assess the differences between batteries and hydrogen fuel-cells. One major difference between these two is in the volumetric energy density. While batteries do not excel in volumetric energy density, hydrogen has a very low volumetric energy density compared to other chemical fuels too, which means that large tanks are required to be able to achieve sufficient range. Moreover, when the mass of the storage tanks and the fuel-cell system, and the efficiency of the fuel-cell are included in this energy density, the numbers worsen. This is unpractical and requires a lot of room inside the aircraft for storage, which gives more wetted area and thus more drag(and increased weight for the structure). While in terms of theoretical limits hydrogen can surpass batteries in this aspect, the currently available technology for hydrogen fuel cells features low efficiencies that make it a worse option, increased by the big efficiency losses during hydrogen production, compression, and in the fuel-cell itself [62].

The second, and probably the most important point, is the infrastructure. For batteries, most of the needed infrastructure is already there. The electrical grid is readily available, charging stations are plenty and not hard to construct, and batteries can even be charged at home. For hydrogen, this is not the case. Very extensive and costly infrastructure would be required, which would difficult the introduction of the vehicle into society. It would also reduce the versatility of the vehicle, since it would only be able to operate in routes where hydrogen stations are available. All of this goes against the mission statement of this project [1]. One of the advantages of an eVTOL aircraft is the ability to take-off and land in many places. Lastly, the technology to produce enough green hydrogen and its infrastructure into the market is not fully ready yet, so it is not guaranteed that hydrogen will be widely available soon enough.

A third concern with hydrogen is the safety regarding storage [43]. There are two ways of storing hydrogen, as a gas or as a liquid. For storing the hydrogen in a gaseous state, a highly pressurised tank is needed. The lower pressures required for cryogenic liquid storage reduce the likelihood of structural failures due to fatigue in the tanks [50]. However, the cryogenic temperatures are a risk since they can injure a person upon touch, plus they require even more costly and complex infrastructure. A lot of care must be put into making sure no hydrogen can leak into the part of the fuselage where people are sitting, which would increase the weight of the aircraft [51]. Lastly, this kind of storage required energy, which results in reduced overall efficiency of the system. On the other hand, batteries, especially lithium ones, are also subject to safety concerns, such as fire and explosions.

Hydrogen fuel-cells also need a lot of development. Their real efficiency is far from their theoretical one; they are expensive, as they commonly use platinum as a catalyst; their performance is very sensitive to pollution of the air entering the system, which can result in significantly reduced performance [9] and thus can be a problem for a vehicle operating in urban environments.

All in all, hydrogen needs more development before it is a feasible option. In the long-term fuel-cells might become a superior option, but for the foreseeable future, batteries are the best option, due to their higher current performance, better safety and most importantly their better practicality in terms of infrastructure.

9.1.3. Battery trade-off

The battery trade-off consists of a quantitative part and a qualitative part. This section will first do a quantitative trade-off, and then mention one qualitative aspect, safety. There are four different types of batteries that were considered as the energy storage system: lithium-ion, lithium-sulfur, lithium-metal and solid state lithium batteries. For the numerical trade-off, five properties of these batteries were considered. The batteries and their properties can be found in Table 9.1.

Table 9.1: Battery characteristics for the different types considered in the trade-off. [31], [37], [60], [64], [67]

	Li-ion	**Li-sulfur**	**Li-metal**	**Solid state**
Specific energy density [Wh/kg]	250	550	500	500
Volumetric energy density [Wh/l]	650	650	1000	1000
Power density [W/kg]	1000	10000	1000	10000
Operational life [cycles]	1000	800	800	10000
Cost [$/kg]	80	87	100	100

The specific energy density is important, because a higher specific energy density results in a lower OEW for the aircraft, which results in better performance. A higher volumetric energy density results in smaller overall batteries, which makes positioning them inside the aircraft easier. A higher power density means that there is more power available for a given battery mass, which means a higher peak power. A higher number of cycles in the operational life means that the battery can perform at an acceptable level for longer, which is better both for maintainability and costs. A lower cost per kilogram will give a less expensive battery, which is good as this allows to reduce the price per battery.

For the trade-off, the specific energy density of the batteries was considered most important, followed by the volumetric energy density and power density. The operational life was deemed less important, as most batteries have suboptimal performance in this aspect, and the batteries can be replaced if needed. The cost was ranked with the lowest weight, since the battery cost is a small part of the total cost of the aircraft and because the cost values are future estimates that depend on a lot of factors, and hence not as reliable as other metrics. This resulted in the trade-off weights that can be found in Table 9.2.

In this trade-off, Li-ion batteries where used as the reference battery, since they are the most popular type nowadays, and the other batteries where bench-marked against it. Thus, Li-ion has a score of 1. The results of this trade-off can be seen in Table 9.3.

Table 9.2: Trade-off weights for the battery trade-off

Property	**Weight**
Specific energy density [Wh/kg]	1
Volumetric energy density [Wh/l]	0.8
Power density [W/kg]	0.8
Operational life [cycles]	0.5
Cost [$/kg]	0.3

Table 9.3: Results from the battery trade-off

Battery type	**Score**
Lithium-ion	1.0
Lithium-sulfur	3.4
Lithium-metal	1.4
Solid state (Lithium)	4.8

Besides the quantitative trade-off requirements mentioned above, on a quantitative basis, the different levels of safety of the batteries will be assessed. In general, solid-state batteries are deemed safer than the liquid batteries, and a lot of research is being conducted to improve the safety even further [59]. Since solid state is a very new battery technology, large steps are still possible in terms of development.

As can be seen in Table 9.3, the solid state battery option is the best one from a quantitative point of view. From Table 9.7 the total required energy can be found, and thus the total battery mass and volume per configuration can be found in the table below.

Table 9.4: Required battery mass and size for the different configurations, based on solid-state batteries

	Tandem wing	**Box wing**	**Single wing**
Required battery mass [kg]	483	575	402
Required battery volume [m^3]	0.242	0.288	0.201

9.1.4. Sensitivity analysis

In this subsection, a sensitivity analysis is conducted for the battery trade-off. By doing the same calculations with different weights, the following observations were made. The specific energy density has the highest weight of the trade-off criteria, see Table 9.2, but changing the weight does not influence the result of the trade-off dramatically, since the specific energy densities are close to each other. The only exception is lithium-ion, which has a significantly lower energy density. The same goes for volumetric energy density, where lithium-metal and solid state perform better, but a change in weight does not alter the outcome of the trade-off. Cost also does not have a major impact on the trade-off, both due to the little variance between the different options and the low weight of this trade-off criterion.

The two trade-off criteria which are most sensitive are power density and operational life. The power density for lithium-sulfur and solid state is an order of magnitude higher than the other options, so a small change in trade-off weight results in a significant change in the final score. However, the ranking of the results does not change.

9.2. Propulsion Subsystem

This section will discuss the different propulsion concepts for the trade-off, and will give both a qualitative and quantitative analysis of the different configurations.

9.2.1. Configurations

There are three different configurations that will be discussed. Drawings of these concepts can be seen in Figure 5.1a, Figure 5.1b and Figure 5.1c. The drawings give an overview of the configuration, but do not contain the accurate details in terms of e.g. number of engines. The tandem wing configuration features distributed propellers over both wings. The propellers are unducted and are mounted on the leading edge of the wings. There are 16 engines in total, equally distributed over the two wings. The box wing configuration also features distributed propulsion, but in the form of 24 ducted fans. The fans are positioned on the top side of the wings, mounted on a flap, and are equally distributed over both wings. The single wing configuration has two engines inside the wings, which are only active during take-off and landing. It also features four bigger tilting engines, two near the front of the fuselage and two near the rear, which provide thrust during cruise and rotate to also work during take-off and landing.

9.2.2. Comparison of the configurations

The advantages and disadvantages of each of the configurations can be seen in Table 9.5. The majority of these advantages and disadvantages cannot be analysed quantitatively during the preliminary phase of this project, since they are very dependent on the exact geometry of the aircraft or consist of non-linear couplings between the propulsion and aerodynamic subsystems, but considering all of them is of paramount importance to perform a proper trade-off of the system.

Table 9.5: Advantages (+) and disadvantages (-) of each configuration in different aspects of the system

	Tandem wing	**Box wing**	**Single wing**
Disk loading	± Medium disk loading	- High disk loading reduces efficiency in hover	+ Lower disk loading increases efficiency in hover
Noise	- Unducted, so no possibility to install acoustic liners	+ Ducts allow for acoustic liners, which can reduce noise	+ Ducts allow for acoustic liners, which can reduce noise
Distributed propulsion	+ Propellers distributed over the leading edge increase the flow speed over the wing, which increases the lift and allows to reduce the wing surface + The flow from the engines can help reduce pressure drag	+ Fans on the trailing edge of the wing can reduce the pressure drag of the wing + The suction of the fans can accelerate the air over the upper surface of the wing, which can help to increase lift + The suction from the fans can potentially reduce or avoid flow separation over the wing + The fans ingest the boundary layer, which increases propulsive efficiency	+ The front row of engines can increase the flow speed over the wing, which can help to increase lift - No distributed propulsion and engines are placed away from the wing, so propulsion-wing interaction effects are smaller
Engine placement	+ Wings can be placed at different heights, which can avoid the second row of engines ingesting the slipstream of the front row	+ Wings are placed at different heights, which can avoid the second row of engines ingesting the slipstream of the front row	- Due to the engine size, it is difficult (and possibly unfeasible) to avoid slipstream ingestion in the second engine, which can result in significant loss of thrust
Redundancy	+ Distributed propulsion with a large number of engines increases the redundancy of the system	+ Distributed propulsion with a large number of engines increases the redundancy of the system	- The lower number of engines reduces the redundancy of the system, and can be critical in OEI conditions

9.2.3. Actuator disk theory

Actuator disk theory is a simple model to obtain preliminary propeller performance characteristics. The propeller is modelled as a propeller with infinitely many blades through which flow gets accelerated with a smooth increase in pressure, and thrust is provided from the exchange in momentum [55]. The theory assumes incompressibility, a discontinuous change in pressure and steady flow. The rotation effects from the blades are also assumed to be negligible, so only axial losses (and not viscous and swirl losses) are accounted for, which leads to high estimated efficiencies.

The disk loading is the ratio between the aircraft weight and total rotor disk area. A higher disk loading results in a lower efficiency [32]. The disk loadings assumed give a value for the total required propulsive area, and are based on other reference aircraft [17]. It is assumed that in hover the inflow velocity is zero. Thus, the exit velocity can be obtained with Equation 9.2:

$$A_{total} = \frac{MTOM}{\text{Disk loading}} \tag{9.1}$$

$$V_{e_{hover}} = \sqrt{\frac{2 \cdot MTOM \cdot g_0}{\rho \cdot A_{total}}} \tag{9.2}$$

Each of the configurations has an assumed number of rotors, which is fixed for this stage of the design. If configurations 1 or 2 are selected for the final phase, this number will be optimised, and if the single wing configuration is selected, this number will remain fixed. The area per rotor is found by dividing the total area over the number of rotors, since the actuator disk theory assumes that all of the area has the same effect. The inner section of the rotors, which houses the shaft that connects the propeller to the engines, does not contribute to the thrust generation, So this has been accounted for when calculating the propeller radii Equation 9.4.

$$A_{rotor} = \frac{A_{total}}{N_{rotors}} \tag{9.3}$$

$$r = \sqrt{\frac{A_{rotor}}{\pi(1-\phi_h^2)}} \tag{9.4}$$

where ϕ_h represents the ratio between the hub radius and the external propeller radius, a value which has also been assumed. The next step is to calculate the efficiency of the propulsion system in cruise. For this Equation 9.6 is used. V_0 is the freestream velocity, and V_e is the flow velocity after the propulsion system. The flow speed after the propulsion system is calculated in Equation 9.5.

$$V_{e_{cruise}} = \sqrt{\frac{2 \cdot T}{\rho \cdot A_{total}} + V_0^2} \tag{9.5}$$

$$\eta_{cruise} = \frac{2}{1 + \frac{V_0}{V_e}} \tag{9.6}$$

The efficiencies obtained can be found in Table 9.6, together with the disk loading, number of engines, area per engine. The efficiencies are all high, which is because the viscous losses, tip losses and swirl losses are neglected, as mentioned at the start of the section.

Table 9.6: Analysis of each configuration through actuator disk theory. For the single wing configuration, the first number is for the tilting rotors, and the numbers between brackets are for the engines inside the wings, if applicable.

	Tandem wing	**Box wing**	**Single wing**
Disk loading [kg/m^2]	250	1000	80
Number of engines [-]	16	24	4 (2)
Propeller area per engine [m^2]	0.47	0.0809	5.3452 (0.5279)
Propulsive efficiency cruise [-]	0.98	0.934	0.993

9.2.4. Required power and energy

The next step is to calculate the power and energy required for each configuration for the mission. For the power required for hover, the equations below were used. For this, Equation 9.7 was used for ducted engines, and Equation 9.8 was used for open propellers. These equations have been obtained from [38], a paper which performs a similar propulsion analysis for the Lilium jet. In these equations T_h is the thrust required for hover, which is equal to the MTOW of the aircraft; ρ is the air density, which was assumed to be at ISA sea level conditions for hover, n is the number of engines and A_{prop} is the area per propeller.

$$P_h^{ducted} = \frac{T_h^{3/2}}{2\sqrt{\rho \cdot n \cdot A_{prop}}} \cdot \frac{1}{\eta_{hover}} \tag{9.7}$$

$$P_h^{open} = \frac{T_h^{3/2}}{\sqrt{2 \cdot \rho \cdot n \cdot A_{prop}}} \cdot \frac{1}{\eta_{hover}} \tag{9.8}$$

To calculate the required power for cruise, Equation 9.9 was used, which was also obtained from [38].

$$P_{cruise} = D_{cruise} \cdot \frac{V_{cruise}}{\eta_{cruise}} \tag{9.9}$$

To obtain the maximum required power, Equation 9.7 and Equation 9.8 were used, using the maximum thrust instead of the hover thrust. The maximum thrust is calculated as $T_{max} = MTOW \cdot \frac{T}{W}$, where $\frac{T}{W}$ is the maximum thrust-to-weight ratio. This value was assumed to be 2.5 for all configurations, based on some preliminary acceleration calculations (i.e. thrust required to achieve a vertical acceleration of 15 m/s^2).

The required energy to provide this power for the entire operations was calculated by multiplying the required power per phase with the time the phase takes, as shown below.

$$E_{req} = P_{req} \cdot 1.2 \cdot t_{phase} \cdot \frac{1}{1000} \tag{9.10}$$

In this equation, the P_{req} is in W, the t_{phase} in h and E_{req} in kWh. The power includes a factor of 1.2 to account for other electrical systems in the aircraft, such as the avionics or the environmental control for the cabin. The required time for vertical flight was assumed to be 4 minutes for the whole mission (i.e. one minute for take-off, one minute for landing, and two minutes for transition). Transition was assumed to require the same power as vertical flight as a preliminary estimate. For cruise, the time was calculated based on the cruise velocity and a distance of 300 km, $t_{cruise} = 300 \cdot 1000 \cdot V_{cruise}$.

Table 9.7: Overview of required power and energy for the configurations

	Tandem wing	**Box wing**	**Single wing**
Cruise power [kW]	110	114	102
Hover power [kW]	1178	1755	640
Maximum power [kW]	4655	6938	2530
Energy for cruise [kWh]	163	171	159
Energy for hover [kWh]	79	117	43
Total required energy [kWh]	242	288	201

9.2.5. Noise analysis

In this subsection the noise of the propulsion subsystem will be analysed. The aircraft will operate in an urban environment, and thus the noise of the aircraft is an important trade-off parameter. To get a quantitative measure of the noise, Equation 9.11 is used [52].

$$\text{SPL}_{1,\text{max}} = 83.4 + 15.3 \log_{10} P_{br} - 20 \log_{10} D + 38.5 M_t - 3(B-2) + 10 \log_{10} N_p. \tag{9.11}$$

This equation gives the maximum sound pressure level at 1 m from the source. P_{br} is the engine power in kW, D is the propeller diameter in m, B is the number of blades of a propeller and N_p is the number of propellers. M_t is the rotational tip Mach number, which can be computed with the following formula:

$$M_t = \frac{\pi D}{c} \frac{n_p}{60} \tag{9.12}$$

Where n_p is the rotational velocity of the propeller in rpm and c is the speed of sound m/s. For equation Equation 9.11 the number of propellers was assumed to be one.

The procedure to calculate the noise differed slightly per configuration. P_{br}, D and N_p have been obtained the same way for all configurations. For P_{br}, the total power for cruise and hover has been calculated in Section 9.2.4, and this value was divided by the number of engines to obtain P_{br}. The propeller diameter D has been calculated in Section 9.2.3. N_p is the number of propellers per engine, which is 1 for all configurations.

The first difference is the number of blades per propeller, which differs per configuration. The first thing worth noting here is that the number of blades per propeller is a design choice that needs to be optimised in the final phase of the project. Thus, the values used for this calculation are reasonable estimates, but not necessarily the values that will be used for the final design. For the tandem and single wing configurations, the number of blades was assumed to be 5. This value is higher than the average number of blades used in

propellers or helicopter rotors, which tends to be 2 or 3, but not uncommon, since it is the same than the one used for the new version of the Airbus H145 [27]. This higher than average number is justified by the higher disk loading of these configurations when compared to average helicopters. The box wing configuration has a much higher disk loading and uses fans (which by definition have more blades than propellers), so the number of blades was higher, 16 per propeller. As seen in Equation 9.11, a higher number of blades means lower noise, which can be explained by the fact that the acceleration of the air passing through the propeller is done by more blades, which means a smaller pressure increment per blade and hence lower noise.

The second difference comes from the limits for tip Mach number. For this analysis, the Mach number of the tip, in Equation 9.11, has been selected based on the allowable limit for the propeller tip speed (based on efficiency limits). The tandem and single wing configurations use conventional propellers, while the box wing configuration uses fans (more blades with wider tips). Conventional propellers start to suffer big tip loses at around Mach 0.7-0.8, while fans have lower limits for tip speed [24]. Hence, the value for M_t for each configuration is different. For tandem and single wing, M_t is 0.7, whereas for the box wing this value is 0.55. Lower tip speeds mean less noise, which means that this particular metric poses and advantage for the box wing configuration. Based on these numbers, the maximum rpm of the propellers were calculated using Equation 9.12. These maximum numbers were assumed to be at hover, so the next step was to calculate the rpm (and hence M_t) at cruise. For the tandem and single wing configurations, due to the bigger size of the propellers, it was assumed that variable pitch propellers could be used, meaning that the rpm stays constant throughout the mission, thus so does M_t. For the box wing configuration, due to the small fans, this was not possible, so in order to reduce the thrust for cruise the rpm need to be reduced, which results in a lower thrust. For this preliminary analysis, it was assumed that the rpm of the engine vary linearly with thrust, and hence with $P^{2/3}$ (see Equation 9.7). Thus, the ratio of cruise to hover power was calculated, and from that the cruise rpm were obtained. Then, M_t was obtained using this value in equation Equation 9.12.

The last thing to mention is that for the single wing configuration the noise of the tilting and wing engines was calculated separately.

This resulted in the estimated noise values per engine. Consequently, to calculate the total noise of each configuration, the noise values for each individual engine were added using Equation 9.13, where L represents the noise in dB.

$$L_{tot} = 10 \log_{10} \left(\sum_{i=1}^{n} 10^{(L_{prop,\ i}/10)} \right) \tag{9.13}$$

The final noise values can be found in Table 9.8. Note that for the single wing configuration, the value between brackets is the noise for the propeller podded in the wing.

Table 9.8: Overview of noise levels, both per propeller and in total for each configuration.

	Tandem wing	**Box wing**	**Single wing**
Noise per propeller in cruise [dB]	114.4	63.1	119.3 (-)
Total noise in cruise [dB]	126.5	76.9	125.4
Noise per propeller in hover [dB]	128.4	96.6	130.8 (110.8)
Total noise in hover [dB]	140.4	110.4	136.8

These values have been calculated for open, isolated propellers. The box and single wing configurations use ducts, which can provide a reduction in noise if properly designed (e.g. installing noise liners). Based on literature and the Lilium jet [33], the ducts for the box wing can be expected to reduce noise levels by 5-10 dB in certain conditions. For the single wing configuration, the size and length of the ducts is smaller than in the box wing with respect to the propeller size, and thus a smaller noise reduction can be expected, <5 dB. However, the noise reduction from ducts is heavily dependent on the design and materials from the ducts, as certain frequencies might even be amplified, which means that these values cannot be estimated quantitatively at this stage. Furthermore, the noise variations due to propeller-propeller interactions cannot be modelled within the scope of this project.

As a closing remark, it is important to critically assess these values and to note that Equation 9.11 is an empirical equation based on propellers installed on conventional aircraft, which means that its accuracy for distributed propulsion and eVTOL aircraft is most likely reduced. Moreover, metrics such as the number of blades and the rpm of the propeller are heavily dependent on the propeller and blade design, which at this

stage of the project has not been determined in detail, which means that these values might be significantly different from those of the final configuration. Furthermore, the box wing configuration achieves the lowest noise level from all options, while it has a significantly higher disk loading, which translates into higher pressure increase to the flow per area and higher downwash speeds, and thus into (expected) higher jet noise, which is not directly seen in the values of Table 9.8. Therefore, in the final phase of the project this noise estimation needs to be revisited and improved.

However, as a means to perform a noise comparison between the configurations, this approach provides a good first estimate of the noise performance of each configuration that can be used in the trade-off.

9.2.6. Sensitivity analysis

This subsection will analyse the variation in the outputs from the previous subsection with respect to a change in thrust-to-weight ratio, disk loading and the number of engines, since these values have been assumed and not calculated.

The first parameter to look at is the thrust-to-weight ratio. This parameter is only a direct influence for maximum power. However, the maximum required power is very sensitive to changes in the thrust-to-weight ratio. Halving or doubling the thrust-to-weight ratio results in a maximum power ranging of 60 and 180 % of the original value respectively, for all configurations.

The disk loading has an effect on multiple parameters. The disk area has an inverse relation with the disk loading, which can also be observed from Equation 9.1. The hover power changes significantly, as doubling the disk loading results in 30 % more required power. The cruise power does not change. The total energy required, and thus also the battery mass and volume, change considerably less, around 10 % when halving or doubling the disk loading.

The change in number of engines has been evaluated for the tandem and box wing configurations. For the single wing configuration the number of engines is fixed. The disk area per propeller is related to the number of engines as described in Equation 9.3. The area per engine is the only parameter that changes.

The conclusion from this analysis is that the disk loading is the most critical parameter from the ones evaluated, since changing its value results in big changes on multiple other parameters. As a result, for the final phase the assumed values will be refined to ensure a correct disk loading is used.

9.3. Verification and Validation

This section is about the procedures for the verification and validation of the propulsion and power analysis.

9.3.1. Verification and validation for preliminary design tools.

Verification can be divided in code verification and calculation verification. The code verification is done to ensure that there are no programming errors within the code. First of all, the compiler automatically checks for syntax errors. For other types of errors, a number of unit tests have been written to test different parts of the programs to make sure they work as intended. These tests include sanity checks such as verifying that flow is accelerated when thrust is positive, that battery mass and volume are positive and that none of the required energies are negative. Moreover, they include checking that a modification in certain parameters has the expected effect in the calculations.

9.3.2. Verification plan

For the calculation verification the equations will be compared against results for which the answer is known. Additionally, a comparison between the models used for this report and other models, such as the DFDC model [66], will be made. For the final design, a more elaborate calculation method will be used, which will require more in depth verification. To verify the noise computations, a comparison with models will be made. Chauhan and Martins [8] and Nathen, Bardenhagen, and Taylor [38] both give power values that are significantly lower than the values obtained in this report, which is an indication that more refinement is needed to obtain an accurate model.

9.3.3. Validation plan

To validate the model, firstly a comparison of the simulations with data from other comparable aircraft will be made. Later in the development process, prototype and model tests need to be performed to validate the simulations. These include wind tunnel tests to validate the simulations on the aerodynamic effects of the propulsion subsystem and its interaction with the aerodynamic surfaces, and flight tests to evaluate the performance of the subsystems on real mission conditions. These tests also need to measure other metrics,

such as required power, energy consumption and noise levels under real conditions. However, these tests cannot be performed within the scope of the DSE.

10 Stability and Control

In this chapter, the three concepts will be investigated in terms of their stability and control characteristics, to see if there are any significant differences which will be utilised for the Trade-off (see Chapter 17) as a main selection criterion. Section 10.1 describes controllability in each of the different flight phases (hover, horizontal flight, and transition). Only with a controllable aircraft can closed-loop stability be achieved. In Section 10.2, the possibility of achieving open-loop stability is being investigated. This is not realistic for all flight phases, but could be desirable to simplify controller design and improve safety.

10.1. Controllability and Closed-Loop Stability

This section investigates the available control inputs in each flight phase per configuration, and the conditions under which controllability can be achieved. This is also important to ensure closed-loop stability, since a control system can only counteract disturbances effectively if the aircraft is controllable. In Section 10.1.1, controllability in hover is investigated, while Section 10.1.2 and Section 10.1.3 analyse horizontal flight and transition, respectively.

10.1.1. Controllability in hover

In hover mode, the oncoming airspeed experienced by the vehicle is very low. Therefore, aerodynamic control surfaces are not an effective means of control and thrust vectoring and differential thrust must be used. In order to quantify the controllability of the eVTOL in hover, the Available Control Authority Index (ACAI) developed by Du et al. [12] is used. It was designed to evaluate available control authority of hovering multirotor vehicles with fixed rotors. While the eVTOL concepts can all tilt some of their rotors, neglecting this possibility for hover control simplifies the analysis considerably while also being conservative.

Du et al. [12] model the dynamics of a hovering multicopter using a state-space system of the form given in Equation 10.1. 8 states are considered, which are given in Equation 10.2. These include the altitude h, the roll angle ϕ, the pitch angle θ, the yaw angle ψ, the vertical speed v_h, the roll rate p, the pitch rate q, and the yaw rate r. Equation 10.3 shows the control variables, which are the total thrust force T, the roll moment N, the pitch moment M, and the yaw moment L. The weight $m_a \cdot g$ is also included in this vector for the sake of convenience.

$$\dot{\boldsymbol{x}} = A\boldsymbol{x} + B\boldsymbol{u} \tag{10.1}$$

$$\boldsymbol{x} = \begin{bmatrix} h & \phi & \theta & \psi & v_h & p & q & r \end{bmatrix}^T \tag{10.2}$$

$$\boldsymbol{u} = \boldsymbol{F} - \boldsymbol{G} = \begin{bmatrix} T & L & M & N \end{bmatrix}^T - \begin{bmatrix} m_a \cdot g & 0 & 0 & 0 \end{bmatrix}^T \tag{10.3}$$

According to Du et al. [12], it must hold that ACAI > 0 for multirotor controllability in hover.

The procedure for calculating the ACAI is described in [12] in detail. The calculation was implemented in Python using the Matlab Toolbox [13] developed by the authors of [12] as an example and means of verification. At this point, only the inputs required to perform the calculation are listed in Table 10.1. Note that since the origin of the coordinate system is the centre of mass, this is also implicitly an input to the calculation.

Tandem wing

In order to calculate the ACAI of the tandem wing configuration, it was assumed that the rotors are the front and aft extremities of the fuselage, and evenly spaced between the wingtips. k_μ was assumed to be 0.1 based on the values used by Du et. al [12]. As for the direction of rotation of the propellers, they were all taken to be rotating inboard.

The resulting ACAI value was 906.9. The minimum number of rotors that are allowed to fail to bring this number to 0 is 3 (if they are all located on one half-wing). This could be improved further by choosing different senses of rotation for the rotors, e.g., an alternating pattern which yields ACAI = 1884.9 and can tolerate 4 rotor failures. However, this would also strongly affect the rotor-rotor and wing-rotor interactions. Therefore, this optimisation will be performed later in the design process.

Table 10.1: Input parameters to the calculation of the ACAI [12].

Symbol	Description
$x_1, x_2, \ldots, x_m$	x-position of each rotor w.r.t the centre of mass
$y_1, y_2, \ldots, y_m$	y-position of each rotor w.r.t the centre of mass
$K_1, K_2, \ldots, K_m$	Maximum thrust of each rotor
k_μ	Ratio between reactive torque and thrust of a rotor
$w_1, w_2, \ldots, w_m$	Direction of rotation of each rotor
$\eta_1, \eta_2, \ldots, \eta_m$	Efficiency parameter of each rotor
m_a	Vehicle mass

A sensitivity analysis (see Figure 10.1a) revealed that the eVTOL remains controllable for all centre of mass positions within the fuselage length (and up to 2.75% outside of it). This is due to the high thrust-to-weight ratio of the aircraft. However, failure tolerance is reduced if the centre of mass is located at the extremities of the fuselage. As Figure 10.1b shows, three rotor failures on the rear starboard wing push the aft limit of the centre of mass forward to 34.4% of the fuselage length. Therefore, to retain the ability to tolerate any three engine failures, the centre of mass should be within 34.4% and 65.6% of the fuselage length.

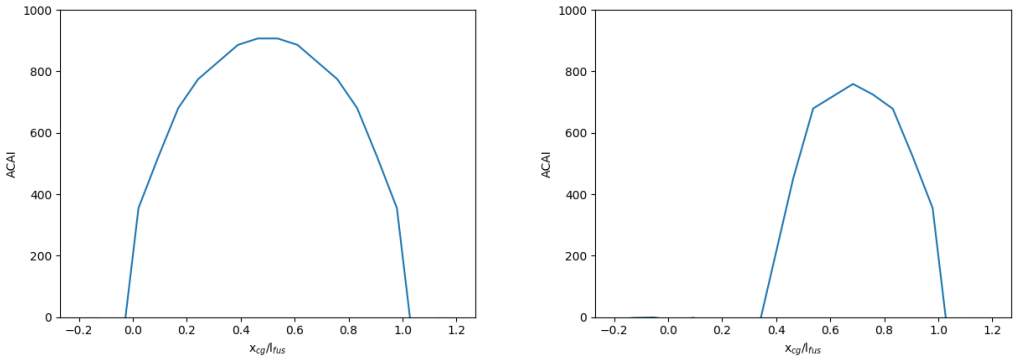

(a) All rotors active.

(b) Three rotor failures on the starboard side of the rear wing.

Figure 10.1: Sensitivity of the ACAI of the tandem wing configuration to the longitudinal centre of mass position.

Further sensitivity studies showed that the value of the ACAI is very sensitive to k_μ. This is due to the importance of this parameter in the yaw control of the model. However, variations in k_μ do not lead to uncontrollable behaviour unless $k_\mu = 0$. Therefore, there is no hard limit on its minimum allowable value. Changing k_μ also does not affect the allowable centre of mass range.

Box wing

The ACAI of the box wing was evaluated in the same way (i.e., with the same assumptions) as the tandem wing, due to the similarity in the configurations. It was assumed that the presence of the vertical elements and the only partial rotation of the wings (as opposed to the full rotation in the tandem wing configuration) do not affect controllability. The ACAI obtained for the fully functioning aircraft is 926.4, and the number of engines allowed to fail before becoming uncontrollable is 5 due to the higher number of engines (again, the most critical failure is if all rotors on one half-wing fail). A sensitivity analysis revealed that this concept would remain controllable up to 2.84% of a fuselage length outside of the fuselage extremities (with all engines functioning). With 5 engine failures on one wing, the centre of mass should be within 39.6% and 60.4% of the fuselage length.

Single wing

For the single-wing configuration, it was assumed that the tilting rotors are located at the extremities of the fuselage, 1.5 fuselage widths away from the symmetry plane. The wing rotors were assumed to be located halfway along the fuselage, at the same lateral distance from the symmetry plane. As for the sense of rotation of the rotors, it was assumed that the tilting rotors rotate inboard (like in the other two configurations) while

the wing rotors rotate in the opposite direction when seen from above in hover. This is based on an example hexacopter configuration from Du et al. [12].

With the assumptions above, the ACAI is 1576.0. However, as soon as any one of the rotors fails, the eVTOL becomes uncontrollable in hover mode. This can be slightly improved e.g. by switching the sense of rotation of the front fuselage-mounted engines. In this configuration, the design is tolerant to one engine failure, as long as it is not one of the rear engines. While a rear engine failure could also be tolerated if rotors are allowed to tilt for yaw control, it is clear that this configuration exhibits less redundancy than the others due to the lower amount of engines. To achieve acceptable safety in hover, the engines would need to be very reliable.

A sensitivity analysis concluded that the centre of mass should be between 8.33% and 91.67% of the fuselage length to ensure controllability with all engines active. Interestingly, the longitudinal position of the wing-mounted rotor did not affect the value of the ACAI. This could be due to the fact that the wing-mounted rotors are not required for pitch control (the fuselage-mounted engines provide enough moment). As Figure 10.2 shows, the value of the ACAI is sensitive to the lateral position of the rotors. It seems like the ideal configuration for controllability would be having the fuselage-mounted rotors between 3.03% and 10.6% of the wingspan, while placing the wing-mounted rotors about 21.4%.

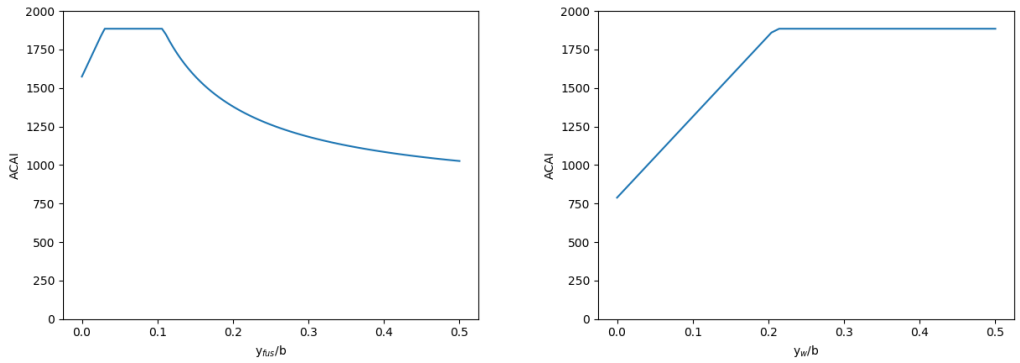

(a) Sensitivity to the lateral position of the fuselage-mounted rotors. **(b)** Sensitivity to the lateral position of the wing-mounted rotors.

Figure 10.2: Sensitivity of the ACAI of the single wing configuration to the lateral position of the rotors.

10.1.2. Controllability in horizontal flight

In horizontal flight, there are nine state variables to be controlled [25], as shown in Equation 10.5. In conventional aircraft, control of these states is achieved using the control variables shown in Equation 10.5 [25]. These are the aileron deflection δ_a (mainly used to create a rolling moment), elevator deflection δ_e (mainly used to create a pitching moment), rudder deflection δ_r (mainly used to create a yawing moment), and trim tab deflection δ_t (used to trim the aircraft).

$$\boldsymbol{x} = \begin{bmatrix} V & \alpha & \beta & \phi & \theta & \psi & p & q & r \end{bmatrix}^T \quad (10.4)$$

$$\boldsymbol{u} = \begin{bmatrix} \delta_a & \delta_e & \delta_r & \delta_t \end{bmatrix}^T \quad (10.5)$$

In order to be controllable like a conventional aircraft in horizontal flight, each configuration must be able to create rolling, pitching and yawing moments (L, M, and N) of sufficient magnitude. All control moments depend on the location of the centre of gravity, since that determines the moment arm that the control force has. However, M is especially affected because the weight acts in the X-Z-plane. Therefore, pitch control will be investigated quantitatively while roll and yaw control will merely be addressed in a qualitative way.

Tandem Wing

The free body diagram of the tandem wing configuration representing straight, symmetric horizontal flight including aerodynamic forces and the weight can be seen in Figure 10.3.

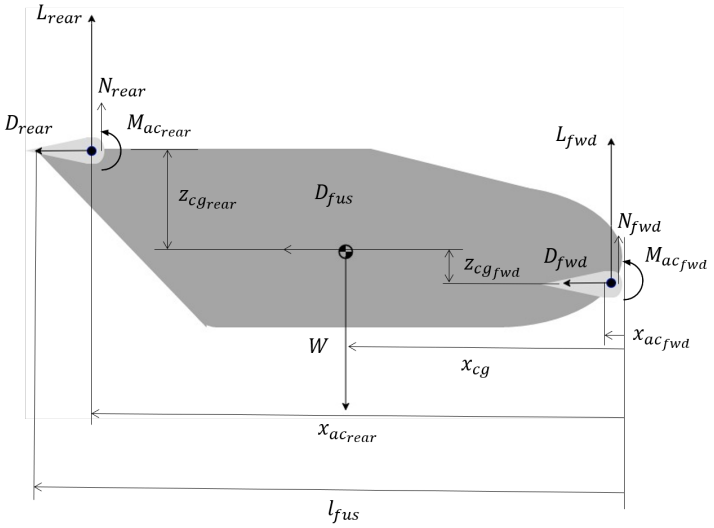

Figure 10.3: FBD showing all aerodynamic loads at horizontal flight with associated distances for the tandem wing configuration.

The moment equation estimated at the centre of gravity (CG) at cruise is as follows:

$$M = M_{ac_{fwd}} - D_{fwd} \cdot z_{cg_{fwd}} + L_{fwd} \cdot (x_{cg} - x_{ac_{fwd}}) + T_{fwd} \cdot z_{cg_{fwd}} - L_{rear} \cdot (x_{ac_{rear}} - x_{cg}) + D_{rear} \cdot z_{cg_{rear}} - T_{rear} \cdot z_{cg_{rear}} + M_{ac_{rear}} + N_{fwd} \cdot (x_{cg} - x_{ac_{fwd}}) - N_{rear} \cdot (x_{ac_{rear}} - x_{cg}) \quad (10.6)$$

where the subscript fwd is for the forward wing and $rear$ is related to the most aft wing. M_{ac} is the aerodynamic moment at the aerodynamic centre, x_{ac} is the horizontal location of the aerodynamic centre and $z_{cg_{rear}}$ and $z_{cg_{fwd}}$ are the vertical distances between the aerodynamic centre of the rear wing and forward wing respectively and the centre of gravity. T is the thrust and N is the normal force caused by propellers.

These aerodynamic loads can be calculated as follows:

$$M_{ac} = C_{m_{ac}} \cdot 0.5\rho V^2 \cdot S \cdot \bar{c} \quad (10.7) \qquad L = C_L \cdot 0.5\rho V^2 \cdot S \quad (10.8) \qquad D = C_D \cdot 0.5\rho V^2 \cdot S \quad (10.9)$$

where $C_{m_{ac}}$ is the aerodynamic moment coefficient, $0.5\rho V^2$ is the dynamic pressure, S is the reference area, C_L is the lift coefficient, C_D is the drag coefficient and finally $\bar{c}$ is the mean aerodynamic chord.

The further the centre of gravity moves forward, the more difficult it becomes to pitch the aircraft up. In order for it to be controllable, the aircraft must be able to attain $C_m > 0$ even at its most forward centre of gravity position.

In order to evaluate the aircraft's natural controllability without differential thrust or thrust vectoring, thrust will be neglected for further estimations. It will also be assumed that the flow is undisturbed at the rear wing due to the distance and height difference between the two wings. It will furthermore be assumed that the moment terms due to drag cancel each other out. This assumes that the vertical cg position is at half the fuselage height. As now the vertical positions and reference areas are the same, the moment terms can be assumed equal in magnitude. The final term that can be neglected is the normal force components which are known to be small and can be neglected when the free stream is normal to the propeller area [8].

By non-dimensionalising and solving for x_{cg}, Equation 10.10 is obtained.

$$x_{cg} > \left(\frac{C_{L_{fwd}} \cdot \frac{x_{ac_{fwd}}}{\bar{c}_{fwd}} + C_{L_{rear}} \cdot \frac{x_{ac_{rear}} S_{rear}}{S_{fwd} \bar{c}_{fwd}} - C_{m_{ac_{fwd}}} - C_{m_{ac_{rear}}} \cdot \frac{S_{rear} \bar{c}_{rear}}{S_{fwd} \bar{c}_{fwd}}}{C_{L_{fwd}} \cdot \frac{1}{\bar{c}_{fwd}} + C_{L_{rear}} \cdot \frac{S_{rear}}{S_{fwd} \bar{c}_{fwd}}} \right) \quad (10.10)$$

$C_{L_{fwd}}$ and $C_{L_{rear}}$ could be influenced by installing mobile surfaces on the trailing edge of the aft and/or

front wing. The distributed rotors would increase their effectiveness and help to achieve higher magnitudes of C_L. The forward is chosen and will include elevators and/or flaps which will increase the control authority over the aircraft.

From Figure 10.4, it can be seen that as there is an increase in $C_{L_{fwd}}$, the min cg limit decreases, which in turn increases the static control authority over the aircraft. It is therefore necessary to apply control or mobile surfaces on the forward wing reaching at least a 40 % increase at stall for a feasible value as can be seen in Section 10.2. This allows for a design $x_{cg_{min}} = 1.570$ m.

The mobile surfaces on the wings could also be used as ailerons, in order to create a rolling moment L. Creating a yawing moment N is a bit more difficult. One option would be to add a vertical tail with a rudder, or add rudders to the winglets on the aft and/or front wing. Another possibility sometimes used by flying wings are split ailerons which allow to increase the drag on one side without inducing a rolling moment. However, the intentional creation of drag would decrease aerodynamic efficiency in turns. Alternatively, differential thrust could be used to create a yawing moment. This would mean that the aircraft does not have yaw control if all engines fail. Also, using differential thrust is less energy efficient than aerodynamic control surfaces.

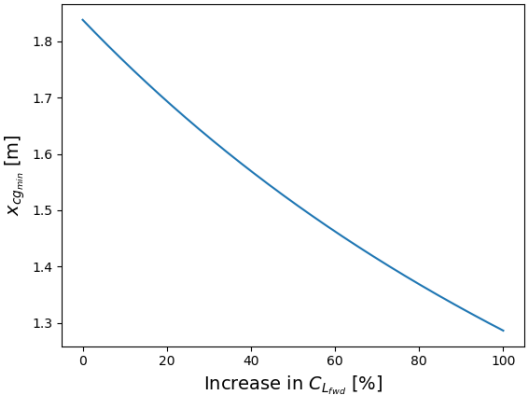

Figure 10.4: Forward cg position as a function of the increase in $C_{L_{fwd}}$ for the tandem and box wing configurations.

Box wing

The box wing configuration is very similar to the tandem wing. Assuming that the vertical struts do not impact pitch, Equation 10.10 can be used to find the forward centre of gravity limit. The result is the same as for the tandem wing configuration due to the fact that both have the same lifting and aerodynamic properties (excluding drag as it was not used for stability and control).

Roll control could be achieved in the same way as for the tandem wing. As for yaw control, the box wing concept may be able to create a moment with rudders installed on the vertical struts connecting the wings. However, these might not be very effective due to the proximity to the centre of gravity. Therefore, as in the tandem configuration, it may be necessary to add a vertical tail, use split ailerons, or resort to using differential thrust for yaw control (at the risk of losing that control in case of engine failure).

Single wing

The FBD for horizontal flight can be seen in Figure 10.5.

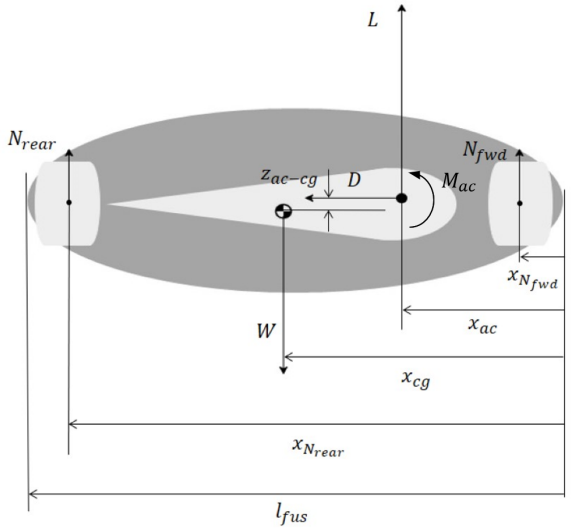

Figure 10.5: FBD showing all aerodynamic loads at horizontal flight with associated distances for the third configuration.

As for previous the aircraft configurations, the controllability of the aircraft without thrust input will be considered. Additionally, it will be assumed that the drag terms due to the rings with the rotors are included in the general aircraft drag. This leads to the following moment equation taken at the CG:

$$M = M_{ac} + L \cdot (x_{cg} - x_{ac}) + D \cdot z_{ac-cg} + N_{fwd} \cdot (x_{cg} - x_{N_{fwd}}) - N_{rear} \cdot (x_{N_{rear}} - x_{cg}) \quad (10.11)$$

where z_{ac-cg} is the distance between the aerodynamic centre and the centre of gravity. Due to the complexity and also the effectively small value of the rings normal forces compared to the entire lift of the aircraft, both N terms are neglected.

The trim equation for the third configuration follows from the non-dimensionalised form of Equation 10.11 and can be used to estimate the minimum allowable centre of gravity position:

$$x_{cg} > x_{ac} - \frac{C_{m_{ac}}}{C_L} \cdot \bar{c} - \frac{C_D}{C_L} \cdot z_{ac-cg} \quad (10.12)$$

In order to compute the value of $x_{cg_{min}}$ (aft cg value), a value for z_{ac-cg} needs to be obtained. It will be assumed that $z_{ac-cg} = \eta/100 \cdot h_{fus}$, where η is a percentage between 0 and 50.

From Figure 10.6 it can be seen that the drag term does not alter the aft cg limit. It can therefore be safely ignored.

Roll control can easily be achieved by installing ailerons on the wing. Pitch and yaw are more difficult, however. One possibility for pitch would be to sweep the wing backwards and place the ailerons at the extremities as far back as possible. Alternatively, horizontal tail surfaces could be added to the rear rotor rings. For yaw control, split ailerons could be used to create differential drag, or a vertical tail surface could be installed. Differential thrust would be less effective than in the other configurations, considering the small lateral distance between the rotors and the centre of gravity.

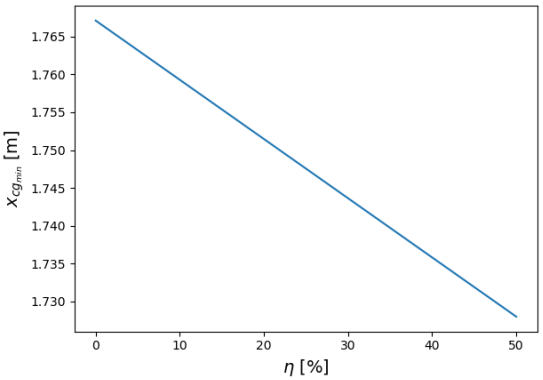

Figure 10.6: Forward cg position as a function of η.

10.1.3. Transitional controllability

Having established how the different configurations can be made controllable both in hover and in horizontal flight, it remains to be shown that the available control inputs can achieve the transition between these two flight modes. This phase of the flight is very difficult to model, so only a qualitative statement will be made in this report.

The dominant aspect of transition is the acceleration/deceleration between stall speed and zero airspeed. In all three configurations, this is achieved by tilting the rotors between their vertical orientation in hover to a horizontal orientation in cruise flight. Due to the low airspeed, most of the control authority will be obtained from the rotors rather than aerodynamic surfaces. Therefore, it is assumed that control of other state variables than horizontal speed is achieved in the same way as in hover.

However, there is one additional complication: due to the high angles of attack attained during transition, there is an increased risk that the rear rotors could enter the wake of the front rotors or front wing, thereby leading to a sudden loss in thrust. This risk is higher for the tandem wing than the box wing, since the entire wing tilting will create a larger wake. However, both configurations have the wings separated both in the horizontal direction, meaning that this will probably not be an issue. For the single wing configuration, on the other hand, there is no vertical separation between the front and back rotors. Especially when the rotors are almost horizontal, this may lead to the front rotors shadowing the rear rotors.

10.2. Open-Loop Stability

The stability properties of all the aircraft configurations for longitudinal and lateral flight will be verified in this section. First, for longitudinal stability, the cruise stability will be estimated which will yield to a

second cg limit following controllability. Secondly, the open-loop stability will be estimated for an ideal pull-up manoeuvre with a particular interest in estimation of the associated stability derivatives. Thirdly, static lateral stability will be estimated in a preliminary manner. Finally, it is essential to mention that hover and transition will not be discussed. It is known that hovering is very rarely an open-loop stable process and transition requires very complex and non-linear aerodynamic modelling which is not intended to be used for the trade-off where a more general and simplified stability model will be implemented for the preliminary conceptual design phase.

10.2.1. Open-loop longitudinal stability at cruise

In this subsection, an analysis will be performed for all configurations in terms of longitudinal open-loop stability at cruise.

Tandem wing

It is known that the limiting factor for static open-loop stability is at high velocities and hence the aircraft must be statically stable at cruise where the highest velocity is achieved.

In order to estimate the stability properties of the design, for a step disturbance in the angle of attack α, the moment equation seen in Equation 10.6 is normalised and differentiated w.r.t. to α leading to:

$$C_{m_\alpha} = \partial C_m/\partial\alpha = -C_{D_{\alpha_{fwd}}} \cdot \frac{z_{cg,fwd} S_{fwd}}{S\bar{c}} + C_{L_{\alpha_{fwd}}} \cdot \frac{(x_{cg} - x_{ac_{fwd}}) S_{fwd}}{S\bar{c}} + C_{D_{\alpha_{rear}}} \cdot \frac{z_{cg_{rear}} S_{rear}}{S\bar{c}} - C_{L_{\alpha_{rear}}} \cdot \frac{(x_{ac_{rear}} - x_{cg}) S_{rear}}{S\bar{c}} \quad (10.13)$$

where $\frac{\partial\epsilon}{\partial\alpha}$ is the downwash effect felt by the rear wing. The latter can be estimated using Equation 10.14 [40].

$$\frac{d\epsilon}{d\alpha} = \frac{K_{\epsilon_\Lambda}}{K_{\epsilon_{\Lambda=0}}} \frac{C_{L_{\alpha_{fwd}}}}{\pi A R_{fwd}} \left\{ \frac{r}{r^2 + m_{tv}^2} \frac{0.4876}{\sqrt{r^2 + 0.6319 + m_{tv}^2}} + \left[1 + \left(\frac{r^2}{r^2 + 0.7915 + 5.0734 m_{tv}^2} \right)^{0.3113} \right] \cdot \left[1 - \sqrt{\frac{m_{tv}^2}{1 + m_{tv}^2}} \right] \right\} \quad (10.14)$$

where $m_{tv} = 2 \cdot v_t/b$ (where v_t is the vertical distance between the rear wing aerodynamic centre and the forward wing aerodynamic centre). An assumption was made based on the geometry of the aircraft that both wings are assumed to be perfectly straight, this results in v_t being equal to the maximum height of the fuselage. The parameter $r = 2 \cdot (x_{ac_{rear}} - x_{ac_{fwd}})/b_{fwd}$ (with b_{fwd} being the span of the forward wing) and K_{ϵ_Λ} is a function of the quarter chord sweep angle $\Lambda_{c/4}$ of the forward wing [40].

Due to the complexity of Equation 10.13, it can be seen that further simplifications must be used in order to ensure a first estimation of the stability properties of the aircraft. The first assumption is related to all C_{D_α} terms. For small disturbances in angle of attack it is known that usual C_{D_α} values are much smaller than C_{L_α}. Additionally, both vertical moment arm z_{cg} are usually smaller than the longitudinal moment arm. Finally, it can be seen from the equation that both moment terms must simplify to reach static stability. These aforementioned explanations lead to cancelling C_{D_α} terms. The final C_{m_α} equation results in:

$$C_{m_\alpha} = C_{L_{\alpha_{fwd}}} \cdot \frac{(x_{cg} - x_{ac_{fwd}}) S_{fwd}}{S\bar{c}} - C_{L_{\alpha_{rear}}} \cdot \frac{(x_{ac_{rear}} - x_{cg}) S_{rear}}{S\bar{c}} \quad (10.15)$$

It is known that for static longitudinal stability $C_{m_\alpha} < 0$. This hence results in the allowable cg position as follows:

$$x_{cg} < \left(\frac{C_{L_{\alpha_{fwd}}} \cdot \frac{x_{ac_{fwd}}}{\bar{c}_{fwd}} + C_{L_{\alpha_{rear}}} \cdot \frac{x_{ac_{rear}} S_{rear}}{S_{fwd} \bar{c}_{fwd}} \cdot (1 - \frac{\partial\epsilon}{\partial\alpha})}{C_{L_{\alpha_{fwd}}} \cdot \frac{1}{\bar{c}_{fwd}} + C_{L_{\alpha_{rear}}} \cdot \frac{S_{rear}}{S_{fwd} \bar{c}_{fwd}} \cdot (1 - \frac{\partial\epsilon}{\partial\alpha})} \right) \quad (10.16)$$

With the required values, the maximum cg value is: $x_{cg_{max}} = 1.685$ m. As it can be seen that $x_{cg_{max}}$ is a function of C_{L_α} of both wings and that the latter is a function of the aspect ratio AR, it must be seen how sensitive the maximum value is to a change in the aspect ratio. This can be seen in Figure 10.7.

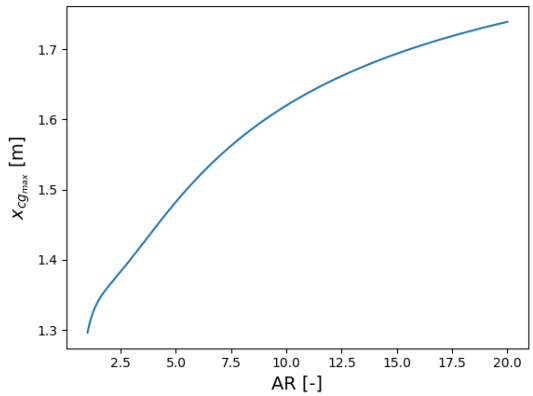

Figure 10.7: Sensitivity analysis on the aft cg position as a function of AR.

From Figure 10.7, it can be seen that the most aft allowable cg position does vary significantly. An increase in aspect ratio is hence favourable for the stability limit. This must be taken into consideration for future design phases.

Box wing
Assuming that disturbances to the initial motion of the aircraft are small, both lateral and longitudinal motions can be decoupled. This leads to both configurations being approximately the same for longitudinal stability, due to their high similarity in the longitudinal direction. Hence this means that the aforementioned equations for the tandem wing configuration can be implemented for the box wing configuration. Using the necessary values from Chapter 8, $x_{cg_{max}} = 1.681$ m for the box wing configurations.

Single wing
The open-loop stability properties of the single wing during horizontal flight will be verified in this section. First, stability will be estimated at cruise and secondly the same will be provided for an idealised pull-up manoeuvre.

As for the previous configuration the C_{m_α} equation must be derived. Differentiating the normalised Equation 10.11 by α and omitting the normal force terms, leads to:

$$C_{m_\alpha} = C_{L_\alpha} \cdot \frac{x_{cg} - x_{ac}}{\bar{c}} + C_{D_\alpha} \cdot \frac{z_{ac-cg}}{\bar{c}} \tag{10.17}$$

Furthermore it is known that for all aircraft, for static longitudinal stability C_{m_α} must be negative which leads to the following cg equation:

$$x_{cg} < \left(x_{ac} - \frac{C_{D_\alpha}}{C_{L_\alpha}} \cdot z_{ac-cg} \right) \tag{10.18}$$

This equation can be further simplified. It can first be assumed that the vertical position of the cg is close to that of the aerodynamic centre and secondly that for small value of α, C_{D_α} is approximately zero. This leads to a very simple stability equation which is analogous to a flying wing and is: $x_{cg} < x_{ac}$. This value was obtained previously in the aerodynamic section and is $x_{cg_{max}} = 1.7947$ m.

10.2.2. Open-Loop longitudinal stability for a pull-up manoeuvre
In this subsection, an analysis will be performed for all configurations during a pull-up manoeuvre.

Generalised ideal pull-up manoeuvre
A general estimate for the change in geometric angle of attack must be first done in order to estimate the required stability derivatives C_{Z_q} and C_{m_q} which effects are dominant during a pull-up manoeuvre.

For an idealised pull-up manoeuvre several aspects will be assumed. First, the velocity V and the load factor n will be assumed to be constant. Secondly, it is assumed that the aircraft motion follows a perfect circle with a radius R, assumed to be significantly larger than the size of the aircraft. The general situation can be portrayed in Figure 10.8.

The change in geometric angle of attack can be estimated by the following equation, where it has been assumed that as the radius R is significantly larger than the overall length of the aircraft, the small angle approximation can be used. Additionally, the radius R can be expressed as a function of the pitch rate q and velocity V with $R = V/q$. From the latter, Equation 10.19 can be rewritten into Equation 10.20.

$$\Delta\alpha \approx sin(\Delta\alpha) = \frac{x - x_{cg}}{R} \tag{10.19}$$

$$\Delta\alpha = \frac{(x - x_{cg})}{\bar{c}} \cdot \frac{q\bar{c}}{V} \tag{10.20}$$

Having derived the general equation for the change in angle of attack, it is now possible to estimate the stability derivatives of the down normal force and pitching moment defined as C_{Z_q} and C_{m_q} respectively. Their definition are as follows:

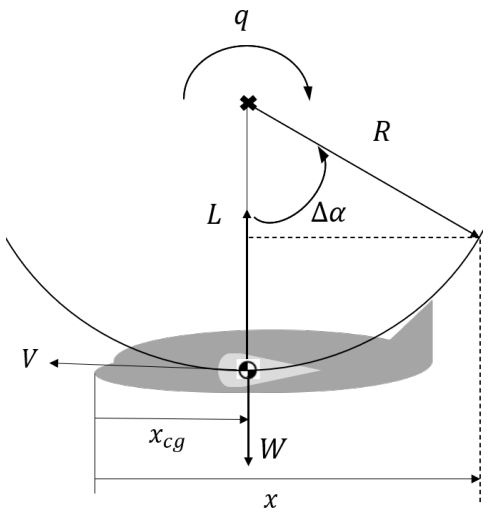

Figure 10.8: Simplified representation of an idealised pull-up manoeuvre with velocity V, radius R and pitch rate q for a generic aircraft.

$$C_{Z_q} = \frac{dC_Z}{d\frac{q\bar{c}}{V}} \qquad C_{m_q} = \frac{dC_m}{d\frac{q\bar{c}}{V}} \tag{10.21}$$

Furthermore, it is known that $C_Z \approx -C_L$. It is now possible to derive an expression for C_{Z_q} and C_{m_q} for all configurations.

Tandem wing and box wing
For the tandem wing and box wing configurations the change in lift is as follows:

$$\Delta C_L = -C_{L_{\alpha_{fwd}}} \cdot \frac{(x_{cg} - x_{ac_{fwd}})}{\bar{c}_{fwd}} \cdot \frac{q\bar{c}_{fwd}}{V} + C_{L_{\alpha_{rear}}} \cdot \frac{S_{rear}(x_{ac_{rear}} - x_{cg})}{S_{fwd}\bar{c}_{rear}} \cdot \frac{q\bar{c}_{rear}}{V} \tag{10.22}$$

As an initial assumption, both mean aerodynamic chords can be assumed to be equal (written from now as $\bar{c}$) leading to:

$$C_{Z_q} \approx C_{L_{\alpha_{fwd}}} \cdot \frac{(x_{cg} - x_{ac_{fwd}})}{\bar{c}} - C_{L_{\alpha_{rear}}} \cdot \frac{S_{rear}(x_{ac_{rear}} - x_{cg})}{S_{fwd}\bar{c}} \tag{10.23}$$

From the latter, the moment coefficient derivative is as follows:

$$C_{m_q} \approx -\left(C_{L_{\alpha_{fwd}}} \cdot \frac{(x_{cg} - x_{ac_{fwd}})^2}{\bar{c}^2} + C_{L_{\alpha_{rear}}} \cdot \frac{S_{rear}(x_{ac_{rear}} - x_{cg})^2}{S_{fwd}\bar{c}^2}\right) \tag{10.24}$$

Single wing
For the single wing the change in lift is as follows:

$$\Delta C_L = C_{L_\alpha} \cdot \frac{(x_{ac} - x_{cg})}{\bar{c}} \cdot \frac{q\bar{c}}{V} \tag{10.25}$$

The normal force derivative and pitching moment derivative can be written as:

$$C_{Z_q} \approx -C_{L_\alpha} \cdot \frac{(x_{ac} - x_{cg})}{\bar{c}} \quad \& \quad C_{m_q} \approx C_{L_\alpha} \cdot \frac{(x_{ac} - x_{cg})^2}{\bar{c}^2} \tag{10.26}$$

Results
The results of the latter are summarised in Table 10.2.

Table 10.2: Longitudinal pull-up stability estimates for all configurations with assumed cg position $x_{cg} \approx x_{cg_{max}}$.

Variable	C_{Z_q} [rad^{-1}]	C_{m_q} [rad^{-1}]
Tandem wing	-2.457	-70.272
Box wing	-2.362	-67.136
Single wing	0.016	0

From Table 10.2, it can be seen that configuration 1 is the most stable for a pull-up manoeuvre as its value of C_{m_q} is the most negative.

10.2.3. Open-loop lateral stability

In order to have static lateral stability the aircraft must have a positive C_{n_β} (being the derivative of the yaw moment coefficient w.r.t to the sides-lip angle β). In this section, first the general estimation method will be presented and secondly the computation for all configurations will be performed.

General equations
As a first estimate of both stability derivative can be done using the method found in [42]. The method takes into account the different parts of the aircraft such as the wing, the fuselage and their interaction.

For C_{n_β}, the wing contribution is as follows:

$$(C_{n_\beta})_w = C_L^2 \cdot \left[\frac{1}{4\pi AR} - \left(\frac{tan(\Lambda)}{\pi AR(AR + 4cos(\Lambda))} \right) \left(cos(\Lambda) - AR/2 - \frac{AR^2}{8cos(\Lambda)} + \frac{6(x_{ac_w} - x_{cg})sin(\Lambda))}{\bar{c} \cdot AR} \right) \right] \quad (10.27)$$

And the fuselage contribution equation is:

$$(C_{n_\beta})_{fus} = -1.3 \cdot \frac{V_{fus}}{Sb} \cdot \frac{D_{fus}}{w_{fus}} \quad (10.28)$$

where V_{fus} and D_{fus} are the fuselage volume and depth respectively. For the volume, an approximation will be used in which the fuselage of all configurations is considered to be an ellipsoid as it is similar in shape, resulting in $V_{fus} \approx 4\pi/3 \cdot w_{fus} l_{fus} h_{fus} = 34.85$ m^3. However, this results in a value approximately equal to -4.17 rad^{-1}, which seems to be a large overestimation. Using [25], it can be seen that the fuselage component is usually of the order of 10^{-2}. Hence as an initial estimate, the value from Equation 10.28 will be divided by 100.

Vertical tail sizing
The previously mentioned value shows that the aircraft is laterally unstable and requires a vertical stabiliser or a fly-by-wire system in order to reach a positive C_{n_β}. In order to estimate the required size of the possible stabiliser, a similar relation to that of C_{m_α} for $(C_{n_\beta})_v$ (the vertical tail component) can be used and is as follows:

$$(C_{n_\beta})_v = (C_{Y_\beta})_v \cdot \left(1 - \frac{d\sigma}{d\beta}\right) \cdot \left(\frac{V_v}{V}\right)^2 \cdot \frac{S_v l_v}{Sb} \quad (10.29)$$

where $(C_{Y_\beta})_v$ is the derivative of the side force coefficient C_Y (of the vertical tail) w.r.t β. This derivative is basically the C_{L_α} of the vertical tail. σ is the side wash (assumed to be 0 for simplicity), V_v is the velocity of the airflow at the vertical tail and l_v is approximately the tail arm between the aerodynamic centre of the vertical tail and the centre of gravity (assumed to be the stability limit).

Before being able to find a preliminary estimate of the vertical tail size, b_v, an equation for $(C_{Y_\beta})_v = C_{L_{v_\alpha}}$ can be found in Equation 10.30 [39], where it is assumed that the vertical tail aspect ratio is very small. Combining Equation 10.29 and Equation 10.30, the relation for b_v can be derived as shown in Equation 10.31:

$$C_{L_{v_\alpha}} \approx \frac{\pi}{2} \cdot AR_v \tag{10.30}$$

$$b_{v_{min}} = \sqrt{\frac{2(C_{n_\beta})_v Sb}{\pi l_v}} \tag{10.31}$$

The minimum tail span can be computed by equating $(C_{n_\beta})_v$ with the sum of the fuselage and wing component found earlier. The latter values are summarised in Table 10.3.

Table 10.3: Lateral stability estimates for all configurations.

Variable	$(C_{n_\beta})_{w+fus}$ [rad^{-1}]	$b_{v_{min}}$ [m]
Tandem wing	-0.031507	0.5248
Box wing	-0.028954	0.5176
Single wing	-0.084536	1.9370

From Table 10.3, it can be seen that the box wing seems to be the most naturally stable as it requires the smallest minimum vertical tail, followed by the tandem wing and lastly the single wing which would require nearly a tail with length of half the fuselage. The latter shows two main aspects of this analysis, the first is that the single wing requires a high amount of attention for lateral static stability and secondly that these estimates are preliminary and will require further scrutiny and optimisation.

Finally, it must be noted that the box wing has already a vertical surface which could help to improve static lateral stability. However this surface is both in front and behind the cg which could lead to either a positive or negative contribution to C_{n_β} depending on the side force distribution over the vertical surface.

10.3. Verification and Validation

It is finally essential to briefly present the Verification and Validation strategy required for Control and Stability, during the preliminary and final stages of the project and possibly afterwards.

10.3.1. Verification and validation for preliminary design tools.

First, it is essential to mention that for the initial phase of the project, validation was not possible due to the preliminary nature of all the obtained estimates and time constraints.

Secondly, in terms of the verification process every value obtained was verified by means of unit and general system tests. For hover controllability, all estimates were verified by using the MATLAB model provided in [13] and comparing them to the implemented model used in this chapter. Whereas for the CG limits and stability derivatives, these were compared to known aircraft models (CFD or other panel methods) obtained in [25]. For both sets of values, the unit tests and system tests were successful.

10.3.2. Verification plan

This section outlines different approaches to verify the preliminary and future numerical model of the aircraft.

Response-to-input - System Testing

The first verification procedure for stability and control simulation model will be to check if for a given specific input to the dynamic model, the output behaviour makes physical sense. This is will be performed by applying three inputs for each of the control surfaces. These inputs will vary in sign and magnitude (negative, positive and zero) and the output's behaviour will be verified qualitatively. As an example if a positive deflection is provided to the aileron, the aircraft is expected to roll in the negative direction ($C_l < 0$ and $p < 0$) and for a positive rudder deflection the aircraft will yaw in the negative direction ($C_n < 0$ and $r < 0$). Finally, for a zero deflection for all control inputs, the response of the system should be zero. When all the qualitative tests are performed for each of the control surfaces, the system test is complete and the model is verified.

Verification of eigenvalues

The eigenvalues of the A-matrices essentially determine the nature of the solution of the state space equations. Based on them, it can be determined whether the solution will converge, diverge or be indifferent, whether it will be periodic or aperiodic, and whether it will damper or undamped. Therefore, it is crucial to ensure that these parameters are verified as errors in the calculations of eigenvalues might render the simulation invalid.

The eigenvalues will be verified by analysis, where the eigenvalues of the derived equations of motion for the symmetric and asymmetric flight will be evaluated by hand. Fortunately, simplifying assumptions can be made for each of the studied flight manoeuvres, which can reduce the size of the matrices considerably. Both sets of eigenvalues will be compared and checked further.

10.3.3. Validation plan

For the Validation process, multicopter flight data will be researched and used to validate the Hover Control simulation model. Whereas for the horizontal flight model, flight data from various aircraft will be found in [25] and other various sources.

Finally, after the project, it would be possible to print a 3D model of the aircraft, and with further wind tunnel data, a more exact computation of the stability derivatives could be performed. As a consequence the stability model could be refined and further optimised in order to model more accurately the dynamic stability behaviour of the aircraft.

10.4. Conclusion

Considering the results from Section 10.1 and Section 10.2, this section summarises the relevant differences between the three configurations in terms of stability and control, which will be used for during the Trade-off process. These can be seen in Table 10.4.

Table 10.4: Summary of stability and control characteristics for each configuration.

	Tandem wing	**Box wing**	**Single wing**
Hover control CG range [m]	1.38-2.62	1.58-2.42	0.33 - 3.67
Allowable engine failures	3	5	0
Horizontal pitch control design $x_{cg_{min}}$ [m]	1.570	1.570	1.765
Ease of lateral control	Moderate	Moderate	Bad
Static longitudinal stability $x_{cg_{max}}$ [m]	1.685	1.681	1.795
Minimum tail size for static directional stability [m]	0.5248	0.5176	1.9370
Damping pitch rate motion C_{m_q} [rad^{-1}]	-70.272	-67.136	0

11 Structures

For the design of any aircraft it is crucial to minimise structural mass while still maintaining a rigid structure able to sustain high loads. Section 11.1 provides a full range of possible flight load factors. Section 11.2 describes loads and approximations of the wing structures. Section 11.3 estimates the weight of the aircraft components with semi-empirical methods and pays special attention to the structural comparison between the tandem and box wing configurations. Section 11.4 presents an initial fuselage shape design and layout. Section 11.5 goes into detail on the design for crashworthiness. Finally, section 11.6 verifies and validates the program used for the stress analysis.

11.1. Structural Design Envelope

To compute the loads acting upon the aircraft in flight, a gust loading diagram and a manoeuvre loading diagram is created. When computing the gust loading diagram Equation 11.1 is used, wherein u is the gust velocity, V is the flight velocity, and W/S is the wing loading. Three gust loads given by Certification Specifications (CS) [15] are $ub, uc, ud = 20.12, 15.24, 7.62$ m/s and three design velocities, namely, design velocity for maximum gust intensity, cruise and dive, are determined. The interpolation of the points and using the formula 11.1 (left) provides the basis for the gust loading diagram. For manoeuvre loading diagram, the approach is slightly different. The loads at stall speed are computed using the formula on the right:

$$n = 1 \pm \frac{\rho \cdot V \cdot C_{L_\alpha} \cdot u}{2 \cdot W/S} \qquad n = \pm \frac{0.5 \cdot \rho \cdot V^2 \cdot C_{L_{max}}}{2W/S} \tag{11.1}$$

This quadratically increasing line is then cut off at the maximum allowable load factor, which is set by the Certification Specifications (CS). The n_{upper} in this case is 2.5. The same procedure is applied for

negative load factors, where n_{lower} is -1, also set by CS. The maximum possible aircraft speed is defined as the dive speed, V_D, after which the envelope drops to zero load factor.

Both diagrams are defined for a specific altitude, in this case the design cruise altitude, as that is the altitude at which the aircraft spends the majority of its time. The diagrams are then combined and the maximum load factor is determined. The diagram is shown in Figure 11.1. It follows that the maximum load factor the structure has to withstand is 3.2 without failing, which is a reasonable result, considering that some transport aircraft have the maximum load factor as low as 2.5. Moreover, the maximum load factor is multiplied by 1.5, a safety factor, that brings the load to the so-called ultimate load factor. The structure should not critically fail at this load, but some structural damage may occur, like buckling or slight yielding.

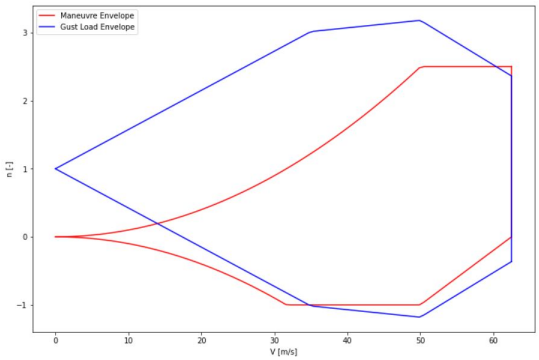

Figure 11.1: The flight envelope

11.2. Load cases

In order to design and analyse the structure, it is important to know what the structure is being designed for. The necessary approach is to identify and analyse critical cases where the limits of the structure are tested. One of such cases is gust and manoeuvre loads during cruise, described in Section 11.2.1. Another case is the vertical take-off, described in section Section 11.2.2.

In order to analyse the cases, an initial estimation of the structure needs to be made. Since the analysis is done for the trade-off, the emphasis is given to how one structure performs compared to another, which is of a different configuration, rather than the actual structural performance. Therefore, to keep the comparison fair, the same wingbox geometry is used for all three configurations, without any stiffening elements, as this task is left for the final stage of the design. The skin thickness was chosen as 3 mm. The loads are evaluated at the root of the wing, where the base of the wingbox is $b = 0.8c_{root}$ and the height of the wingbox is $h = 0.8h_{root}$.

For the above stated load cases, several critical failure modes are to be analysed. It was found that for aircraft components, the three most common causes of failure are fatigue, corrosion and overload, in that order [18]. Corrosion is not going to be analysed in this report since it is not crucial for the trade-off, but overload and fatigue are. When it comes to overload, bending moments, shear forces, buckling stresses are to be analysed. Fatigue is analysed using the Paris equation. [47]

For overload, bending loads are computed using the bending stresses equation, assuming full elasticity of the material. Additionally, since using a symmetrical wingbox, term I_{xy} reduces to 0. The moment of inertia, being a geometric property, is trivial to compute with a set of rectangles and their Steiner terms. For shear flows and stresses, the shear flow equation is used, wherein again, due to the fact that I_{xy} is 0, the equation simplifies to the following:

$$\sigma_z = \frac{M_x y}{I_{xx}} + \frac{M_y x}{I_{yy}} \qquad q_2 - q_1 = \int_{s1}^{s2} \frac{\delta q}{\delta s} ds = -\frac{V_y}{I_{xx}} \int_{s1}^{s2} ty ds - \frac{V_x}{I_{yy}} \int_{s1}^{s2} tx ds \tag{11.2}$$

Since the wing box is a closed section, it needs to be 'cut' somewhere in order to analyse the section like an open one. Luckily, due to symmetry, cutting the in the middle of the bottom flange and the middle of the left web does not introduce any redundant shear flows, since they are 0 in those spots, and thus simplifies the calculation process.

Adding shear flow due to torque is trivial, as it is simply $q = T/2A$, where T is torque and A is the enclosed area. All the shear flows are added together and shear stress is then easily found by simply diving the flow at the specific location by the thickness.

During analysis of buckling, the buckling of the top panel was computed. This is done using the equation for buckling of thin plates:

$$\sigma_{cr} = C \frac{\pi^2 E}{12(1-\nu^2)} \left(\frac{t}{b}\right)^2 \tag{11.3}$$

Where E is the Young's modulus, ν is the Poisson ratio, t is the thickness of the plate and b is the side where the impressive load is not applied. C is a function of the aspect ratio of the plate and the boundary conditions of the plate. The top plate of the wingbox under analysis is assumed to be clamped at the root and to be simply supported on other sides, which makes the coefficient C to be equal to 5.41.

As mentioned before, fatigue is analysed using the Paris relation to provide preliminary comparison between the configurations [47]. This equation assumes constant amplitude fatigue loading and is used in estimation of crack growth and not crack initiation. For crack initiation, a simple S-N curve, otherwise known as Wöhler's curve, can be used for a material of choice. As materials trade-off has not yet been made, the comparison can be made between the wingboxes using the same material, for example Aluminium 2024-T3, as it is one of the most popular aluminium alloys used in aircraft wings due to its high tensile strength [53]. Construction of the S-N curve is an experimental procedure, however, methods exist where this curve is semi-empirically. One of such experimental examples is show in Figure 11.2. The relationship in Figure 11.2 is described by the Basquin's Law, as ${S_a}^m \cdot N = C$, where S_a is the load level, $m = 4.10$ and $C = 3.15 \cdot 10^{14}$, which depend on material properties [30]. Note that the scale is logarithmic. Using this relationship it is possible to get estimates on fatigue life of the selected concepts by simply plugging in the respective load level.

The Paris law is used to predict fatigue crack growth in a structure under constant amplitude loads.

$$N_{a_0 \to a_f} = \int_{a_0}^{a_f} \frac{1}{f_R(\Delta K)} da \tag{11.4}$$

where a is the crack length, and $f_R(\Delta K)$ represents crack growth resistance of the material. Using the Paris relation with $\beta = 1.125$:

$$\frac{da}{dN} = C\Delta K^m = C(\beta \Delta\sigma\sqrt{\pi a})^m \tag{11.5}$$

Substituting Equation 11.5 into Equation 11.4 results in:

$$N = \frac{1}{C\Delta\sigma^m} \int_{a_0}^{a_f} \frac{1}{(\beta\sqrt{\pi a})^m} da \tag{11.6}$$

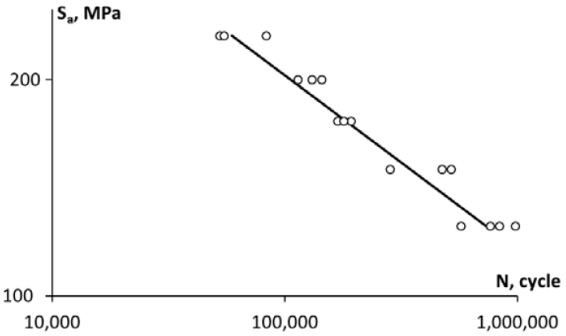

Figure 11.2: The S-N curve for 2024-T3 aluminium alloy under axial tension-compression [30].

Where β is a geometry factor related to crack propagation,
m is the Paris exponent and C is the Paris constant, both are dependent on the material. The initial crack length is chosen to be $0.375 \cdot 1.2$mm as this is the smallest length that can be detected by the mechanoluminescence film [19]. The final crack length is chosen to be half of the thickness of the wingbox thickness. β is defined as 1.125 as the assumption that the crack is initiated at the edge of the plate is made, as this case is more critical than cracks in the centre of the material. The number of cycles is then determined numerically using numerical integration.

11.2.1. Cruise

For the cruise flight condition, the maximum positive load factor is considered for the trade-off. The loads on the aircraft are shown on diagram 10.5 for the single wing configuration and on diagram 10.3 for the tandem and box wing configurations, with values of some parameters taken from the results of other departments or from initial sizing. These loads are first solved for a simple longitudinal equilibrium situation, and the solved values of those loads are then applied on the wing's aerodynamic centre line to create a distribution of shear forces and bending moments (NVM diagrams) as well as internal torque along the half span of the wing. For this, the weight of the wing and the aerodynamic force and moment are assumed to be uniformly distributed along the span of the wing.

From table 11.1, the single experiences largest bending stresses but also the largest number of cycles until failure. The former can be explained by that fact that there is only one wing to carry lift forces, and thus the bending loads are higher. The reason for larger number of cycles is not clear but could maybe be attributed to the wider panel where the crack sits. Moreover, a better decision is to analyse the single wing configuration at the engine cutout. Even though the bending moments and shear forces there are smaller than in the root, the cross-section is much smaller and therefore undergoes large stresses and torsional twists. Overall, buckling of the top panel is the critical failure mode in all three configurations. This can be attributed to the fact that a simple wingbox structure has been used without any stiffening elements. Lower

critical buckling stress of the single wing concept is most likely due to an a longer wing, making parameter b bigger in Equation 11.3.

Table 11.1: Stresses occurring in the wing root under loads in cruise

	Tandem wing	**Box wing**	**Single wing**
Bending axial stress (σ)[MPa]	70.6	69.3	79.5
Critical buckling stress (σ_{crit})[MPa]	6.26	6.0	1.9
Number of cycles (Paris Law) [10^6]	9.35	1.71	13.2
Shear stress (τ)[MPa]	30.1	30.2	2.0
Number of cycles (SN curve) [10^6]	3.95	4.15	2.41

11.2.2. Vertical take-off

For the vertical take-off condition, the wings or engines are rotated and maximum thrust is applied, as this would be the most critical situation to analyse during take-off. These situations are depicted in figures 11.3. The results from the numerical structural analysis are given in the Table 11.2. Critical buckling and life cycles are omitted since both of these take bending stresses as inputs, compression of the top plate for buckling and cycling between compression and tension of the plates for fatigue. Since the bending stresses stresses for this situation are several times lower than those for cruise, fatigue or buckling would not be critical in this situation.

Table 11.2: Stresses occurring in the wing root under loads in vertical take-off

	Tandem wing	**Box wing**	**Single wing**
Bending moment (σ)[MPa]	23.0	43.3	3.9
Shear stress (τ)[MPa]	3.6	134.7	3.9

It is evident that the stresses during vertical take-off are much less severe since maximum thrust is roughly equal to the weight of the aircraft. During cruise, the lift is approximated by multiplying the weight by the ultimate load factor. Bending stresses are larger in the tandem and the box wing due to propulsion being evenly distributed between the 2 wings. The sing wing has only one engine on each side of the wing providing an upward force. This is being counteracted by the weight of the engine itself and the wing, resulting in low bending moment around the root.

As for the shear, there is a large spike in the box wing due to the propulsion system being situated at the trailing edge of the wing, generating a large moment around the shear centre, resulting in large shear loads. The non-rotating wings aid negatively to this, as this feature increases the moment arm, producing an even larger torque. Additionally, during vertical take-off the forces would not be distributed as evenly as during lift, imposing sharp spikes in shear forces induced in the structure in the locations of the engine attachments. This is a topic to analyse during the final stage of the project.

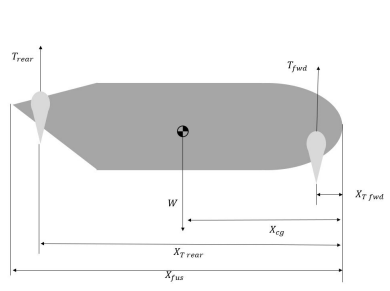

(a) Vertical take-off configuration of the tandem wing.

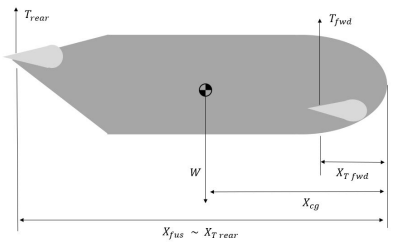

(b) Vertical take-off configuration of the box wing.

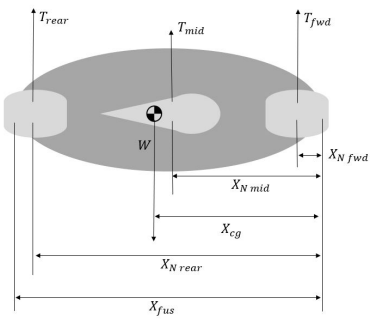

(c) Vertical take-off configuration of the single wing.

Figure 11.3: Free Body Diagrams of the vertical take-off.

11.3. Aircraft Component Weight and Centre of Gravity Estimation

Including weight of the aircraft in the trade-off is crucial, however estimation of weight components for eVTOLs has not been researched extensively due to novelty of the concept. Therefore, a method of semi-empirical estimation is used to estimate the wing and fuselage weights, as these are the weights that will differ a lot between the 3 configurations. The estimation methods used are taken from a book by Dr. Jan Roskam [44]. The specific method used is for general aviation airplanes and is called the "Cessna method". The method is defined for the imperial units, but conversion is made when outputting the result in code.

The wing weight is estimated using the following equation:

$$W_w = 0.04674(W_{TO})^{0.397}(S)^{0.360}(n_{ult})^{0.397}(AR)^{1.712} \tag{11.7}$$

where W_{TO}, S, n_{ult}, AR are take-off weight from Class I estimation (Chapter 6), wing area, ultimate load factor and aspect ratio, respectively. For tandem and box wing configurations, the area and aspect ratios are considered separately for each wing, and then are added to the wing group.

The fuselage weight is estimated using the following two equations:

$$Wf_{lowwing} = 0.004682(W_{TO})^{0.692}(P_{max})^{0.379}(l_{f\_n})^{0.590} \tag{11.8}$$

$$Wf_{highwing} = 14.86(W_{TO})^{0.144}\left(\frac{l_{f\_n}}{P_{max}}\right)^{0.778}(l_{f\_n})^{0.383}(N_{pax})^{0.455} \tag{11.9}$$

where $P_{max}, l_{f\_n}, N_{pax}$ are fuselage length, maximum perimeter of the fuselage and number of passengers, respectively. For this method, the pilot (and any crew members) is included in the number of passengers. For tandem and box wing, both formulas are used to compute the weight of the fuselage and the average is taken, to account for both high and low wing.

Using the above listed formulas and the relevant values, and the below tables, Table 11.3 to Table 11.5 are produced.

Table 11.3: Component weight fractions for the tandem wing concept.

Tandem wing			
	Mass	% of OEM	% of MTOM
Front wing	120.4	9.2	6.4
Back wing	120.4	9.2	6.4
Fuselage	90.2	6.9	4.8
Passengers	475.0	0.0	36.3
Cargo	85.0	0.0	4.6
Battery	499.5	38.2	26.7
Landing gear	77.2	5.9	4.1
Propulsion	400.0	30.6	21.4
Total Mass		1307.7	1867.7

Table 11.4: Component weight fractions for the box wing concept.

Box wing			
	Mass	% of OEM	% of MTOM
Front wing	120.1	8.7	6.2
Back wing	120.1	8.7	6.2
Fuselage	90.2	6.5	4.7
Passengers	475	0.0	34.4
Cargo	85	0.0	4.4
Battery	572.5	41.5	29.5
Landing gear	77.2	5.6	4.0
Propulsion	400.0	29.0	20.6
Total Mass		1380.1	1940.1

Table 11.5: Component weight fractions for the single wing concept.

Single wing			
	Mass	% of OEM	% of MTOM
Wing	211.5	17.1	11.8
Fuselage	112.5	9.1	6.3
Passengers	475	0.0	38.5
Cargo	85	0.0	4.7
Battery	433.1	35.1	24.1
Landing gear	77.2	6.3	4.3
Propulsion	400.0	32.4	22.3
Total Mass		1234.3	1794.3

These values were obtained through one iteration. In this case, the single wing configuration is the lightest one. However, since a semi-empirical methods are used to calculate the weights, thus these do not take into account unconventional configurations. Particularly for the single wing configuration, the method does not take into account the fact that a vertical take-off propeller in embedded in the wing. This would

increase the weight of the wing greatly since it has to sustain vibrational loads produced by a large propeller engine. Moreover, a cutout in the wing would negatively affect torsional stiffness of the wing, causing it to twist greatly, needing for reinforcements.

11.3.1. Tandem vs box wing

Another point that is important to mention is the difference between the tandem wing and the box wing configuration. The approximated wing weights are very similar, which is not an accurate estimation. This is because the connection between the two wings acts as a support structure, possibly relieving some loads. However, the research on the general effect of closing the wing on its structural weight is inconclusive. Some studies claim the structure of a box wing can be up to 35 % lighter than that of the conventional wing [26], while others reason that it is around 23 % heavier [10]. Because of this, quantitative results cannot be found at this stage and qualitative points have to be relied on.

The main structural advantage of the box wing is its increased torsional rigidity compared to the equivalent tandem configuration. This happens because the torsion of a given wing structure is resisted by the deflection of the other wing's tip. However, for a box wing with 2 equally sized wings and assuming the same aerodynamic loads on both wing surfaces, the wing tip connection doesn't relieve significant stresses in pure bending, at least at small deflection angles. This is because both wings deflect vertically by the same distance, so the tip connection doesn't carry any axial load to change the root bending moments. This reasoning is reinforced by a study measuring the effect of the tip connector inclination on the different internal loads. In the study it was found that the inclination angle "significantly affects the torsional force, dragwise shearforce, and dragwise bending moment distributions", but "for out-of-plane bending moment and shear force distributions, there were only minor variations". For a horizontal take off airplane, this meant that "no significant variations in wing structural design drivers as a function of tip fin inclination were observed." [26]

A logical explanation for this is that for the wings of a conventional take-off airplane, upwards bending moment is the critical load case. This effect has even more certainty for high aspect ratios, since for a uniform load and torque distribution, the root bending moment depends on the square of the beam length, while the root internal torque only depends linearly on the beam length, so the bending moment becomes relatively stronger than torsion in high aspect ratio wings. With this knowledge, it is important to decide whether the considered configurations are loaded more extremely in torsion or bending. Because of the reasons explained in the paragraph above, the cruise is assumed to impose root bending moments that are more critical for the wing box than internal torque is. On the other hand, the hover mode should be analysed more deeply. The tandem configuration has wings that rotate in their entirety for hover mode. The propeller thrust vector passes relatively close to the shear centre of the wing box and the thrust creates bending moments around the wingbox axis that's more resistant to bending because of the airfoil geometry. Therefore, Hover mode is not critical for the tandem configuration. The box wing configuration, however, has thrust vectoring propulsion close to the trailing edge of the airfoil, which may create large torsional loads on the structure in hover flight, because the applied vertical load creates a large moment around the shear centre of the wing box. Fortunately, this propulsion system is implemented only in the box wing concept, so those large torsional loads are handled by the wing tip connector as explained before.

In conclusion, the closed wing is beneficial for the structure only in the configuration with trailing edge thrust vectoring propulsion because of the large torsion introduced in vertical flight. The closed wing would not structurally benefit the current tandem configuration, and it would only pose problems with the wing rotation. For the structural trade-off, the tandem and box wing configurations are equally feasible.

11.4. Fuselage Initial Design

It was decided to use the same fuselage for the 3 concepts, to facilitate the trade-off and focus only on major differences between the configurations. Before designing the fuselage, some constraints on component sizes were collected. The headroom height measured from the floor should be 1.5 m, the height at the passenger's shoulder should be at least 0.95 m, the seat pitch should be around 0.8 m and the width of a seat is around 0.6 m. The chosen configuration is a simple 2 rows of 2 passengers, with a separated single-seat cockpit in the front. Initially an aisle was considered for easy access to seats, but the concept was abandoned after a new, better idea was created. The initial fuselage design is shown in figure 11.4

The 2 rows of 2 passengers configuration is more compact and equally comfortable with this new design. The choice to face the front 2 seats backwards was made to reduce the necessary number of passenger cabin doors from 4 to 2, thus reducing weight. Additionally, the cockpit was designed to be 1 m long, to allow for the pilot's seat and the controls and dashboard. For aerodynamic reasons the fuselage cross section is the smallest multi-arc oval-like shape wrapped around the necessary inside space. The cross section of the

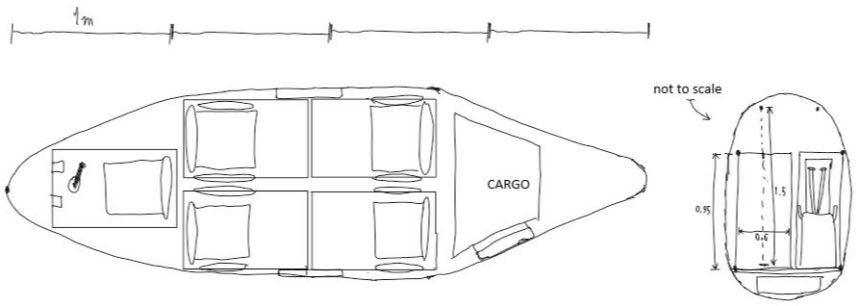

Figure 11.4: Drawing of initial fuselage design

passenger cabin can be seen on the right of figure 11.4. Behind the passenger cabin is the tail curve, which decreases the cross section area gradually to prevent excessive boundary layer separation and pressure drag. The cargo compartment is positioned inside this tail, filling up most of the empty space. There is also empty space below the cabin floor, which can be used either for batteries or for an energy absorbing structure. This trade-off will be discussed further in section 11.5.

The width of the fuselage is 1.3 m, the length is 4 m and the height is 1.6 m. This is only a preliminary fuselage concept and an optimised design of the fuselage will be created for the final report.

11.5. Crashworthiness

Another important aspect for the trade-off is the crashworthiness of a design. This section analyses the 3 designs with respect to the behaviour during a defined crash situation.

A crashworthy VTOL vehicle design is defined by its ability to protect its payload from harm during a ground impact. In this project the focus is on protecting humans, since they are the most sensitive and important payload. From the past incident analysis it is known that injury during a helicopter crash comes from excessive acceleration during impact, a contact injury by a body part hitting a hard surface, and environmental injuries such as from fire, smoke or water [63].

In the midterm trade-off only the effect of the vehicle configuration on crashworthiness is considered and more detailed analysis and design will follow in the final report. Because the fuselage is a constant across the 3 designs, the environmental injuries are not considered for now; that should not depend on the configuration so it's unnecessary for the trade-off. Similarly, injury from impact of body parts on hard surfaces will probably be prevented by the 3 configurations in the same way, by including seat harnesses and ensuring the fuselage structure is strong enough not to collapse onto the passengers.

First, the effect of different configurations on crash behaviour will be analysed. For single wing VTOL vehicles, the safest wing placement is a low wing, because a high wing is extra mass above the passengers that has to be decelerated by the structure during a crash. A low wing configuration therefore allows for a much lighter fuselage structure. However, there is a major disadvantage to the single wing configuration. For aerodynamic stability and controllability, the wing must be positioned close to the centre of gravity, which for a low wing happens to be below the passenger cabin, and "stiff lifting structures underneath the cabin can negatively affect the crashworthiness behaviour, so one must guarantee enough energy absorption for these structures in the event of a crash" [7]. In other words, the space under the passenger cabin would be better used for an energy absorbing structure to protect passengers from excessive impact acceleration. The tandem and box wing configurations don't have this problem, as the wings are positioned in the extreme front and back locations. For both of these configurations, the back wing is a high wing above the cargo compartment or behind it. Because no valuable payload is stored under the wing, the aforementioned disadvantage of a high wing can be ignored. In the front, however, there is a stiff wing root structure under the pilot's seat. This is still a problem, but less critical than the stiff wing under the passenger cabin in the single wing concept, because it is easier to overcome without altering the wing structure. Possible solutions to protect the pilot during a crash are a special energy absorbing seat assembly [63], or an ejection seat for the pilot to use just before impact.

Next, some useful facts and ideas about crashworthy design collected from the research can be discussed and applied to the configurations to find any additional basis for the trade-off. Firstly, batteries are also stiff elements, so they should not be placed below the passenger cabin, for the same reason a wing should not be placed there. Additionally, batteries might catch fire after a crash, so keeping them away from passengers

is a good idea. Those two facts imply it's beneficial to put batteries in the wings, which the tandem and box wing configurations can do better than the single wing plane, because the latter's in-wing engines take up potential battery space. Next, the landing gear will have to be designed to absorb as much energy as possible while not puncturing through the cabin. The rest of the energy will have to be absorbed by energy absorbing materials below the cabin. There are multiple options for such a material, for example metal rings, tubes, or a hexagonal matrix [63]. All this needs to be done with minimum peak deceleration.

In conclusion, the single wing configuration performs worse and poses more problems than the tandem and box wing configurations when it comes to crashworthiness, mainly because of the wing placement relative to the passenger cabin and the ability to store batteries in the wings, where they pose a smaller mechanical and environmental threat to the passengers. However, no difference has been found between the box wing and tandem configurations. The optimally crashworthy design is a box wing or tandem configuration that stores all batteries in the wings, has properly designed landing gear, uses energy absorbing structures between the lower fuselage skin and the cabin floor, and optionally features energy absorbing seats.

11.6. Verification and Validation

Verification and validation is crucial during any sort of simulation In case for structural design, numerical tools have been built in order to facilitate iterative design and to facilitate an easy change between the configurations for comparison.

11.6.1. Verification and validation for preliminary design tools

Verification has been done on a basic level, such as simple unit tests and basic 'back of the envelope' analytical calculations and derivations. These include simple hand-drawn free body diagrams of the wings and wing boxes and basic NVM-plots. Although the calculations have been verified on a simple level, a lot of assumptions and approximations have been made, which explains the inaccurate results of the models.

11.6.2. Verification plan

However, given the complexity of the code, more testing is needed. This involves utilising more unit tests and also introducing system tests to better test the interaction of the architecture. More sophisticated analytical models should be produced in order to test the accuracy of the numerical results. On top of that, the models are going to be improved and made more detailed, requiring additional testing of the new features.

11.6.3. Validation plan

Validation could be done through either a real-life experiment of a simple load case, like a cantilever beam under point loads. This would validated the equilibrium equations and deflection calculations. However, this is outside of the scope of the project and an alternative solution has to be found. One of these solutions would be to use a very elaborate and well-validated Finite Element Analysis software, if available or finding data extracted from a real-life experiment done by a third party.

At the moment, the values of stresses obtained from the model seem to underestimate the stresses greatly. This can later be fixed through extensive testing and validation. Nevertheless, the values can still be used for comparison and provide a good basis for structural trade-off.

12 Operations and Logistics

The Operations and Logistics of a system are very important to consider during the trade-off as they involves a lot of stakeholders. First, storage and standby operations are considered for all three concepts. Then, operation of the vehicle is described briefly, such as the flight mission itself, loading and unloading of passengers and more. After that, the actions related to the use and support of the system are be identified. The actions to be considered are: inspection, replacing and charging batteries, replacing and repairing damaged parts. Last but not least, the end-of-life logistics are discussed. The logistical advantages and disadvantages of each design then can be analysed and added to the complete trade-off process.

Starting off with ***Storage & Standby***, the main concern is the wingspan. As opposed to aerodynamic efficiency, for sideways clearance on taxiing or hangar storage, a small wingspan is beneficial. The wingspan of the tandem and the box concepts is very similar and thus roughly the same amount of storage volume is required. The third configuration has almost triple the wingspan of the other two, making it less beneficial when it comes to storage. As the aim of the project is to design a personal air-transport vehicle, a large

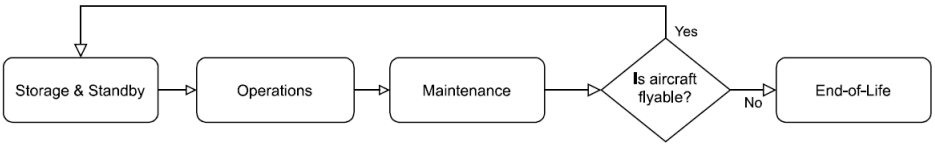

Figure 12.1: Generalised Operations and Logistics flow block diagram.

wingspan presents an issue of extra infrastructure required in order to facilitate the vehicle. A regular helipad sized space is sufficient to store the tandem and the box wing concepts, making it possible to store the vehicle on the property of private owners.

Operations involves mainly the mission itself and ground operations. In essence, the nominal mission is simply transportation of passengers between two locations, including taxiing, performing flight (details on which are given in Figure 7.1) and taxiing once again. The mission is very similar to a conventional passenger aircraft, with few differences such as the fact that that the aircraft under investigation are able to hover, and thus sometimes taxiing would not be necessary and that, as opposed to conventional aircraft, landing and take-off do not require a runway, reducing the infrastructure required substantially. Communications between the pilot and Air Traffic Control still remain a necessity throughout the mission, but in the future could possibly be modified in order to ease the travel and make it more 'personal' and robust. Communications between the pilot and the passengers could be done through simple intercom as the goal is to design the cabin's sound isolation well enough to eliminate a need for the in-flight headsets.

Ground operations, however, are different for all three configurations. During the fuselage design it was decided that the optimal configuration has 4 seats in a rectangular pattern behind the cockpit which houses the pilot. The exact arrangement can be seen in Figure 11.4. With this information the passenger accessibility to the cabin can be analysed. The box wing configuration has a clear difficulty with loading and unloading passengers from the side, because the passengers would have to pass under the wingtip connection to reach the side door. However, if the rear wing is high enough, they could possibly pass under the rear wing to access the cabin. The single wing aircraft presents a difficulty for entering passengers in another way, as the door is above the main wing. The passengers would have to climb onto the wing and enter from there, similarly to how it is done in small low-wing conventional aircraft. Finally, the tandem configuration is the easiest for the passengers to get into since there is no obstruction for the door from the sides, but on the other hand, the propellers are in close proximity to the passengers approaching the plane, which presents a risk of injury if not handled properly by the pilot or ground operators.

Moving onto ***Maintenance***, the general approach is again very similar between the configurations, with only some distinguishable specifics. As for the energy source being the same, the turnaround time including charging or battery replacement should not vary substantially between the 3 concepts. General inspection techniques can be used on all aircraft, like performing visual, mechanical, electrical and power checks. However, the time required for maintenance and repair varies. Assuming a full maintenance is performed, the tandem wing seems to be the simplest, with just 2 wing-rotation mechanisms and a medium number of open propellers. The box wing configuration may require a more extensive inspection due to the greater number of ducted engines due to the distributed propulsion system and the propulsion-rotation mechanisms. The single wing may require extra maintenance of the wing-embedded propeller system and the individual rotating mechanisms of the 4 main engines. The above mentions do not include other subsystem maintenance as it would be similar between the configurations. For these, the pilot could be informed about an issue through the on-board computer and later communicate the issues to the maintenance team upon landing. In the end, the maintenance operator (who could also be the pilot itself due to the small size of the aircraft, provided proper training), would deem the aircraft flyable or not. In case it is not, the aircraft would move on to the *End-of-Life* operations.

The ***End-of-Life*** operations largely involve dismantling the aircraft with the aim to either repurpose the parts, recycle or discard them if not recyclable. Dismantling time would most likely differ between the configurations. The box wing configuration would most likely take the longest due to the large amount of engines and complex wing. Next the single wing, due to its large engines which would most likely require heavy machinery to remove and complex wing design due to the embedded engines. Lastly, the tandem wing, with medium number of engines and fairly simple wing designs should take the least amount of time. After the dismantling, the parts would be analysed and either reused in the aircraft currently on the production line. Depending on the materials used, parts would either be recycled or discarded, with metals being easier to recycle than composite materials. Although the exact materials used are not known at this stage of the

design, the single wing is most likely to take the longest to complete the *End-of-like* stage.

To conclude, the tandem and the box wing configurations are beneficial when it comes to the operations and logistics, with the tandem wing performing slightly better in ground operations, maintenance, and end-of-life. The single wing concept is underperforming in nearly all aspects. Nevertheless, it is important to mention that operations and logistics also depend on the detailed design, specially involving maintenance and end-of-life stages.

13 Financial Plan

This chapter will discuss the long-term monetary objectives of the business and the strategies to achieve them as crafted within the the financial plan. Section 13.1 details the procedure used to estimate the production cost of a single eVTOL unit for all three different concepts and Section 13.2 expands on the operational costs derived from them. Section 13.3 will deal with the financial health of the business by computing the Return on Investment (ROI). Section 13.4 will close the chapter detailing the plan of attack post-DSE if the business were to continue being set up.

13.1. Unit Cost Analysis

This section describes the Eastlake Method (a modified version of the DAPCA-IV method) to reflect development and operational costs of a GA aircraft, as seen in Gudmundsson [21]. The team has used this formulation to estimate the unit cost for a single eVTOL aircraft for three different concepts, under the assumptions that the size and characteristics of such an eVTOL is similar to existing small GA aircraft.

The method starts with the computation of the man-hours required for the engineering phase, tooling and manufacturing phase through Equation 13.1, 13.2 and 13.3 respectively. These equations depend on the OEW $W_{airframe}$, maximum level airspeed expressed in KTAS per configuration and the number of aircraft to be produced in a five-year span, which was determined to be 1 000 from the market analysis [1].

Gudmundsson also makes use of a number of different factors depicted by the symbol F with a corresponding subscript to indicate the influence of a system or process in the total cost. F_{CERT} is used to scale the cost based on the certification class of the aircraft. F_{CF} is influenced by the type of flap system used. The eVTOL contains no High Lift Devices (HLD), and thus omits this factor throught the whole process. On the other hand, F_{COMP} accounts for the complexity of including composite materials. Finally, F_{PRES} depends on whether the aircraft to be designed has a pressurised cabin - which is not the case for the team's eVTOL designs.

$$H_{ENG} = 0.0396 \cdot W_{airframe}^{0.791} \cdot V_H^{1.526} \cdot N^{0.183} \cdot F_{CERT} \cdot F_{CF} \cdot F_{COMP} \cdot F_{PRESS} \tag{13.1}$$

$$H_{TOOL} = 1.0032 \cdot W_{airframe}^{0.764} \cdot V_H^{0.899} \cdot N^{0.178} \cdot Q_m^{0.066} \cdot F_{CERT} \cdot F_{CF} \cdot F_{COMP} \cdot F_{PRESS} \tag{13.2}$$

$$H_{MFG} = 9.6613 \cdot W_{airframe}^{0.74} \cdot V_H^{0.543} \cdot N^{0.524} \cdot F_{CERT} \cdot F_{CF} \cdot F_{COMP} \tag{13.3}$$

The total cost computation from these aspects follow through from the man-hours needed for each of these processes. As a result, the total costs of engineering, tooling and manufacturing can then be computed with Equation 13.4. Gudmundsson published his book in 2013, and states that the Consumer Price Index relative to the year 2012 CPI_{2012} accounts for the yearly inflation rate when estimating aircraft costs compared to those in the year 2012. These equations include salary rates R, where the values 120, 60, 50 dollars per hour are used for engineering, tooling and manufacturing respectively as suggested by Gudmundsson. As a result, the engineering C_{ENG}, tooling C_{TOOL} and manufacturing C_{MFG} costs can be computed through Equation 13.4:

$$C = 2.0969 \cdot H \cdot R \cdot CPI_{2012} \tag{13.4}$$

The total cost of development support follows from Equation 13.5, where N_P represents the number of prototypes to build and test, having the team choose four for the certification phase.

$$C_{DEV} = 0.06458 \cdot W_{airframe}^{0.873} \cdot V_H^{1.89} \cdot N_P^{0.346} \cdot CPI_{2012} \cdot F_{CERT} \cdot F_{CF} \cdot F_{COMP} \cdot F_{PRESS} \tag{13.5}$$

The total cost of flight test operations involves a full certification flight-test program and follows from Equation 13.6:

$$C_{FT} = 0.009646 \cdot W_{airframe}^{1.16} \cdot V_H^{1.3718} \cdot N_P^{1.281} \cdot CPI_{2012} \cdot F_{CERT} \tag{13.6}$$

The total cost of quality control entails the technicians and equipment required to demonstrate that the product is being designed and manufactured appropriately. It is computed with Equation 13.7:

$$C_{QC} = 0.13 \cdot C_{MFG} \cdot F_{CERT} \cdot F_{COMP} \tag{13.7}$$

The total cost of materials is calculated with Equation 13.8:

$$C_{MAT} = 24.896 \cdot W_{airframe}^{0.689} \cdot V_H^{0.624} \cdot N^{0.792} \cdot CPI_{2012} \cdot F_{CERT} \cdot F_{CF} \cdot F_{PRESS} \tag{13.8}$$

The total cost to certify, C_{CERT} is the collection of all costs prior to certification that are needed to develop the product: C_{ENG}, C_{DEV}, C_{FT} and C_{TOOL}. It is considered as the total fixed costs used later for the break-even analysis. In addition to the total fixed costs, there are several aircraft systems needed for every aircraft unit whose cost can be broken down. The costs of the engine powerplant and propellers computed from Equation 13.9 and Equation 13.10 respectively based on the shaft-horsepower and number of engines per configuration [28].

$$C_{PP} = N_{PP} \cdot \left(0.0022 \cdot P_{SHP}^3 - 0.4209 \cdot P_{SHP}^2 + 48.62 \cdot P_{SHP} + 1612\right) \tag{13.9}$$

$$C_{PROP} = \begin{cases} 3145 \cdot N_{PP} \cdot CPI_{2012} & \text{fixed-pitch propellers (tandem and box wing)} \\ N_{PP} \cdot CPI_{2012} \cdot CPI_{2012} \cdot D_P^2 \cdot \left(\frac{P_{SHP}}{D_P}\right)^{0.12} & \text{constant-speed propellers (single wing)} \end{cases} \tag{13.10}$$

The cost of the battery can be estimated through its mass m_{BAT} and specific energy density E_{kg} with Equation 13.11:

$$C_{BAT} = m_{BAT} \cdot E_{kg} \tag{13.11}$$

As a result, Equation 13.12 yields the unit cost per aircraft by combining the total fixed cost, manufacturing cost, quality control cost and material cost per aircraft with the engine, battery, landing gear (C_{LG}) and avionics (C_{AV}) costs. Gudmundsson also suggests an estimation for the last two.

$$\text{Unit Variable Cost} = \frac{C_{CERT} + C_{MFG} + C_{QC} + C_{MAT}}{N} + C_{LG} + C_{AV} + C_{PP} + C_{PROP} + C_{BAT} \tag{13.12}$$

Finally, Equation 13.13 computes the number of aircraft required to produce and sell to reach the break-even point, the point where the total revenue is equal to the total costs and from which all posterior sales will result in profit.

$$N_{BE} = \frac{\text{Total Fixed Cost}}{\text{Unit Price} - \text{Unit Variable Cost}} \tag{13.13}$$

Table 13.1 collects the results of evaluating the Eastlake cost estimation method for all three different aircraft configurations.

13.2. Direct Operational Cost

For calculating the operational cost of the aircraft a number of different aspects have to be taken into account. As in Section 13.1 the method used is Eastlake for General Aviation aircraft, but with some modifications to account for the fact that the plane is electric. The first part to calculate is the maintenance cost, C_{AP},

Table 13.1: Summary of unit costs and break-even expectation per eVTOL concept.

	Tandem wing	Box wing	Single wing
Total Fixed Cost [$]	157 556 420	164 371 115	150 552 029
Unit Variable Cost [$]	1 061 323	1 246 304	1 107 110
Unit Price [$]	2 000 000	2 000 000	2 000 000
Break-Even Number of Units	110	132	109

which is calculated by Equation 13.14 below.

$$C_{AP} = F_{\mathsf{MF}} \cdot R_{\mathsf{AP}} \cdot Q_{\mathsf{FLGT}} \tag{13.14}$$

$$C_{\mathsf{INS}} = 500 + 0.015 \cdot \mathsf{C}_{AC} \tag{13.15}$$

Where R_{AP} is the hourly rate for a certified mechanic, which is assumed to be $60\$/h$. Q_{FLGT} is the number of flight hours per year which is estimated to be 1055, and F_{MF} the ratio of maintenance to flight hours which using Eastlake's method gives 0.38 for all the eVTOL concepts. For storage a cost of 3000 $ per year is assumed, as indicated by Gudmundsson. For the insurance cost per year, Equation 13.15 is used.

Where C_{AC} is the price of the aircraft. The inspection costs for the aircraft as well as the engine overhaul is also included. Where the inspection cost can be assumed to be 500 $ per year [21] and the engine overhaul can be computed by Equation 13.16. All of these apply to both general aviation aircraft and the eVTOL; however, the following cost apply only to the eVTOL, as they are related to the battery and energy consumption. The battery replacement cost per year was calculated with Equation 13.17:

$$C_{\mathsf{OVER}} = 5 \cdot N_{PP} \cdot Q_{\mathsf{FLGT}} \tag{13.16}$$

$$C_{B,REP} = \frac{B_m \; C_{kg} \; Q_{\mathsf{FLGT}}}{F_{cycle} \; N_{cycles}} \tag{13.17}$$

Where B_m is battery mass in kg, C_{kg} is the price of the battery per kilogram, N_{cycles} is the number of discharge cycles of the battery. The last two are obtained from table 9.1. Finally, F_{cycle} is the number of flight hours per cycle, to calculate this, the target mission range is assumed, 300 km, and then is divided by the cruise speed for each concept. The cost of the energy also has to be taken into account. For this calculation a price of 0.41 $\$ - \mathrm{kWh}$ is used, which is the electricity price in Germany [57]. The following formula is used to calculate the total cost of electricity.

$$C_{B,REP} = \frac{B_m \; E_{kg} \; C_{kWh} \; Q_{\mathsf{FLGT}}}{F_{cycle}} \tag{13.18}$$

The specific energy of the batteries E_{kg} is obtained from Table 9.1. Finally, the following table presents the total direct operational costs for each aircraft concept divided into the relevant sub parts.

Table 13.2: Operational costs breakdown. All costs (except flight hour) are given in [$/year]

	Tandem wing	Box wing	Single wing
Maintenance Cost	24054	24054	24054
Storage Cost	3000	3000	3000
Battery replacement cost	33527	43814	29318
Annual Insurance Cost	38000	38000	38000
Engine Overhaul Fund	84900	127100	32150
Energy cost	69520	90852	60793
Total yearly cost	253001	326821	187316
Cost per flight hour [$]	240	310	178

13.3. Return on Investment

Once the cost breakdown has been determined, the team then started developing a timeline and allocating monetary resources destined to the different business phases planned. Crafting the financial plan is closely related to the Project Design & Development logic, explained later in Section 13.4. The business and the eVTOL idea was launched with the start of the DSE during the spring of 2021. This also marks the start of the engineering and development phase, where the team's main focus is the design and development of the eVTOL product. The development cost includes all those early investments needed to startup the company.

In the case for this particular eVTOL product, a preliminary estimate of these costs include engineering, development support and other costs as described in Section 13.1. The team believes that a strong initial investment of around $210 million is needed to reach the end of the development stage. Having the finished, detailed design is a milestone set to 2025.

Overlapping the latest stages of the development phase, the team has deemed appropriate to allocate a fraction of the manufacturing cost to start building the first number of prototypes to be used for testing and certification. According to the FAA [16], modern commercial aircraft can take between three to five years to certify, while new designs range between five and nine years. The team expects that certification for a small eVTOL, similar to small general aviation aircraft should take for around five years despite being a new category of aircraft. As a result, the aircraft should be fully certified by 2030. However, in order to start production and sales immediately after, the team plans to spend the remaining manufacturing, quality control, material and certification costs over the remaining certification period - totalling close to $ 600 million investment without profit. Yearly breakdown of these costs is presented in Table 13.3, where more money is spent as the design and certification phases develop.

The first units are expected to be manufactured and sold by 2031, the first year where the business will create revenue and profit. At this point, production costs are high and thus the team has established a production cost 20% higher than the one estimated from Section 13.1. The production cost is expected to reach its nominal value by 2035, where 200 aircraft shall be produced and sold. In contrast to the market analysis conducted earlier [1] , the new insight gained has made the team move up the objective of producing and selling 200 aircraft per year from 2040 to 2035, after which the team expects to keep growing, selling more units and cutting even more production costs. The team has capped the potential number of sales to 1250 per year after 2035 with a production cost of 90 % the stipulated value from Section 13.1 as a conservative approach. Reasons to believe in a future decrease in costs include the employee's learning curve, optimisation of different processes, end to outsourcing parts and processes for a cheaper, own development and many more. The team has unanimously set a retail price tag of $ 2 million, with a sensible profit margin and deemed competitive as required from the market analysis.

Additionally, the business has to deal with other non-technical costs including CapEx (or Operating Expense) and taxes. Deloitte [11] conducted a statistical study claiming that the average CapEx tends to be 12 % of the total revenues. Furthermore, corporate tax rates for businesses headquartered in The Netherlands is of 25 %.

Table 13.3 collects all expected cash flows in a timely fashion, depicting the different stages and evolution of the business. The spreadsheet crafted to do so computes the Net Present Value (NPV), Internal Rate of Return (IRR) and Return on Investment (ROI) for the tandem wing concept (collected in table 13.4), following the trade-off selection detailed in chapter 17. The model assumes a yearly discount rate of 6 %. Figure 13.1 then illustrates the long-term strategy and plan constructed from conducting this financial investigation.

Table 13.3: Profit & Loss (P&L) Statement.

	Development					Certification				
Timeline	2021	2022	2023	2024	2025	2026	2027	2028	2029	2030
Cash-Flow	-1 575 564.20	-16 799 774.87	-28 872 857.12	-44 628 499.17	-117 175 448.40	-42 058 914.77	-58 180 127.26	-81 498 132.51	-83 786 680.38	-103 569 569.46

Timeline	2031	2032	2033	2034	2035	2036	2037	2038	2039	2040	2041	2042	2043	2044	2045
Units sold	5	25	50	100	200	500	1 250	1 250	1 250	1 250	1 250	1 250	1 250	1 250	1 250
Selling Price	2 000 000.00	2 000 000.00	2 000 000.00	2 000 000.00	2 000 000.00	2 000 000.00	2 000 000.00	2 000 000.00	2 000 000.00	2 000 000.00	2 000 000.00	2 000 000.00	2 000 000.00	2 000 000.00	2 000 000.00
Unitary Cost	1 273 588.01	1 273 588.01	1 167 455.67	1 114 389.51	1 061 323.34	1 050 710.11	1 008 257.17	955 191.01	955 191.01	955 191.01	955 191.01	955 191.01	955 191.01	955 191.01	955 191.01
Revenue	10 000 000	50 000 000	100 000 000	200 000 000	400 000 000	1 000 000 000	2 500 000 000	2 500 000 000	2 500 000 000	2 500 000 000	2 500 000 000	2 500 000 000	2 500 000 000	2 500 000 000	2 500 000 000
Cost of Sales	6 367 940.03	31 839 700.17	58 372 783.65	111 438 950.60	212 264 667.82	525 355 052.84	1 260 321 465.15	1 193 988 756.46	1 193 988 756.46	1 193 988 756.46	1 193 988 756.46	1 193 988 756.46	1 193 988 756.46	1 193 988 756.46	1 193 988 756.46
Gross Margin	3 632 059.97	18 160 299.83	41 627 216.35	88 561 049.40	187 735 332.18	474 644 947.16	1 239 678 534.85	1 306 011 243.54	1 306 011 243.54	1 306 011 243.54	1 306 011 243.54	1 306 011 243.54	1 306 011 243.54	1 306 011 243.54	1 306 011 243.54
% Sales	36%	36%	42%	44%	47%	47%	50%	52%	52%	52%	52%	52%	52%	52%	52%
Operating Expense	-1 200 000.00	-6 000 000.00	-12 000 000.00	-24 000 000.00	-48 000 000.00	-120 000 000.00	-300 000 000.00	-300 000 000.00	-300 000 000.00	-300 000 000.00	-300 000 000.00	-300 000 000.00	-300 000 000.00	-300 000 000.00	-300 000 000.00
Profit from Operations	2 432 059.97	12 160 299.83	29 627 216.35	64 561 049.40	139 735 332.18	354 644 947.16	939 678 534.85	1 006 011 243.54	1 006 011 243.54	1 006 011 243.54	1 006 011 243.54	1 006 011 243.54	1 006 011 243.54	1 006 011 243.54	1 006 011 243.54
Taxes	-608 014.99	-3 040 074.96	-7 406 804.09	-16 140 262.35	-34 933 833.05	-88 661 236.79	-234 919 633.71	-251 502 810.88	-251 502 810.88	-251 502 810.88	-251 502 810.88	-251 502 810.88	-251 502 810.88	-251 502 810.88	-251 502 810.88
Net Profit	1 824 044.97	9 120 224.87	22 220 412.26	48 420 787.05	104 801 499.14	265 983 710.37	704 758 901.13	754 508 432.65	754 508 432.65	754 508 432.65	754 508 432.65	754 508 432.65	754 508 432.65	754 508 432.65	754 508 432.65
%	18%	18%	22%	24%	26%	27%	28%	30%	30%	30%	30%	30%	30%	30%	30%
Net Profit Adjustment															
Cash-Flow	1 824 044.97	9 120 224.87	22 220 412.26	48 420 787.05	104 801 499.14	265 983 710.37	704 758 901.13	754 508 432.65	754 508 432.65	754 508 432.65	754 508 432.65	754 508 432.65	754 508 432.65	754 508 432.65	754 508 432.65

Table 13.4: Summary of NPV, IRR and ROI obtained for the eVTOL tandem wing concept.

Net Present Value (NPV) [$]	1 027 905 397
Internal Rate of Return (IRR)	18 %
Initial Investment [$]	578 145 568
Return on Investment (ROI)	77.79 %

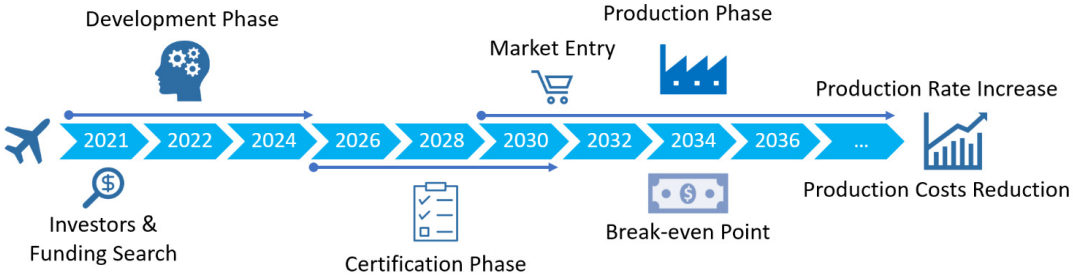

Figure 13.1: Timeline and long-term strategy for the eVTOL model market launch and expectations.

13.4. Project Design & Development Logic

This section will address the Project Design and Development logic, which consists on the planning of the activities to be performed after the current phase of the project ends (end of the DSE). Figure 13.2 contains a flow diagram of these actions.

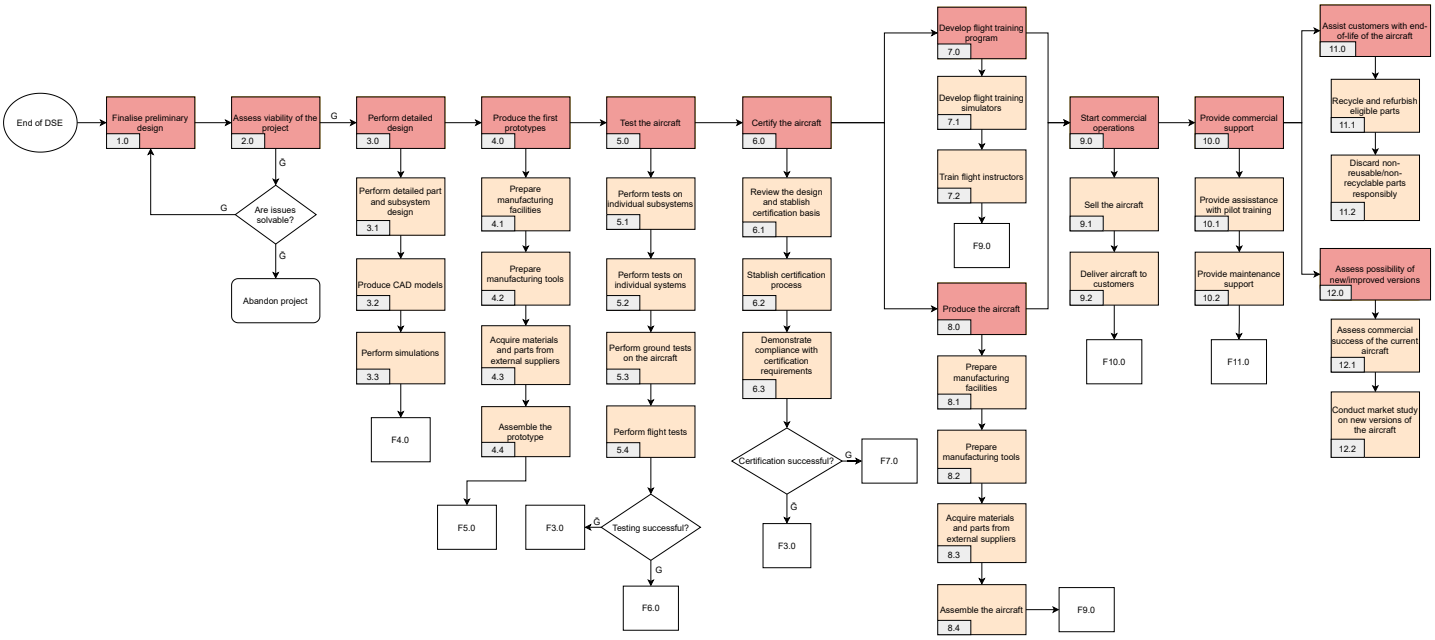

Figure 13.2: Flow diagram of actions to be performed for the project continuation after the Design Synthesis Exercise

The first step after the DSE is to finalise the preliminary design, addressing all areas that could not be finalised within the resources of this project. Once the preliminary design is finalised, the team needs to perform a viability assessment of the design, and make sure it complies with requirements. If the design is feasible, the next step is to perform a detailed design. In case it is not feasible, the teams needs to analyse whether the issues found are solvable. If so, the preliminary design needs to be modify such that the issues are solved; otherwise, the project would need to be abandoned.

In the detailed design phase, there are three steps to be performed: the detailed part and subsystem design, the creation of CAD models of such parts and subsystems, and detailed simulations of the performance of the vehicle.

After the detailed design, the first prototypes need to be built. This includes preparing the manufacturing facilities need for this, preparing the manufacturing tools to be used, acquiring the necessary materials and parts from external suppliers, training the staff and assembling the prototype.

Once the prototypes are built, the aircraft can be tested. The testing phase should start with tests on individual subsystems and parts. After these are tested, the whole aircraft can start ground tests to assess the integration of the subsystems. If these tests are passed, the aircraft can start the final phase of testing, the flight tests. In this phase, the whole aircraft is tested in missions of increasing difficulty, from hover tests and short flights to exemplary missions. In case the tests are not successful, the detailed design needs to be amended so that the issues encountered are solved.

Once the tests are completed and passed, the aircraft can go into certification. The certification process described here is the process followed by EASA [14]. First, the team should present the design to EASA, who will decide the certification category that applies to the aircraft. Following this, the team and EASA will decide how the compliance with the certifications requirements will be demonstrated. Lastly, this compliance should be demonstrated, after which EASA will certify the process. If the certification were not successful, the team would need to go back to the detailed design phase to amend the issues found.

After certification is successful, two parallel steps will need to be carried out. On the one hand, a flight training program has to be developed, which includes flight testing software and simulators, and training flight instructors. On the other hand, the aircraft needs to enter commercial production, for which the manufacturing facilities and tools need to be prepared, materials and parts from external suppliers need to

be acquired, and the aircraft need to be assembled.

After these steps, the company can start with commercial operations, selling the aircraft and delivering it to customers. Once the first aircraft are in the market, the company has to provide commercial support to customers, through assistance with training the pilots and with maintenance of the vehicles. After some years in the market (circa 15 years, the design operational life of the aircraft), the first aircraft will start to retire. The company should then provide EOL support to its customers, recycling and refurbishing the parts which can be used in newer models, and discarding in a responsible manner the parts and materials that cannot be recycled.

As a last consideration, the company should assess the commercial success of the aircraft, and evaluate the possibility of releasing improved models with e.g. more passenger capacity or different ranges.

14 Sustainability Plan

Since sustainability was an important part of the mission need, it is something that needs to be considered from an early design stage. Important to not is that sustainability concerns the entire life cycle of the aircraft, and not only operation. This chapter mainly concerns itself with environmental and social sustainability. The third, economic pillar of sustainability is only briefly addressed, since Chapter 13 covers it as well.

14.1. Environmental Sustainability

A study performed by Kasliwal et al. [29] found that eVTOLs emit less greenhouse gases than cars on ranges longer than 50 km, due to the longer amount of time spent in cruise. To maximise the time spent in cruise, vertical flight and transition should thus be done in a short timespan. Furthermore it was found that the design parameters having the most influence on global warming were the aircraft lift-to-drag ratio, grid carbon intensity and battery specific energy. During development, focus should thus lie on these three parameters.

André and Hajek [4] performed a similar study to Kasliwal et al., which confirms most of their findings, but also found that weight is an important factor. Additionally, when considering the entire lifecycle, it was found that the impact of production (without battery) is generally an order of magnitude less than the impact of operation. End-of-life impacts are about an order of magnitude less than production. Batteries production on the other hand does account for a significant part of the total lifecycle emissions. Still, the study highlights the importance to put priority on the sustainability of aircraft operations above production and end-of-life.

In order to make the eVTOL environmentally sustainable during operation, the minimisation of energy consumption over a 300 km mission will be set as the design optimisation target. Since the energy consumption is directly proportional to the climate impact during operation, this will tend to make the vehicle as sustainable as possible. To achieve this, the performance evaluation of the vehicle will be integrated with an optimisation algorithm (e.g., genetic algorithm), which optimises all design parameters.

As mentioned previously, battery production also has a significant impact on the life-cycle emissions of eVTOL vehicles. Melo et al. [34] found in their life-cycle analysis that lithium-sulfur batteries place a smaller burden on the environment than other chemistries. Another promising technology are solid state batteries, which are predicted to enter the market soon and achieve very long lifetimes with high energy densities [64]. The long lifetimes are relevant to sustainability since they minimise the amount of times that the batteries need to be replaced (thus reducing the number of batteries produced per vehicle). However, the sustainability of many batteries is constrained by the limited availability of the raw materials needed to manufacture them. Lithium, Nickel and Cobalt are in growing demand and need to be recycled in order to allow for a sustainable, circular economy [35]. Recycled batteries also have a lower production greenhouse impact [35] which can be beneficial for the sustainability of the eVTOL project as a whole. Therefore, the possibility of battery recycling will be investigated as a means of reducing the environmental footprint of the eVTOL.

14.2. Social Sustainability

Choice of batteries is also be influenced by social sustainability. According to Mossali et al. [35], cobalt mines for battery production have been under scrutiny for human rights violations. In order to act in a socially sustainable way, battery chemistries without Cobalt will be investigated most closely. For example,

Barke et al. [5] suggest that lithium-sulfur can provide a socially and environmentally sustainable alternative to lithium-ion batteries. According to Hoque et al. [23], hydrogen fuel cells perform better than batteries regarding social and environmental sustainability, but may not be economically sustainable due to the high prices associated with hydrogen. This could however improve in the future.

One of the major challenges for urban air mobility is the acceptance by the general public. This is in part related to the noise produced by VTOL vehicles with rotors. The final phase of this project will aim to characterise the noise properties of the vehicle and create a design that complies with ICAO regulations. This will be achieved by optimising disk loading and considering the use of ducted fans and noise liners.

One positive aspect of all eVTOLs with regard to social sustainability is the absence of harmful emissions during operation. The current aviation sector based on fossil fuels emits fine particulate matter and tropospheric ozone which are harmful to human health and cause 16000 annual premature deaths worldwide [65]. Road transport based on hydrocarbon fuels also emits harmful particulate matter, so eVTOLs could contribute to a cleaner air in urban areas as opposed to current transportation methods.

14.3. Economic Sustainability

In order to ensure that the project is economically sustainable in the long term, the product must address a market need that will grow in the future. Electric VTOLs will be desirable to enable faster door-to-door travel times, and can also be a part of the restructuring of urban transport. There is a growing public interest in reducing the number of private cars, and eVTOLs could provide a solution for this scenario [46]. Furthermore, since eVTOLs are not dependent on fossil fuels, their market growth will not be inhibited by their increasing scarcity. However, the depletion of other resources (especially for battery manufacturing) may affect eVTOLs, so this must be considered in the design process.

15 RAMS

In order to save costs of failures, as well as minimise their occurrences, the reliability, availability, maintainability and safety characterises of any design must be considered. These are key to designs in the aerospace industry as there is a large cost associated with designs that are not maintainable (i.e. are unable to fulfil requirements after a certain duration or failure) and not highly available (i.e. are unable to be operational for a large percentage of its design life), as well as unreliable and / or unsafe [3]. Firstly, availability will be briefly defined and discussed.

Availability can be defined by the ratio of the expected uptime to the nominal mission duration [6]. Design aspects that impact availability include turnover time, endurance, loiter time as well as other extraneous factors. Therefore, the power subsystem is designed as such to support the high range, and to have high energy density. This is one of the factors considered during trade-off, the battery that is the most suitable, however, includes other factors. Since the design is optimised for range and not endurance, which in a way hinders availability, but to a degree that compromises the mission. That being said, the turnover time (that is primarily dependant on battery recharging) is not considered, which also hinders availability for the battery that is selected. However, between the three concepts all three can potentially be equally available, all else being equal.

Safety is an important characteristic of design, which is mainly discussed by the crashworthiness. As it is essentially the lack of the propensity for a system not to fail, and to attenuate the impact of failure, it is mostly a question of structural integrity. A key aspect of design is not only the measured safety but also the passenger's perception thereof. There have been numerous surveys [45] where passengers' perception of cabin safety was recorded. It was mentioned that despite most passengers being relatively unenthusiastic about the briefings themselves, they were fairly confident with the cabin safety equipment itself. Therefore, the most important aspect of this is to demonstrate the use of cabin safety equipment itself, which significantly boosts the impression of safety.

Maintainability is the ability for a system to be continuously improved and kept in its original condition. This includes replacement of parts and disassembling, but also involves its ability to meet novel requirements, should they appear [6]. For this reason, parts or assemblies that are relatively novel are those that hinder maintainability despite being innovative. As a result, the single wing and box wing configurations, as they involve assemblies with relatively novel concepts such as a cutout in the wing for the single wing and the struts that connect the wing to the tail for the box wing involve new structures that are difficult to maintain.

Reliability entails the probability that the system will perform its required function under given condi-

tions for a stated time interval [6]. It furthermore decreases as a function of system complexity. Because of this, the more complex the system is, the more difficult it is to predict points of failures and therefore decreases the mean time between failures (MTTF). Reliability also depends on extrinsic factors such as the operating condition and the mission profile, although that is not relevant for the purpose of the trade-off [6]. Hence, high complexity of the design is not preferred, similarly to maintainability, and for that reason, the box wing is considered the least reliable, due to its rotating propulsion and highest number of engines, making it the most complex. This is followed by the single wing, which is axiomatically structurally complex due to the cutouts in the wing. Finally, the tandem wing has the least complexity and the mechanisms of failure are arguably the most similar to conventional aircraft, potentially allowing the design to be the most reliable one.

All in all, it is clear that in every engineering design RAMS characteristics are always considered to some extent to minimise failures and costs associated. As such, it was found that the availability is potentially similar for all three configurations, but that was not the case for reliability and maintainability for which the tandem configuration is considered the best, due to its design complexity and modes of failure that strongly resemble those of conventional aircraft.

16 Technical Risk Analysis

Technical risk is a part of every system and subsystem. In order to deliver a successful design, it is not enough to simply use the latest design technologies, but also make sure that all the important risks are identified and managed. In Section 16.1 relevant risks are listed, and newly found risks are explained. All risks are given a score and plotted in a risk map in Section 16.2, and the most severe risks are managed.

16.1. Risk Assessment & Identification

In this section, the most relevant technical risks associated with the aircraft design are identified. A short explanation is given as to why a risk is relevant, and a score is given based on the likelihood and consequence of each risk. The scale used to determine the scoring is given in Table 16.1 and Table 16.2 for the probability of occurrence and the consequence, respectively.

Table 16.1: Score associated with probability of occurrence. Obtained from [20]

Score	% Probability	Chance
1	$p < 1\%$	very low
2	$1\% \leq p < 30\%$	low
3	$30\% \leq p < 50\%$	medium
4	$50\% \leq p < 70\%$	high
5	$p \geq 70\%$	very high

Table 16.2: Score associated with consequence of the risk.

Score	Probability
1	Negligible impact
2	Small performance reduction
3	Moderate performance reduction
4	Partial mission failure
5	Complete mission failure

Below is the list of all technical risks identified earlier in the Baseline report. As they have been described in detail in the Baseline report, with scores given, both before mitigation and after mitigation, the same descriptions will not be given in this chapter. However, the risk maps, Table 16.3 and Table 16.6, are given for both set of risks.

- **RT.1** - Calculation errors
- **RT.2** - Not meeting range requirement
- **RT.3** - Not meeting lift-to-weight ratio requirement
- **RT.4** - Power failure
- **RT.5** - Engine failure during cruise
- **RT.6** - Cabin fire
- **RT.7** - Engine failure during vertical flight/hover
- **RT.8** - Damage during maintenance/ground operation
- **RT.9** - Failing certification
- **RT.10** - Unexpected centre of gravity shift during flight
- **RT.11** - Flutter before reaching maximum speed
- **RT.12** - Running out of energy during flight
- **RT.13** - Lightning strike
- **RT.14** - Control failure
- **RT.15** - Hard landing
- **RT.16** - Maximum load factor exceeded
- **RT.17** - Unacceptable noise level

- **RT.18** - Aircraft too difficult to control
- **RT.19** - Pilot incapacity
- **RT.20** - Bird strike
- **RT.21** - Engine/wing actuator jammed
- **RT.22** - OEW too high
- **RT.23** - Aircraft price is too high
- **RT.24** - Aircraft operations are unsustainable
- **RT.25** - Operating cost too high
- **RT.26** - Aircraft less performant than competition
- **RT.27** - Aircraft fails to attract customers
- **RT.28** - Depletion of natural resources

16.1.1. Additional risks

In this subsection, additional risks are added with their respective explanations. These risks were identified during the design and trade-off phase, where the older technical risks were identified in the Baseline report, and thus those are more generalised risks.

RT.29 - Unstable liquid electrolyte batteries. The use of batteries in all three configurations involves obvious risks. One of such risks comes from the fact that liquid electrolyte batteries are unstable. This may cause overheating of even an explosion. Although it is not common for such batteries to explode or overheat if treated properly, the effect if such an explosion could be quite detrimental to the mission and passengers' safety.

RT.30 - No validation of models. Not enough resources are available to properly validate all models used throughout the design process. This might lead to the undetected use of an invalid model. This could lead to bad predictions of aircraft parameters, and thus to a badly optimised design. Although the probability of this is low, the consequence can be moderate.

RT.31 - Emergency landing on water. Having a fully electric vehicle becomes an important hazard if the electronics and wiring is not fully protected from the environment, such as water/moisture. An extreme case of this would be a crash-landing on water. Due to the damage to the structure, the vulnerable circuitry and batteries could get exposed to water, putting passengers and the pilot into a dangerous situation. Again, the chance of such a crash landing happening is low, but the outcome would be disastrous.

RT.32 - Inaccurate estimation of stability. Due to the wide variety of eVTOL configurations, there are no design tools for stability that can be readily applied. This might lead to an inaccurate estimation of control derivatives, which are already hard to estimate for conventional aircraft. The probability of an inaccurate stability model is thus medium. The consequence can be considered moderate, as it can lead to dangerous situations when flight-testing new control systems on naturally unstable aircraft.

RT.33 - No available landing spots. An important area for operation for eVTOL's is in cities, where space is costly. This will likely lead to relatively small 'vertiports'. A consequence of this can be lack of space when multiple aircraft try to land. Using effective air traffic management systems, the probability of this risk is still medium, as eVTOL flights will not always be scheduled days in advance. To avoid this, the different aircraft already have a 30 [min] loiter time in cruise, and a 30 [s] loiter time while hovering. The consequence of no landing spots is moderate, as the aircraft will have to divert or even land in an unprepared area. It should however not damage the aircraft or injure the passengers, because it can land vertically.

RT.34 - Circuitry exposure to moisture. The eVTOL should be able to operate in adverse weather conditions, such as rain, mist or snowfall. In hindsight, these weather conditions introduce undesirable moisture to the power system. The probability of such occurrence should be high given a good waterproof design, examples of which are readily available in the industry. The consequence is moderate as, at most, partial mission failure takes place.

RT.35 - Flight load factor exceeds the maximum load factor. During computation of the Manoeuvre and Gust loading diagrams, maximum load factors are set by Certification Specifications. Although is not likely that the aircraft will exceed these as a lot of research goes into establishing these maximums, it is still possible. This would impose loads on the wings that are not expected and are not tested for (only during design). Because of this, a safety factor of 1.5 is applied to the maximum load factors, making an ultimate load factor, for which the structure is designed. Exceeding this too is highly improbable. The consequence of exceeding maximum load factors can be considered as partial mission failure, as the aircraft would be able to land safely but will most likely need extensive repairs or even disposal.

RT.36 - Tandem wing concept-related risks

- **RT.36a - Wing rotating mechanism failure** Since the tandem wing concept is a tilt-wing design, the consequence of a failure of the rotating mechanism is more severe than for a tilt-rotor design. If one wing tilts is stuck, or tilts uncontrollably, a large moment can be created, which might make the

aircraft uncontrollable. The effects of this can be reduced by rotating the functioning wings to the same position as the malfunctioning wing. Since rotation happens during transition, where usually the speed and altitude are low, it could prove difficult to react in time, although a computer could help. A stuck wing might also make a vertical landing impossible, requiring a conventional landing.

- **RT.36b - Propeller strike**

  The open propellers of the tandem wing concept can lead to the propeller striking the ground. Since for VTOL operations, the propellers will be tilted upward when lading or taking of, this is not likely to cause issues. If the aircraft would also be used for conventional landings, propeller strikes are more likely to happen. Proper landing gear design and positioning should largely alleviate this risk.

- **RT.36c - Propeller causing injury**

  Another risk associated with the open propellers is that passengers or ground crew could be injured if the propellers are rotating while on the ground. The consequences of this are severe, possibly leading to death. Apart from the risk of physical injury, the propellers being at head and leg height might make the aircraft less attractive for customers.

RT.37 - Box wing concept-related risks

- **RT.37a - Flap failure** Similar to RT.36a, a failure of the flap mechanism may make introduce high aerodynamic moments and make the aircraft difficult or impossible to control. The effect will however be less severe than in the case of a tilt wing.

RT.38 - Single wing concept-related risks

- **RT.38a - Engine failure during hover** Although already addressed by RT.7, engine failure during hover is considered again for the single wing concept, as this concept is still very sensitive to engine failures. The consequence of an engine failing in hover are very severe, as failure of one engine can already make the aircraft uncontrollable.
- **RT.38b - Stability in transition** The large ducts around the propellers can act as control surfaces. This can help make the aircraft more controllable during flight, but can introduce problems during transition. The rotation of the ducts can introduce aerodynamic moments on the aircraft, which have to counteracted in order for the aircraft to be controllable.

16.2. Risk analysis

Table 16.4 shows the risk scores for all the additional risks. These are also tabulated in Table 16.3, where the other risks are also presented.

Table 16.3: Risk map with the additional technical risks added.

Consequence						
	5	RT.6, RT.12, RT.14, RT.19	RT.4, RT.11, RT.29, RT.32, RT.38a			
	4	RT.8, RT.9, RT. 13, RT.22, RT. 27, RT.31, RT. 36a, RT.37a, RT.38b	RT.2, RT.18, RT.21, RT.25, RT.30, RT.35, RT.36c	RT.5, RT.7		
	3	RT.20, RT.23, RT.28, RT.36b	RT.3, RT.16, RT.24, RT.26, RT.33, RT.34,			RT.1
	2	RT.10	RT.17		RT.15	
	1					
		1	2	3	4	5
		Probability				

Table 16.4: Scores for newly identified risks

Risk (RT)	29	30	31	32	33	34	35	36a	36b	36c	37a	38a	38b
Probability score	2	2	1	2	2	2	2	1	1	2	1	2	1
Consequence score	5	4	4	5	3	3	4	4	3	4	4	5	4

16.3. Risk prevention and mitigation

Below are the risks that need to be mitigated as these exceed the acceptable threshold. For each risk a prevention strategy and a contingency plan are given.

RT.29 - Unstable liquid electrolyte batteries
Prevention Keeping the batteries cool can help prevent them from overheating or even exploding. Splitting the battery in several portions and separating them can prevent a chain reaction in case on the batteries does indeed overheat or explode. Another preventative measure would be to use solid state batteries which are stable and much safer. Firewalls could be installed around the batteries in order to protect the rest of the aircraft and passengers from any damage, or at least reduce the damage.

Contingency plan In case the batteries show any signs of overheating, the issue must be immediately reported to the pilot. He/she then can regulate the temperature accordingly and possibly cut off the faulty battery from the rest to avoid a chain reaction. Needless to say, the pilot should land the aircraft as fast as possible.

RT.30 - No validation of models.
Prevention Although insufficient resources are present at the current design stage to validate all models, this is something that can be avoided by using validated models from previous research instead of making new ones.

Contingency plan At a later design stage, testing can be performed on subsytems to validate them. Although this might require redesign if it is found out that some models were not valid, it is better to find this out before building a complete prototype.

RT.32 - Inaccurate estimation of stability
Prevention With eVTOLs gaining interest, there is more research in the field and thus better methods are invented in order to estimate stability in quick and precise manner. Computational Fluid Dynamics (CFD) software could be used in order to analyse the stability and get precise data.

Contingency plan In case the aircraft is deemed unstable, which would be found during testing, it has to be redesigned. An addition of a specific control surface, like a vertical tail for example, could fix the problem, depending on the issue at hand.

RT.35 - Flight load factor exceeds the maximum load factor.
Prevention It is hard to prevent this risk, as the pilot does not know what load factors he/she is going to encounter. However, the pilot can refrain from performing hard manoeuvres. This would decrease the probability of such an instance occurring even further.

Contingency plan In case such loads are indeed met, there is already a safety factor that will prevent the structure from failing. Needless to say, the structure can still fail, but not critically. Such failures could be yielding or buckling. Extensive repairs will have to be made once the aircraft has landed.

RT.36c - Propeller causing injury
Prevention To prevent the open propellers from injuring people, they could be surrounded by a ring. As the propellers are usually horizontal while the ground, this should prevent people from running into them accidentally. Note however that the propellers can still be accessed, although it should be less likely. Completely covering the propeller by a grid should prevent this risk almost completely, although this is not preferred as it would reduce the efficiency of the propulsion system.

Contingency plan There is little that can be done once someone has been injured. It can however be required for every vertiport to be equipped with first aid kits and to be accessible to ambulances.

RT.38a - Engine failure during hover
Prevention Engine failures can be prevented partially by testing the engines before each flight, and by performing regular inspections of the power and propulsion subsystem. It is however still possible for an engine to fail unexpectedly.

Contingency plan To reduce the effects of an engine failure in hover, redundancy should be designed for. This is critical for the single wing concept. To add redundancy without changing the concept significantly, extra counter-rotating engines and propellers could be added in each fan. This not only adds redundancy, but could also increase efficiency.

16.3.1. Revised risk scores

Based on the prevention or mitigation strategies outlined in the previous part, every risk was given a new score. These can be found in Table 16.5, where the altered scores are colored grey. The effects of managing the risks can also be seen in Table 16.6, where no serious risks are present anymore.

Table 16.5: Risk scores after managing the worst risks. The altered scores are highlighted in grey.

Risk (RT)	29	30	31	32	33	34	35	36a	36b	36c	37a	38a	38b
Probability score	1	1	1	1	2	2	1	1	1	1	1	2	1
Consequence score	3	4	4	4	3	3	3	4	3	4	4	3	4

Table 16.6: Risk map after managing the most severe risks

Consequence						
	5	RT.6, ***RT.11***, RT.12,RT.14, RT.19				
	4	***RT.4***, RT.8, RT. 9, RT.13, ***RT. 21***, RT.22, ***RT. 25***, RT.27, ***RT. 30***, RT.31, ***RT. 32***, RT.36a, ***RT. 36c***, RT.37a, RT.38b				
	3	RT.20, RT.23, RT.28, ***RT.29***, ***RT.35***, RT.36b	***RT.2***, RT.3, ***RT. 7***, RT.16, ***RT. 18***, RT.24, RT. 26, RT.33, RT. 34, ***RT.38a***			
	2	RT.10, RT.15	***RT.1***, ***RT.5***, RT. 17			
	1					
		1	2	3	4	5
		Probability				

17 Trade-Off

The design trade-off between the different configurations can be found in this chapter. Section 17.1 briefly describes the method used, level of compliance is given in Section 17.2. The trade-off itself and the sensitivity analysis are given in Section 17.3 and Section 17.4, respectively.

17.1. General Methodology

Having previously defined the required selection criteria and their associated weights (see Chapter 4), it is now possible to define the grading scheme and by extension the overall trade-off process. The grading scheme will be comprised of levels of compliance (grades) to a specific selection criterion. These will be associated to a specific colour and will improve the visualisation of the trade-off process.

With the various required tools defined, it is now possible to present the trade-off process. This will be summarised in a trade-off matrix, with the selection criteria put in a row and the configurations in a specific column. The column width will be proportional to the weight of its associated selection criterion. Each cell will also be coloured in order to visualise their level of compliance to that specific selection criterion. When the trade-off matrix is finalised, a qualitative assessment of all configurations w.r.t. the grading given will allow the team to select a winning configuration.

17.2. Level of Compliance

It is now the turn to define the different levels of compliance (with their associated colour and grade) that a selection criterion can be met. These are as follows:

- **Excellent**: this means that the configuration exceeds requirements or is the best for that particular criterion (Green). Its numeric grade is 1 (or 100 %).
- **Good**: this level is associated to a nominal performance which meets requirements (Blue). This is associated to a grade of 0.8 (or 80%).

- **Standard**: this level refers to an acceptable level of compliance with requirements but that still is less optimal or with a lower performance when compared to the rest of configurations (Gray). Due to its lower performance when compared to the Good level of compliance, it is associated to a grade of 0.6 (or 60%).
- **Sub-optimal**: this level refers to the fact that the configuration has multiple but correctable deficiencies (Yellow). This relates to a grade of 0.4 (or 40%).
- **Unacceptable**: this level shows that the configuration's performance for that selection criterion is non-correctable and must be discarded or completely redesigned if selected (Red). Due to the aforementioned comments, its associated grade is 0.

Each configuration will hence be graded using the previously described selection criteria and grading scheme.

17.3. Trade-Off Matrix

Initially, it was found that the single wing configuration is the most optimal option with, possibly, the tandem wing being a second feasible option. This result is due to the fact that when only accounting for quantitative measures for **Power**, the single wing obtains an *Excellent* grade. In terms of **Control and Stability**, it must be noted that even though the cg range is at preferable higher values, it is also much more limited than for the other options. This would initially allow the single wing to obtain a *Standard* grade in that aforementioned category. However, cg range for both tandem wing and box wing can also be altered easily using mobile aerodynamic surfaces without reducing the lifting capacity of the aircraft, whereas for the single wing a different and more complicated control system might be required. Additionally, it must be noted that the single wing does not allow for any engine failure during hover in terms of control authority, reducing its grade to an unacceptable level. Due to requirement VTOL-STK-6, this requires additional attention for a re-design of the configuration which factors in an additional scheduling risk, which is leading it to be unacceptable in the limited time frame of this project. An update in the grading taking into the consideration the latter must be done. Finally, it was also found that this configuration is the most naturally unstable of the three which further confirms its grading.

Secondly, it can be seen that both the box wing and the single wing have a sub-optimal grade for **Passenger Comfort**, which mainly relates to passenger boarding. In fact, for the box wing, the vertical connection between the wings impedes passengers to board, whereas for the single wing, passenger would need to board the aircraft by going on top of the wing. Both issues can still be correctable and possible operational solutions can be found without requiring a total or partial (sub-)system re-design.

Furthermore, due to the preliminary nature of the analysis, specifically for the propulsion and power parameters, a qualitative aspect to the **Power** criterion must added to the quantitative nature for a more accurate grading. In fact, the single wing has engines that are straight behind each other. The first set of engines accelerates the air, leading the inflow velocity for the rear-part of the engines already to have a higher velocity. This slipstream ingestion can reduce thrust and result in more necessary power for cruise. This can be avoided for both the tandem wing and box wing configurations (due to their different wing heights), but it will probably be not possible for the single wing due to the big size of the engines [58]. The risk factor of the uncertainty for being able to compensate the decrease in efficiency must hence be included in the trade-off. This leads to an update of the single wing's **Power** grade to *Standard*.

Using the previously mentioned qualitative aspects, the final trade-off matrix can be found in Table 17.1.

Table 17.1: Final Trade-off matrix between possible configurations.

Criterion / Option	**Power** (5/20)	**Energy Consumption** (5/20)	**Control & Stability** (4/20)	**Cost** (2/20)	**Noise** (3/20)	**Pass. Comf.** (1/20)
Tandem wing	Cruise power = 110024 W & Hover power = 1177550 W [Blue]	422 MJ [Gray]	CG: 1.570-1.685 m & Allowed number of engine failure: 3 [Blue]	C_{unit} = \$1061323 [Blue]	140.4 dB [Yellow]	Nominal [Blue]
Box wing	Cruise power = 113762 W & Hover power = 1755275 W [Gray]	557 MJ [Yellow]	CG: 1.570-1.681 m & Allowed number of engine failure: 5 [Blue]	C_{unit} = \$1246304 [Yellow]	110.4 dB [Blue]	Vertical wing connection. [Yellow]
Single wing	Cruise power = 102327 W & Hover power = 639938 W with possible high decrease in efficiency [Gray]	398 MJ [Blue]	CG: 1.765-1.795 m & Unacceptable allowed number of engine failure: 0 [Red]	C_{unit} = \$1107110 [Gray]	136.8 dB [Gray]	Boarding on top of wing [Yellow]

From Table 17.1, the following grades are given:

- Tandem wing: 6.9/10
- Box wing: 6/10
- Single wing: 4.9/10

Hence, the best configuration remains to be the tandem wing with a possible alternative choice being the box wing. The single wing's performance in the **Control and Stability** criterion is unacceptable and additional effort would be required to make the system stable and safe which hence confirming its lowest ranking.

Before being able to present the winning configuration which would conclude the design configuration selection, it is essential to check how sensitive the trade-off process is to a change in weights.

17.4. Sensitivity Analysis: Weights

In order to verify the robustness of the trade-off procedure, a sensitivity analysis on the criteria weight change will be performed.

The influence of the criteria weights was investigated to determine how the trade-off procedure and concept grade outputs will vary accordingly. To do this, the same exact trade-off method was performed with different weight values according to their importance. Firstly, a new trade-off was constructed where all weights were assumed to be equally distributed among the six different criterion. Then, the trade-off outcome was reported in each of the six cases where a criterion's weight was reduced to zero and redistributed equally among the other five criteria. Table 17.2 collects the average grades and standard deviations calculated from the seven new tables. The trade-off ranking remained unchanged (being tandem wing first, then box wing and single wing last) except for the case where the stability and control criteria was entirely removed - which brought up the single wing only to second place.

Table 17.2: Trade-off output summary after criteria weight sensitivity.

Concept	Average Grade	Grade Standard Deviation
Tandem wing	7/10	2.24 %
Box wing	6/10	4.09 %
Single wing	4.7/10	7.52 %

Furthermore, a six-by-six matrix was constructed to investigate how small changes to each criteria weight would affect the final scoring for a selected concept. This matrix was parametric on a multivariate level, resulting in a large number of different possible weight value combinations that not always added up to 100 % but was generally close. Table 17.3, Table 17.4 and Table 17.5 collect the variation in grade (expressed as a decimal) for a selected range of different criteria weights. From this analysis, the team observed how the results gathered from the original trade-off are repeated all over again when there are small changes to the weight values. Header symbols are abbreviations for the criteria defined in Chapter 4 and seen in Table 17.1.

Table 17.3: Sensitivity grades for the Tandem Wing.

		P / EC \SC							
	Tandem wing	0 / 0.29 \0.15	0.2 / 0.25 \0.15	0.21 / 0.26 \0.15	0.22 / 0.27 \0.15	0.23 / 0.28 \0.15	0.25 / 0.1 \0.15	0.25 / 0.16 \0.15	0.25 / 0.29 \0.15
C / N \ PC	0.41 / 0.1 \0.05	0.7020	0.8380	0.8520	0.8660	0.8800	0.7880	0.8240	0.9020
	0.23 / 0.12 \0.05	0.5660	0.7020	0.7160	0.7300	0.7440	0.6520	0.6880	0.7660
	0.19 / 0.14 \0.05	0.5420	0.6780	0.6920	0.7060	0.7200	0.6280	0.6640	0.7420
	0.15 / 0.16 \0.05	0.5180	0.6540	0.6680	0.6820	0.6960	0.6040	0.6400	0.7180
	0.35 / 0.1 \0.05	0.6540	0.7900	0.8040	0.8180	0.8320	0.7400	0.7760	0.8540
	0.29 / 0.1 \0.05	0.6060	0.7420	0.7560	0.7700	0.7840	0.6920	0.7280	0.8060
	0.15 / 0.11 \0.05	0.4980	0.6340	0.6480	0.6620	0.6760	0.5840	0.6200	0.6980

Table 17.4: Sensitivity grades for the Box Wing.

		P / EC \SC							
	Box wing	0 / 0.29 \0.15	0.2 / 0.25 \0.15	0.21 / 0.26 \0.15	0.22 / 0.27 \0.15	0.23 / 0.28 \0.15	0.25 / 0.1 \0.15	0.25 / 0.16 \0.15	0.25 / 0.29 \0.15
C / N \ PC	0.41 / 0.1 \0.05	0.5000	0.6040	0.6140	0.6240	0.6340	0.5740	0.5980	0.6500
	0.23 / 0.12 \0.05	0.4440	0.5480	0.5580	0.5680	0.5780	0.5180	0.5420	0.5940
	0.19 / 0.14 \0.05	0.4440	0.5480	0.5580	0.5680	0.5780	0.5180	0.5420	0.5940
	0.15 / 0.16 \0.05	0.4440	0.5480	0.5580	0.5680	0.5780	0.5180	0.5420	0.5940
	0.35 / 0.1 \0.05	0.4760	0.5800	0.5900	0.6000	0.6100	0.5500	0.5740	0.6260
	0.29 / 0.1 \0.05	0.4520	0.5560	0.5660	0.5760	0.5860	0.5260	0.5500	0.6020
	0.15 / 0.11 \0.05	0.4040	0.5080	0.5180	0.5280	0.5380	0.4780	0.5020	0.5540

Table 17.5: Sensitivity grades for the Single wing.

		P / EC \SC							
	Single Wing	0 / 0.29 \0.15	0.2 / 0.25 \0.15	0.21 / 0.26 \0.15	0.22 / 0.27 \0.15	0.23 / 0.28 \0.15	0.25 / 0.1 \0.15	0.25 / 0.16 \0.15	0.25 / 0.29 \0.15
C / N \ PC	0.41 / 0.1 \0.05	0.5580	0.6460	0.6600	0.6740	0.6880	0.5560	0.6040	0.7080
	0.23 / 0.12 \0.05	0.4620	0.5500	0.5640	0.5780	0.5920	0.4600	0.5080	0.6120
	0.19 / 0.14 \0.05	0.4500	0.5380	0.5520	0.5660	0.5800	0.4480	0.4960	0.6000
	0.15 / 0.16 \0.05	0.4380	0.5260	0.5400	0.5540	0.5680	0.4360	0.4840	0.5880
	0.35 / 0.1 \0.05	0.5220	0.6100	0.6240	0.6380	0.6520	0.5200	0.5680	0.6720
	0.29 / 0.1 \0.05	0.4860	0.5740	0.5880	0.6020	0.6160	0.4840	0.5320	0.6360
	0.15 / 0.11 \0.05	0.4080	0.4960	0.5100	0.5240	0.5380	0.4060	0.4540	0.5580

18 Selected Configuration and Layout

The aim of this report was to document the selection process of one of the three concepts presented in the baseline report. To do so, a multidisciplinary approach to analyse the strengths and weaknesses of each of the three concepts, in sufficient depth, was necessary. Through the process of analysing the different options, a better defined configuration and layout had to be chosen for each of the three concepts. All the concepts have some aspects in common such as the fuselage layout, which is presented in Figure 11.4. As can be observed a 1-2-2 seat configuration is chosen for passenger comfort, with large cargo located at the back to minimise the cross-section. Furthermore, solid state batteries were chosen for all the different configurations as the energy source, as it was deemed to be an aspect independent of the configuration.

After the trade-off presented in Chapter 17, the best overall configuration out of the three was the tandem configuration, for which a conceptual drawing is shown in Chapter 5. This concept uses leading edge open propellers for propulsion, providing a higher air velocity over the wing. In order to achieve vertical take-off and landing, a system will be designed to allow the entire wing to rotate about its spanwise axis. By doing this, the downwash of the propellers will not hit the top surface of the wing when taking-off or landing vertically. A total of 16 engines will be used with a propeller area of 0.47 m^2 per engine. Regarding the wing planform, due to the low cruising speed, no sweep is applied at quarter chord. A 0.4 taper ratio was chosen in order to obtain a nearly elliptical lift distribution; furthermore, both wings were chosen to be identical, as according to literature, for a tandem configuration, having equal span wings reduces induced drag. Nevertheless, this might change later in order to make the aircraft more stable. For lateral stability, it was found that a vertical tail would be needed.

Finally, by analysing and simulating the flight performance during cruise, transition and hover for the configuration, as well as computing the critical loading cases that the eVTOL will encounter during service, it was possible to compute a class II weight estimation for the aircraft, which yielded a Maximum Take-Off Mass of 1867.7 kg and an Operational Empty Mass of 1307 kg.

Bibliography

[1] Javier Alba Maestre et al. *Baseline Report - Multi-Disciplinary Design and Optimisation of Long-Range eVTOL Aircraft*. 2021. DOI: 10.5281/zenodo.5575953.

[2] Javier Alba Maestre et al. *Project Plan - Multi-Disciplinary Design and Optimisation of Long-Range eVTOL Aircraft*. 2021.

[3] "An overview on reliability, availability, maintainability and supportability (RAMS) engineering". In: *International Journal of Quality and Reliability Management* 25 (3 2008), pp. 330–344. ISSN: 0265671X. DOI: 10.1108/02656710810854313.

[4] Nicolas Andŕe and Manfred Hajek. "Robust Environmental Life Cycle Assessment of Electric VTOL Concepts for Urban Air Mobility". In: June 2019. DOI: 10.2514/6.2019-3473.

[5] Alexander Barke et al. "Life cycle sustainability assessment of potential battery systems for electric aircraft". en. In: *Procedia CIRP*. The 28th CIRP Conference on Life Cycle Engineering, March 10 – 12, 2021, Jaipur, India 98 (Jan. 2021), pp. 660–665. ISSN: 2212-8271. DOI: 10.1016/j.procir.2021.01.171. URL: https://www.sciencedirect.com/science/article/pii/S221282712100202X (visited on 04/30/2021).

[6] Alessandro Birolini. *Basic Concepts, Quality & Reliability (RAMS) Assurance of Complex Equipment & Systems*. Springer Berlin Heidelberg, 2017, pp. 1–24. DOI: 10.1007/978-3-662-54209-5_1.

[7] Saullo G. P. Castro. *Urban Air Mobility CourseModule 1 Structures Part 2/2 Reader*. Delft, Netherlands: Delft University of Technology, Faculty of Aerospace Engineering, 2021.

[8] Shamsheer S. Chauhan and Joaquim R.R.A. Martins. "Tilt-wing eVTOL takeoff trajectory optimization". In: *Journal of Aircraft* 57 (1 2020), pp. 93–112. ISSN: 15333868. DOI: 10.2514/1.C035476.

[9] X. Cheng et al. "A review of PEM hydrogen fuel cell contamination: Impacts, mechanisms, and mitigation". English. In: *Journal of Power Sources* 165.2 (Mar. 2007), pp. 739–756. DOI: https://doi.org/10.1016/j.jpowsour.2006.12.012.

[10] D. Scholz D. Schiktanz. *BOX WING FUNDAMENTALS – AN AIRCRAFT DESIGN PERSPECTIVE*. 2011.

[11] Deloitte. *A bumpy ride ahead. Cash & working capital insights into the airline sector*. 2019. URL: https://www2.deloitte.com/content/dam/Deloitte/uk/Documents/corporate-finance/deloitte-uk-a-bumpy-ride-ahead-airline-sector.pdf.

[12] Guang Xun Du et al. "Controllability analysis for multirotor helicopter rotor degradation and failure". In: *Journal of Guidance, Control, and Dynamics* 38.5 (Jan. 2015), pp. 978–984. ISSN: 15333884. DOI: 10.2514/1.G000731. arXiv: 1403.5986. URL: https://arc-aiaa-org.tudelft.idm.oclc.org/doi/abs/10.2514/1.G000731.

[13] Guang-Xun Du and Quan Quan. *A Matlab Toolbox for Calculating an Available Control Authority Index of Multicopters*. Mar. 2016. URL: http://rfly.buaa.edu.cn/resources.

[14] EASA. *Aircraft certification*. URL: https://www.easa.europa.eu/domains/aircraft-products/aircraft-certification.

[15] EASA. *EASA Special Condition for VTOL and Means of Compliance*. 2020. URL: https://www.easa.europa.eu/document-library/product-certification-consultations/special-condition-vtol.

[16] Federal Aviation Administration. *Airworthiness certification*. 2021. URL: https://www.faa.gov/aircraft/air_cert/airworthiness_certification/#:~:text=The%5C%20certification%5C%20was%5C%20completed%5C%20in,between%5C%205%5C%20and%5C%209%5C%20years..

[17] Mykhaylo Filipenko. *(8) Back to the Future: A rough comparison of 70s VTOL concepts to current eVTOL designs LinkedIn*. 2020. URL: https://www.linkedin.com/pulse/back-future-rough-comparison-70s-vtol-concepts-evtol-filipenko/.

[18] S. J. Findlay and N. D. Harrison. *Why aircraft fail*. Nov. 2002. DOI: 10.1016/S1369-7021(02)01138-0.

[19] Yuki Fujio et al. "Invisible crack visualization and depth analysis by mechanoluminescence film". In: *Journal of Alloys and Compounds* 832 (Aug. 2020), p. 154900. ISSN: 09258388. DOI: 10.1016/j.jallcom.2020.154900.

[20] Eberhard Gill. *Lecture 1 - Course Organization & Systems Engineering - AE3211-I Systems Engineering & Aerospace Design (2020/21 Q3)*. URL: https://brightspace.tudelft.nl/d2l/le/content/293146/viewContent/1909569/View (visited on 04/27/2021).

[21] Snorri Gudmundsson. *General Aviation Aircraft Design: Applied Methods and Procedures*. 2013. DOI: 10.1016/C2011-0-06824-2. URL: https://www.sciencedirect.com/book/9780123973085/general-aviation-aircraft-design?via=ihub=.

[22] Jeff Holden and Nikhil Goel. *Fast-Forwarding to a Future of On-Demand Urban Air Transportation*. Oct. 2016. URL: https://www.uber.com/elevate.pdf (visited on 04/19/2021).

[23] Najmul Hoque et al. "Life Cycle Sustainability Assessment of Alternative Energy Sources for the Western Australian Transport Sector". en. In: *Sustainability* 12.14 (Jan. 2020). Number: 14 Publisher: Multidisciplinary Digital Publishing Institute, p. 5565. DOI: 10.3390/su12145565. URL: https://www.mdpi.com/2071-1050/12/14/5565 (visited on 04/30/2021).

[24] Hoverhawk. *Propeller and Fan Tip Speed Calculator*. URL: https://hoverhawk.com/propspd.html.

[25] J.A. Mulder, W.H.J.J van Staveren, J.C. van der Vaart, E. de Weerdt, C.C. de Visser, A.C. in 't Veld & E. Mooij. *AE3202 Flight Dynamics Lecture Notes*. Delft, The Netherlands: Delft University of Technology, 2013.

[26] Paul Olugbeji Jemitola. *Conceptual Design and Optimization Methodologyfor Box Wing Aircraft*. 2012.

[27] Johnson, Oliver. *Airbus Helicopters launches 5-bladed H145 upgrade*. 2019. URL: https://verticalmag.com/news/airbus-helicopters-launches-5-bladed-h145-upgrade/.

[28] Yasamin Karamian et al. "Spricho, an on demand energy efficient eVTOL Airtaxi". In: (2019).

[29] Akshat Kasliwal et al. "Role of flying cars in sustainable mobility". en. In: *Nature Communications* 10.1 (Apr. 2019). Number: 1 Publisher: Nature Publishing Group, p. 1555. ISSN: 2041-1723. DOI: 10.1038/s41467-019-09426-0. URL: http://www.nature.com/articles/s41467-019-09426-0 (visited on 04/29/2021).

[30] Adam Lipski. "Rapid determination of the Wöhler's curve for aluminum alloy 2024-T3 by means of the thermographic method". In: vol. 1780. American Institute of Physics Inc., Oct. 2016. ISBN: 9780735414426. DOI: 10.1063/1.4965936.

[31] Ya Tao Liu et al. "High Volumetric Energy Density Sulfur Cathode with Heavy and Catalytic Metal Oxide Host for Lithium–Sulfur Battery". In: *Advanced Science* 7 (12 June 2020). ISSN: 21983844. DOI: 10.1002/advs.201903693.

[32] Martin D Maisel, Demo J Giulianetti, and Daniel C Dugan. *The History of the XV-15 Tilt Rotor Research Aircraft: From Concept to Flight*. 2000.

[33] McIntosh, Alastair. *Technology behind the Lilium Jet*. 2021. URL: https://lilium.com/newsroom-detail/technology-behind-the-lilium-jet.

[34] Sofia Pinheiro Melo et al. "Life Cycle Engineering of future aircraft systems: the case of eVTOL vehicles". en. In: *Procedia CIRP*. 27th CIRP Life Cycle Engineering Conference (LCE2020)Advancing Life Cycle Engineering : from technological eco-efficiency to technology that supports a world that meets the development goals and the absolute sustainability 90 (Jan. 2020), pp. 297–302. ISSN: 2212-8271. DOI: 10.1016/j.procir.2020.01.060. URL: https://www.sciencedirect.com/science/article/pii/S2212827120301062 (visited on 04/29/2021).

[35] Elena Mossali et al. "Lithium-ion batteries towards circular economy: A literature review of opportunities and issues of recycling treatments". en. In: *Journal of Environmental Management* 264 (June 2020), p. 110500. ISSN: 0301-4797. DOI: 10.1016/j.jenvman.2020.110500. URL: https://www.sciencedirect.com/science/article/pii/S0301479720304345 (visited on 04/29/2021).

[36] Polaczyk N. et al. *A review of current technology and research in urban on-demand air mobility applications*. 2019, pp. 333–343.

[37] Hiroshi Nagata and Yasuo Chikusa. "A lithium sulfur battery with high power density". In: *Journal of Power Sources* 264 (Oct. 2014), pp. 206–210. ISSN: 03787753. DOI: 10.1016/j.jpowsour.2014.04.106.

[38] P Nathen, A Bardenhagen, and J Taylor. *Architectural performance assessment of an electric vertical take-off and landing (e-VTOL) aircraft based on a ducted vectored thrust concept*. 2021.

[39] F. Oliviero. *Lateral and Ground Stability*. Feb. 2021.

[40] F. Oliviero. *Requirement Analysis and Design Principles for AC Stability and Control (Part 1)*. Feb. 2021.

[41] Fabrizio Oliviero. "AE2111-II Systems Design: AircraftDesign-2_2019 BS- Lift & Drag Estimation (1)". In: ().

[42] Daniel P Raymer. *Aircraft Design: A Conceptual Approach*. 1992.

[43] Stephen Rondinelli, Roberto Sabatini, and Alessandro Gardi. "Challenges and Benefits offered by Liquid Hydrogen Fuels in Commercial Aviation". In: 2014. DOI: 10.13140/2.1.2658.9764.

[44] Jan Roskam. *Airplane design Part V: Component Weight Estimation*. DARcorporation, 1986. ISBN: 9781884885501.

[45] Ratchada Ruenruoy, Paul A Craig, and Wendy S Beckman. *PASSENGERS' PERCEPTION OF THE SAFETY DEMONSTRATION ON BOARD AN AIRCRAFT*. 2015.

[46] Tom Rye and Robert Hrelja. "Policies for reducing car traffic and their problematisation. Lessons from the mobility strategies of British, Dutch, German and Swedish Cities". In: *Sustainability (Switzerland)* 12 (19 Oct. 2020). ISSN: 20711050. DOI: 10.3390/su12198170.

[47] "Designing against Fatigue of Structures". In: *Fatigue of Structures and Materials*. Ed. by Jaap Schijve. Dordrecht: Springer Netherlands, 2009, pp. 559–586. ISBN: 978-1-4020-6808-9. DOI: 10.1007/978-1-4020-6808-9_20. URL: https://doi.org/10.1007/978-1-4020-6808-9_20.

[48] D Schiktanz and D Scholz. *BOX WING FUNDAMENTALS-AN AIRCRAFT DESIGN PERSPECTIVE*.

[49] Daniel Schiktanz. "Conceptual Design of a Medium Range Box Wing Aircraft". In: (July 2011).

[50] U. Schmidtchen et al. "Hydrogen Aircraft and Airport Safety". In: *Renewable and Sustainable Energy Reviews* 1 (4 Dec. 1997), pp. 239–269. ISSN: 13640321. DOI: 10.1016/S1364-0321(97)00007-5.

[51] D Silberhorn et al. *ASSESSMENT OF HYDROGEN FUEL TANK INTEGRATION AT AIRCRAFT LEVEL*. 2019.

[52] Dick G. Simons and Mirjam Snellen. *Reader Aircraft Noise and Emissions (part A)*. Delft University of Technology, July 2020.

[53] Ben Smye. *Aluminum alloys for aerospace - Aerospace Manufacturing and Design*. 2018. URL: https://www.aerospacemanufacturinganddesign.com/article/aluminum-alloys-for-aerospace/.

[54] The Vertical Flight Society. *eVTOL Aircraft Directory*. 2021. URL: https://evtol.news/aircraft.

[55] Z. S. Spakovszky. *11.7 Performance of Propellers*. 2006. URL: https://web.mit.edu/16.unified/www/FALL/thermodynamics/notes/node86.html.

[56] R JA Vos FPP Melkert FPP BTC Zandbergen SSE. *Aerospace Design and Systems Engineering Elements I-AE1222-II A/C Preliminary Sizing (class I weight estimation method)*.

[57] Statista. *Electricity prices for households in Germany from 2010 to 2020, semi-annually*. URL: https://www.statista.com/statistics/418078/electricity-prices-for-households-in-germany/.

[58] Tom C A Stokkermans et al. "Aerodynamic Interaction Effects Between Propellers in Typical eVTOL Vehicle Configurations". In: (2021). DOI: 10.2514/1.C035814. URL: https://doi.org/10.2514/1.C035814.

[59] Guoqiang Tan et al. "Solid-State Li-Ion Batteries Using Fast, Stable, Glassy Nanocomposite Electrolytes for Good Safety and Long Cycle-Life". In: (2016). DOI: 10.1021/acs.nanolett.5b05234. URL: https://pubs.acs.org/sharingguidelines.

[60] *The SES Li-Metal Technology*. URL: https://www.ses.ai/technology/.

[61] Maxim Tyan et al. "Comprehensive preliminary sizing/resizing method for a fixed wing – VTOL electric UAV". In: *Aerospace Science and Technology* 71 (2017). ISSN: 12709638. DOI: 10.1016/j.ast.2017.09.008.

[62] Volkswagen AG. *Hydrogen or battery? A clear case, until further notice*. 2019. URL: https://www.volkswagenag.com/en/news/stories/2019/08/hydrogen-or-battery--that-is-the-question.html.

[63] Xianfeng Yang et al. "Crashworthy design and energy absorption mechanisms for helicopter structures: A systematic literature review". In: *Progress in Aerospace Sciences* 114 (Apr. 2020), p. 100618. ISSN: 03760421. DOI: 10.1016/j.paerosci.2020.100618.

[64] Luhan Ye, Xin Li, and John A Paulson. "A dynamic stability design strategy for lithium metal solid state batteries Check for updates". In: *218 Nature* 593 (2021). DOI: 10.1038/s41586-021-03486-3. URL: https://doi.org/10.1038/s41586-021-03486-3.

[65] S. H. L. Yim et al. "Global, regional and local health impacts of civil aviation emissions". English. In: *Environmental Research Letters* 10.3 (Feb. 2015), p. 034001. DOI: 10.1088/1748-9326/10/3/034001.

[66] Harold Youngren, Mark Drela, and Scott Sanders. *DFDC*. 2005. URL: https://web.mit.edu/drela/Public/web/dfdc/.

[67] Ghassan Zubi et al. *The lithium-ion battery: State of the art and future perspectives*. June 2018. DOI: 10.1016/j.rser.2018.03.002. URL: https://doi.org/10.1016/j.rser.2018.03.002.